INVESTIGATION OF MICRO-SCALE STRESS DISTRIBUTIONS AND CONCENTRATIONS IN HYBRID FIBER-REINFORCED COMPOSITES

HİBRİT KOMPOZİT MALZEMELERDE MİKRO ÖLÇEKTE GERİLME VE GERİLME YIĞILMALARININ İNCELENMESİ

ECEM TURAN

ASSOC. PROF. BARIŞ SABUNCUOĞLU

SUPERVISOR

Submitted to

Graduate School of Science and Engineering of Hacettepe University

as a Partial Fulfillment to the Requirements

for the Award of the Degree of Master of Science

in Mechanical Engineering

January 2023

ABSTRACT

INVESTIGATION OF MICRO-SCALE STRESS DISTRIBUTIONS AND CONCENTRATIONS IN HYBRID FIBER-REINFORCED COMPOSITES

Turan, Ecem

M.S., Department of Mechanical Engineering

Supervisor: Assoc. Prof. Dr. Barış Sabuncuoğlu

January 2023, 136 pages

Hybrid composite materials are a specialized version of composite materials that constitute at least two different fiber materials. Hybrid composites are promising materials for various engineering applications. These materials can be specialized by selecting fiber materials that suit best with application field. Hybrid composites are employed in many fields, such as aerospace, automotive, construction, etc. Due to their application areas and the high potential of enlargement of their application fields in the future, having sufficient knowledge of these materials is essential.

Due to their complex internal structure, the effect of different parameters on these materials has been subjected to studies intensively. In general, studies focus on axial direction, parameters, and impact on axial load-carrying capability. This thesis study focuses on effects of different structural parameters in transverse direction and their effect on structure. The main aim of this study is investigation of different characteristic structural parameters of composite materials on stress distribution and stress concentrations at micro scale on hybrid composite materials composed with carbon and glass fibers.

During this thesis study, representative volume elements-both hexagonal and random RVE-utilized to model the structure. FEA modeling is used and a FEA model prepared for each investigated case for finite element modeling. Abaqus[2] program utilized for FEM modeling. To parametrize the study, a set of code used to create FEA models, Python[3, 4] program used for this process. In postprocess stage FEA output data is used as an input for normalization and stress concentration calculations and post process viewing programs, Mathcad[5] and Hyperview [6] programs are utilized for postprocess. Results of this study is aimed to use in prediction of behavior of these materials under certain loading conditions.

Keywords: composite materials, hybrid composite materials, FEA modeling, micromechanical modeling, stress concentration, representative volume element.

ÖZET

HİBRİT KOMPOZİT MALZEMELERDE MİKRO ÖLÇEKTE GERİLME VE GERİLME YIĞILMALARININ İNCELENMESİ

Turan, Ecem

Yüksek Lisans, Makine Mühendisliği Bölümü
Danışman: Doç. Dr. Barış Sabuncuoğlu

Ocak 2023 , 136 sayfa

Hibrit kompozit malzemeler, kompozit malzemelerin en az iki farklı fiberden oluşan özelleşmiş bir türüdür. Hibrit kompozitler farklı mühendislik uygulamarında kullanılma potansiyeline sahiptir. Bu malzemeler kullanılacağı mühendislik alanı için en uygun fiber malzemesi seçilerek özelleştirilebilir. Hibrit kompozitler, havacılık, otomotiv, yapı gibi farklı uygulama alanlarında kullanılmaktadır. Mevcut uygulama alanları ve gelecekte kullanımının yaygınlaşma potansiyelinin yüksek olması sebebiyle, bu malzemeler ile ilgili yeterli bilgi birikimine sahip olmak yüksek öneme sahiptir.

Karmaşık iç yapısı sebebiyle, farklı parametrelerin bu malzemeler üzerindeki etkisi, araştırmalarda çokça çalışılmıştır. Genel olarak, araştırmalar eksenel yön ve eksenel yönde yük taşıma kapasitesi üzerine odaklanmıştır. Bu tez çalışmasında farklı yapısal parametrelerin yanal yönde ve yapı üzerindeki etkileri üzerinde durulmuştur. Bu tez çalışmasının ana amacı kompozit malzemelerin karakteristik özelliklerini belirleyen bazı parametrelerin karbon ve cam fiberler kullanılarak oluşturulmuş hibrit kompozitler üzerinde mikro düzeyde gerilim dağılımları ve gerilim konsantrasyonları üzerindeki etkilerinin araştırılmasıdır .

Tez çalışması sırasında , yapıyı modellemek amacıyla temsili hacim elemanları-altıgen ve rastgele hacim elemanları- kullanılmıştır. Sonlu elemanlar analizi method kullanılmıştır, her bir parameter için farklı bir sonlu elemanlar modeli oluşturulmuştur. Sonlu elemanlar modellemesi için Abaqus program kullanılmıştır. Çalışmanın parametirize bir hale getirilebilmesi ve sonlu analiz modellerinin oluşturulabilmesi için kodlar kullanışmıştır, bu aşamada Python program kullanılmıştır. Sonuçların incelenmesi aşamasında, datalar sonlu elemanlar analizi programından alınmış, ve normalizasyon ve gerilim dağılımı hesaplamalarının yapılabilmesi ve son incelemelerin yapılabilmesi için girdi olarak kullanılmıştır, Mathcad ve Hyperview programları sonuçların incelenmesi için kullanılmıştır. Çalışmanın sonuçlarının bu malzemelerin çalışmada belirtilen yük koşulları altında davranışlarına dair bilgi ve ön bilgi oluşturması için kullanılması amaçlanmıştır.

Anahtar kelimeler: kompozit malzemler, hibrit kompozit malzemeler, sonlu elemanlar analizi modellemesi, mikromekanik modelleme, stress konsantrasyonu, temsili hacim elemanı

ACKNOWLEDGEMENTS

I would like to express my sincere appreciation to my supervisor, Assoc. Prof. Dr. Barış Sabuncuoğlu for his guidance, technical support, helpful advice, and encouragement throughout the research.

Secondly, I would like to thank each member of my family, and especially my parents, for their support at each stage of my life, undergraduate and graduate level studies, and my thesis preparation duration.

TABLE OF CONTENTS

LIST OF TABLES

I

LIST OF FIGURES

SYMBOLS AND ABBREVIATIONS

SYMBOLS

ξ	Reinforcing factor
G	Shear modulus
E	Elastic modulus
Y	Poisons ratio
E_f	Elastic modulus of fiber material
E_m	Elastic modulus of matrix material
V_f	Fiber volume
V_m	Matrix volume
E_1	Elastic modulus in axial direction
E_2	Elastic modulus in transverse direction
K_{RR}	Normalized radial stress concentration
$K_{R\Theta}$	Normalized tangential (shear) stress concentration
σ_{r_θ}	shear stress
$\sigma_{\theta\theta}$	radial stress

ABBREVIATIONS

RVE	Representative volume element
Sc	Stress concentration
Scf	Stress concentration factor
FEA	Finite element analysis
FEM	Finite element model
C	Carbon
G	Glass
Hex	Hexagonal
BC	Boundary conditions
PBC	Periodic boundary conditions
UD	Unidirectional
S_norm	Normalized stress concentration

CHAPTERS

1. INTRODUCTION

1.1. Motivation, Aim and Objectives of the Study

Regarding current studies and the demand for specialized materials, it can be said that hybrid composite materials are used in various structural applications. Since these materials can be specialized further regarding application needs such as low weight, cost reduction or low electrical permeability, demand for these materials will increase. Since the amount of study on these materials in the transverse direction is limited, estimation of the mechanical behavior of these materials becomes a difficult case. The motivation of this thesis study is to increase knowledge about these materials. Rising know-how will lead to an increase in the utilization of these materials

A number of studies in axial direction loading can be found in the literature, but resources and studies on transverse loading on these structures are very limited. The known fact about composite materials is the axial load-carrying capability is much better than the transverse side. Main aim of the study is to investigate micro-scale stress distributions and concentrations in carbon glass hybrid reinforced composites in the transverse direction. All the load cases used in this study are transverse loading cases and all of the stress concentrations and stress distributions investigated during the study are the results of this type of loading.

Main objective of this master's thesis is to analyze the hybridization effect on the micro-scale stress concentrations. This study will lead to make further predictions about these materials and their behaviors; consequently, these developments will ease the usage of these materials in engineering applications and increase the utilization of hybrid composites in a new variety of applications.

1.2. Research Methodology

Research methodology of this thesis is shown in a diagram in Figure 1.1. This thesis study begins by giving introduction-level information about hybrid composite materials. Also, brief information about previous researches and studies on the hybridization effect, micromechanical modeling based on different RVE types and FEA modeling studies is given in this section. After that, research method employed in this study is defined within research and methodology section, also studied parameters, parameter-related FEM models, FEA model BC's and post-process method of outputs are given in this section. Then FEA models are created using Python code and FEA models are set and accomplished. After that, results are obtained using python code and Abaqus post-process. Then, results were used to calculate the stress concentration factor and contour plots were drawn for normalized stress values using the Hyperview program. Lastly, all of the final results are collected and evaluated; final remarks and conclusions are given from them and future prospects of the study are revealed.

Figure 1.1 Summarized representation of research methodology.

1.3. Outline of the Study

This thesis study is composed of six chapters, an appendix and reference parts. Brief information about each chapter is as follows:

Chapter 1, *Introduction:* General information about the thesis study is given, including aim of the study, research methodology and outline.

Chapter 2, *Literature Review:* Information about past and recent studies related to the research field of this thesis study, such as usage fields, micromechanical modeling, hybridization effect, and studies on different RVE types, are revealed in this chapter.

Chapter 3, *Methodology:* This chapter supplies information about the method followed during the thesis study. Detailed information about studied parameters, corresponding FEM models, and process about FEA model creation with both Python and Abaqus pre-process are given in this stage. Also, information about post-process, refining and rearranging results with specific mathematical formulations is explained in this stage.

Chapter 4, *Results and evaluation:* Results, tables, stress concentration graphs and contour plots are stated in this chapter. All outputs of the study are revealed in this chapter in their final evaluation form. Also, this chapter includes basic comments and inferences from the results.

Chapter 5, *Conclusion:* A summary of the study as a whole is presented in this section. Besides, outcomes of the study can be found within this chapter.

Chapter 6, *Future work:* Further studies, based on this study to deepen and solidify the background that the research relies on stated in this section.

2. LITERATURE REVIEW

2.1. General Information about Hybrid Composites

There is a continuous search in engineering for new materials to use in every aspect of our lives to increase efficiency, using less resources and ease our lives. For a long time, composite materials have been a part of our daily lives. Composite materials have been used in many applications due to their superior properties, such as high stiffness, low weight etc. Hybrid composite materials are a specialized version of composite materials. Hybrid composites have an opportunity to produce materials with improvements on selected properties. This opportunity gives engineers to work with materials that are produced dedicated to usage places.

Hybrid composites are materials that are manufactured with the same production method as standard composite materials, but Hybrid composite materials are a specialized version of standard composite materials. Hybrid composites are produced using standard matrix materials, but more than 1 type of fiber is utilized within the structure.

With the help of different material combinations, structural materials with highlighted beneficial properties can be achieved. Carbon and glass fibers and combinations of these two fibers have been used in this study. Carbon&Glass fiber combinations are one of the widely used fiber duos in applications due to their high strength and low cost. A macro scaled view of carbon glass hybrid composites is given in Figure 2.1

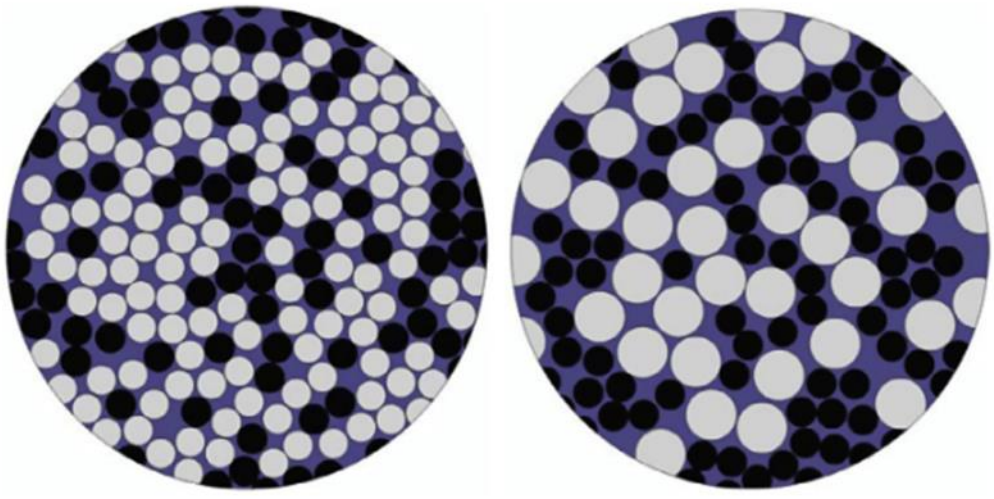

Figure 2.1 Macro-scale view of hybrid composites[7].

Hybridization can be achieved with different ways in composites. These methods can be said as interlayer, intralayer and intra-yarn. A representation of different hybridization methods can be seen in Figure 2.2.

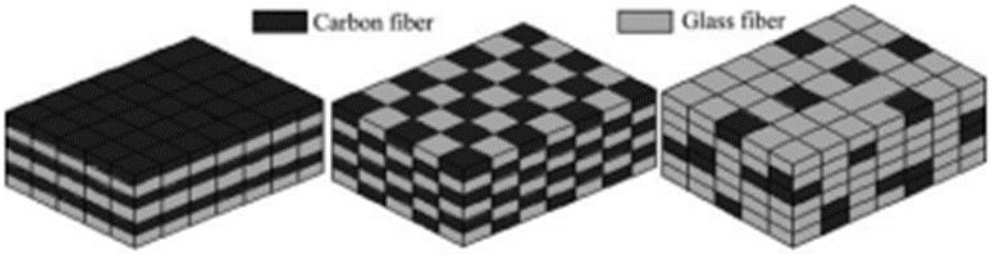

Figure 2.2 Interlayer, intralayer and intra yarn hybrid composite representation [8].

Hybrid composites are produced with combinations of two different types of fibers, as the most critical and brittle fiber is carbon fiber and the second fiber is called hybridization fiber [9, 10]. Generally hybridization fiber is selected with higher failure strain.

Mechanical properties of hybrid composite materials can be calculated using a variety of analytical methods. Mostly used of these methods are: Halpin Tsai equations, Chamis formulations, Rule of mixtures and Inverse Rule of Mixtures. In general, Rule of mixture is the most common way to predict the micromechanical properties of composite materials and iROM is used for hexagonal-shaped fibers extensively. On the other hand, these relation system gives inaccurate results in terms of stress concentrations that result from fiber matrix interactions under transverse loading. Instead of Rule of mixtures and iROM, Halpin Tsai equations are used to calculate transverse modulus by some of the researchers such as Crookston[11]. In general Halpin Tsai equations used extensively for the transverse modulus of hybrid composites, these equations can be given as below [1].

$$E_1 = E_f * V_f + E_m * V_m \quad \textbf{(1)}$$

$$\frac{E_2}{E_m} = \frac{1 + \xi * \eta * V_f}{1 - \eta * V_f} \quad \textbf{(2)}$$

$$\eta = \frac{\frac{E_f}{E_m} - 1}{\frac{E_f}{E_m} + \xi} \quad \textbf{(3)}$$

E_f and E_m refers to fiber and matrix modulus values respectively. E_1 is elastic modulus of composite in axial direction and E_2 is elastic modulus in transverse direction. In these equations ξ refers to reinforcing factor and defined by three parameters that are: fiber geometry, packing geometry and loading conditions [1]

Representation of Halpin Tsai equations and transverse modulus is given in Figure 2.3

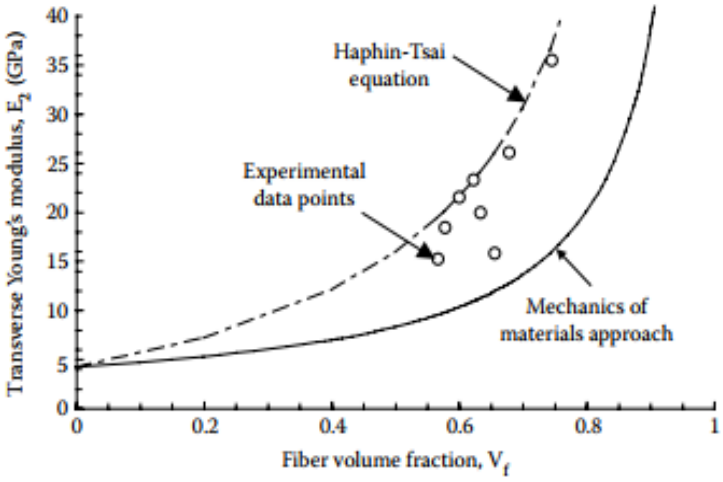

Figure 2.3 Experimental data vs theoretical assumptions of Halpin-Tsai

Hybrid composites have been used widely in a variety of different fields. Some of the usage examples of hybrid composites can be given as: in aerospace industry, at commercial aircraft's cockpit glare shields, for the places where high strength is not required and when remarkable cost efficiency can be achieved, hybrid composites can be used widely. Zweben [12], in his study, gives the idea of usage area of advanced composites and potential usage area of these types of composite structures. Hybrid composites that are produced from glass, carbon or basalt fibers have been used in wind turbine panel production. In marine applications, hybrid composites are preferred in ship hull production due to their strength, low weight, ability to produce at complex geometrical shapes, low electromagnetic recognition and less maintenance requirements. In the construction section, a pedestrian crosswalk project whole structure compromised from carbon&glass hybrid composites was completed and has been used actively[13].

Figure 2.4 A pedestrian bridge in Okinawa Japan made of hybrid composite structure [13].

Also, there are ongoing studies to produce hybrid composite suspension parts in heavy automotive industry (within the scope of LiMech project) In AMRC Sheffield university.

Various studies have been made on the production methods of hybrid composites. Zin et al. [14] studied on various production methods of hybrid composites for automotive and aerospace applications, in terms of both open and closed mold fabrication methods, hand lay-up, spray-up; regarding various restraints such as geometric complexities, part scales etc., and requirements such as high pressure due to strength needs etc.

2.2. Studies on Hybridization Effect

As hybrid composites provide a wide range of application possibilities, there have been many research studies related to the development of this type of composite in the literature.

Hayashi [15] discovered the hybridization effect and stated that the failure strain of the low elongation fiber in a hybrid composite structure is higher than that of in homogenous composite structure.

Hybridization causes changes in material behavior. Response to material changes regarding different loading types. Swolf et.al.[16] studied on maximizing hybridization effect on hybrid composite materials.

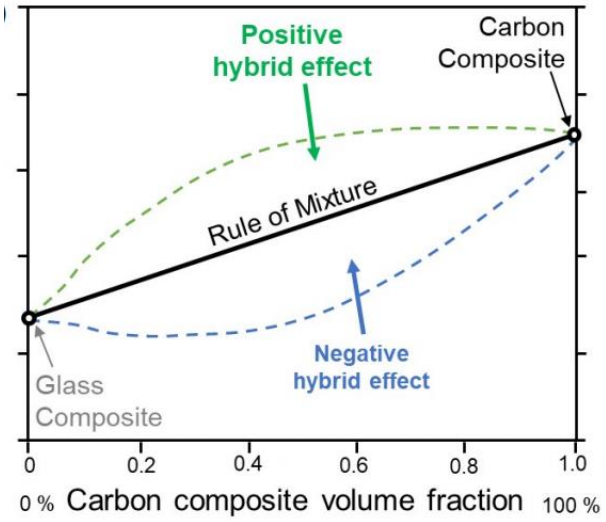

Figure 2.5 Representation of hybridization effect on axial mechanical properties[17]

Improvements that are achieved by hybridization can be given as followings:

- Improvements in axial load-carrying capability:

  Positive hybridization effect on mechanical properties at the axial direction of hybrid composites can be seen in Figure 2.5. On the other hand, Kretsis [18] studied on behaviors of hybrid composites under axial loading.

Improvements on rupture&fracture mode and elongation value: Manders[19] has been shown the effect of hybridization on elongation values with his studies. A representation of hybridization on elongation value can be seen in Figure 2.6

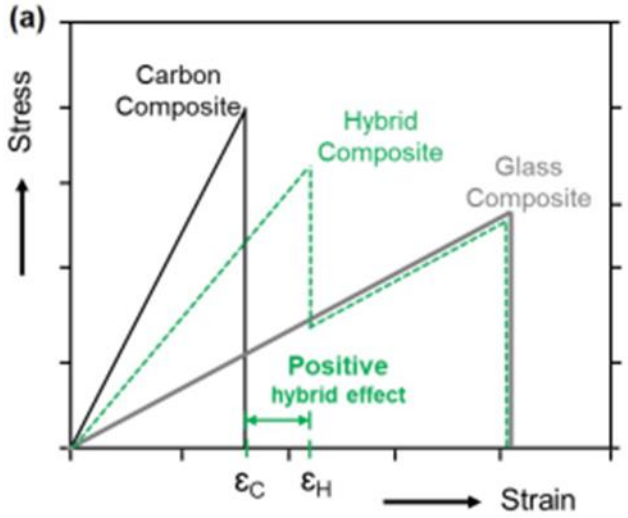

Figure 2.6 Effect of hybridization on elongation [17]

-Improvements in repeated impact response behavior:

Sevkat (2010) showed that damage accumulation on carbon fiber materials can be decelerated by making hybridization with glass fibers at outer layers [20]. A Representation can be seen in Figure 2.7

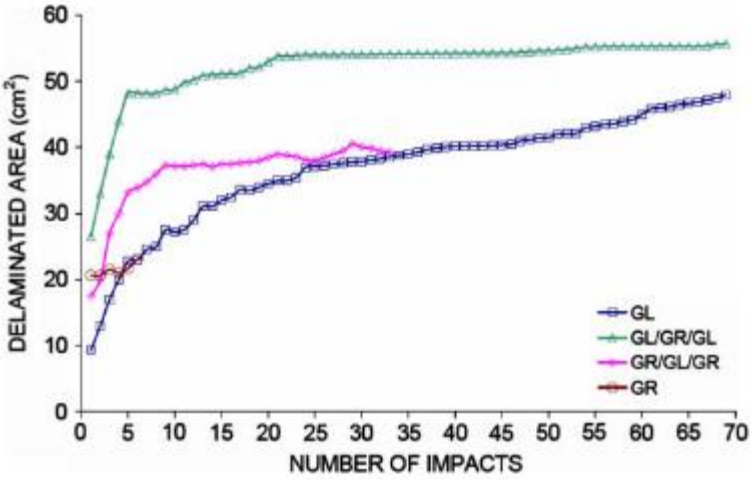

Figure 2.7 Delamination under repeated impact and hybridization effect wrt different hybrid combinations [20].

- Improvements in fatigue behavior:

  Dickson& Fernando managed to show positive hybridization effect on fatigue stress levels on carbon&glass and structures even though they couldn't set a direct linear relationship[21, 22]. This effect revealed in Figure 2.8

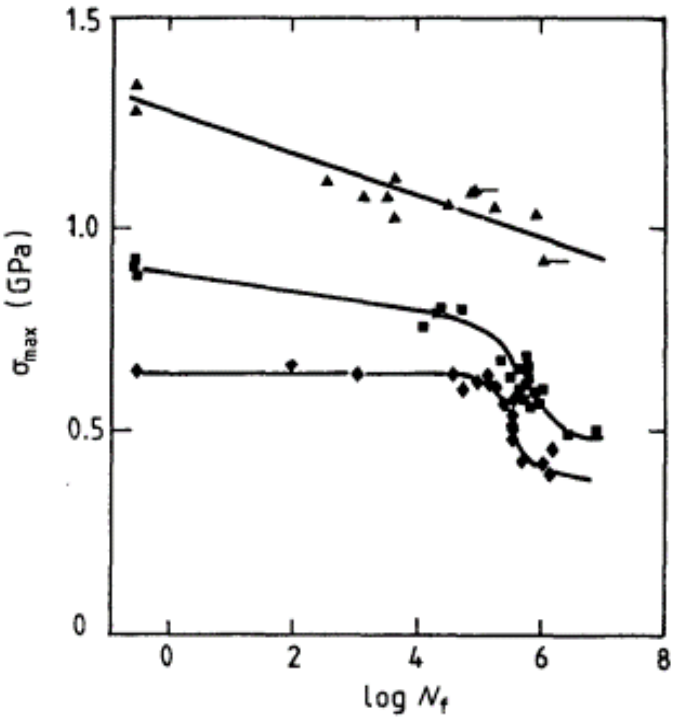

Figure 2.8 Fatigue life vs stress curve regarding various composite structures both homogenous and hybrid composites [21, 22].

- Improvements in flexural rigidity:

  Dong found that as a transition from homogenous carbon fiber to glass fiber at the portions where compressive forces become dominant, a negative hybridization effect observed, but as the hybridization ratio increases, stability on flexural rigidity has been achieved, and a positive hybridization effect occurred. On the other hand, a further increase in glass fiber ratio causes an abrupt decrease in flexural rigidity. Main reason behind this behavior is bending occurs on outermost sides and becomes zero at the neutral axis[23]. A representation regarding flexural rigidity can be seen in Figure 2.9

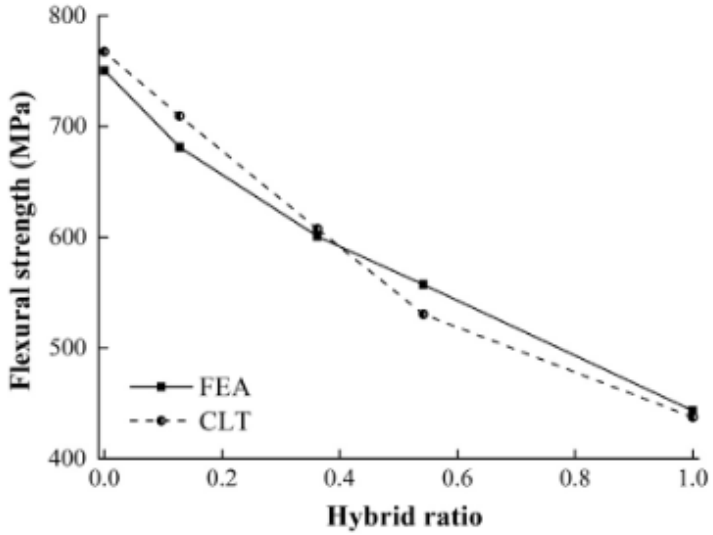

Figure 2.9 Flexural strength comparin FEA and CLT results wrt changing hybrid ratio [23].

2.3. Studies on Micromechanical Modeling

In studies made on composite materials to investigate stress values on matrix and fiber-matrix interface, a variety of micromechanics models have been made by modeling these two gradients separately. Sabuncuoğlu et al. [24-28], stress analysis on composite materials under transverse loading. In his studies, to be able to examine fiber-matrix interface, he modeled these two structures separately. They studied on the effect of different fiber section geometries on stress concentration values. Also, Sabuncuoğlu studied radial and tangential shear stress distributions wrt different fiber volume ratio values, stress redistribution around broken fibers, matrix effect.

Besides of these, there are a variety of studies on negative effects of hybridization on fatigue analysis, such as crack propagation. Chavalier [29], in his studies, he made investigations on the characterization of transverse compressive loading and showed that the studies made on this subject must be supported with experiments, in his studies, under transverse tension loading when early damage accumulation takes place and damage accumulates on fiber matric interface, models gives the true and expected results but on

the other hand, under transverse compression loading when macro scale damage occurs, he stated that experimental results and modeling results separate from each other. To understand this situation, further experiments must be made.

Sun [30] studied on loss of load-carrying capability of unidirectional fiber composite materials from the micromechanics aspect. Especially under high shear loads, he compared the rupture envelopes of envelopes found from model simulations and classical rupture envelopes. He studied on different rupture envelopes but found irregularities between model results and classic theoretical envelopes. To cope with this difference, he proposed a new set of rupture mechanisms developed mainly based on model findings, and this new method shows a good agreement with model results.

Sharma [31] studied on micromechanics modeling of biaxial rupture envelopes of carbon fiber structures. In this study, he showed that effect of matrix on transverse strength is at a minimal level, and for the combined loading compression and shear, fiber-matrix interface and friction at this interface become important on strength value.
Regarding investigated studies in the literature, it is observed that there are not many studies on the transverse direction to reveal the effect of different parameters such as fiber material , fiber radius, fiber volume ratio, etc. and different combinations of these materials. This study mainly focuses on that issue.

In general, most of the studies are employed representative volume elements for modeling. Main motivation to use this type of representative volume element is assuming that hybrid composite structures compromises of homogenously distributed fibers and assuming these representative volume elements as a periodic unit that repeats itself.

Sun [32] makes a description of how a suitable model should be as: working on the FEM that represents the model in the most realistic way. Different representative volume elements were used previously in studies found in literature and continue to use. Most known of these representative volume elements are square representative volume elements, hexagonal representative elements, circular representative volume elements and

random representative volume elements[33]. Each of these periodic volume elements has both advantageous and disadvantageous sides. For example, square volume elements have been selected mainly due to their symmetricity and ease of application of boundary conditions. S. Li[34-36] studied on different unit cells and discussed details of different RVE's such as boundary conditions, max fiber volume ratio that can be achieved etc. an explanation of comparison of different RVE's in terms of transverse isotropy can be found in that study. Bayat and Aghdam[37] made a study using both square and hexagonal RVE; they stated that axial results are similar in these models, but results become to differ when transverse cases are considered. It can be said that in terms of transverse properties, square RVE reveals the real case worse than hexagonal RVE.

Main RVE types; square RVE, cylindrical RVE, hexagonal RVE and random RVE, have been used intensively within studies since these approximations correlate with real composite structures better than other RVE types.

In this study, firstly, hexagonal RVE is used in investigations. Cowin and Mehrabadi revealed with their studies; hexagonal RVE gives the most realistic results in terms of preserving transverse isotropy. Also, Love studied and made a mathematical demonstration on these subjects [38]. A representation of hexagonal RVE can be seen in figure Figure 2.10

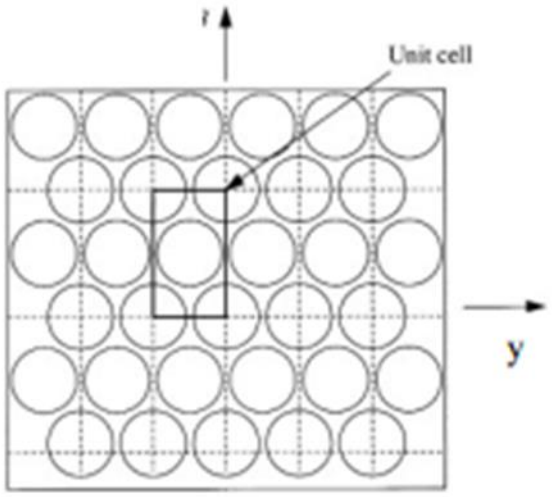

Figure 2.10 A version of Hexagonal RVE representation [33]

Adams et al. [39-41] made investigations on homogenous composite structures in terms of longitudinal, transverse and shear loading.

Another RVE type used within the studies both in this study and literature is random RVE. There is an extensive study on random microstructure modeling in composites to be able to correlate real cases better. It is a known fact that fiber distribution in an UD composite structure may not be uniform and may not repeats itself periodically. Swolf et al. [7] studied on stress concentrations in unidirectional hybrid composites with random packing. Aghdam et al. [42] revealed a method of dividing random RVE into sub-cells and conducted a study on micromechanical and thermal properties of structures with the help of these sub-cells. Romanov et al. [43] studied on the statistical aspect of micromechanical modeling in terms of fiber distribution and fiber modeling using RMG(random microstructure generation).

In random RVE modeling, various difficulties are encountered and subjected to different studies. Random distribution causes a deviation from symmetricity in terms of boundary conditions. Wongsto et al. [44] studied on a methodology that uses average fiber spacing to correlate the boundary conditions of the symmetrical unit cell with a randomly distributed fiber arrangement over a transverse cross-section. Trias et al. [45] studied on variance in the same mechanical properties of a particular composite structure between random models and periodic models. Chen et al. [46] studied on interface stress distribution on transversely loaded homogenous composite structures-carbon/epoxy- using the boundary element method in terms of square packing and random packing RVE. Buryachenko et. al.[47] used quantitative description method and numerical simulations on random RVE structured composite materials regarding the material's effective elastic moduli. Gusev et. al.[48] studied on glass composites assuming transversely random structure. Melro et al. [49, 50] studied on damage initiation and propagation on composites using random RVE FEM model, cohesive elements and employing continuum model approximations to predict the strength and elastic mechanical properties. Gonzales and Lorca [51] studied on CFRP and GFRP using a FEM model structured with random fiber

inclusions and computational micromechanics under compression and stated that the main failure control parameter was found as matrix shear bands and interface crack propagation. Guerrero and Mayugo [52-54] conducted different studies on hybrid composites to see the effect of thermal stresses and dynamic effects, size effects, and stress around broken fibers.

There are various studies on micromechanical calculations by analytical approaches. Huang [55] studied on a theoretical approach to be able to calculate the ultimate strength of unidirectionally fiber-reinforced composites. Wilczynski and Lewinski [56] studied on an analytical approach to predict homogenous unidirectional fiber-reinforced composites for isotropic reinforcement.

3. METHODOLOGY

In this chapter, research methodology is explained in detail. Methodology chapter contains information from the parameter selection, parametric and standard model creation to the end of the mathematical calculations. Models are created by using both Abaqus preprocessor and Python programs that allow user to work parametrically. By making required changes on Python codes and implementing them into Abaqus, a FEA model can be created easily without time consumption. Base Python codes used in this study were created and used previously within the studies by Sabuncuoğlu [25] for parametric hexagonal & random RVE studies, Muyago& Guerrero [53] for parametric random RVE studies. Explanation of geometrical properties of the model, unit system, and boundary conditions applied to each model is defined within each section in this chapter. Lastly, data analysis section for the output evaluation method is introduced and analytical approach is explained.

By using a variety of Python codes, parametric model creation is achieved and analysis models are accomplished and run. On the other hand, for some of the models Abaqus pre-process module is utilized to create FEA model. During model creation step 2 main geometry types are followed to simulate that are hexagonal RVE and random RVE. The key point of the geometry creation step is maintaining the specified fiber volume ratio wrt related FEA model requirements

An overall research methodology flowchart is given in Figure 3.1.

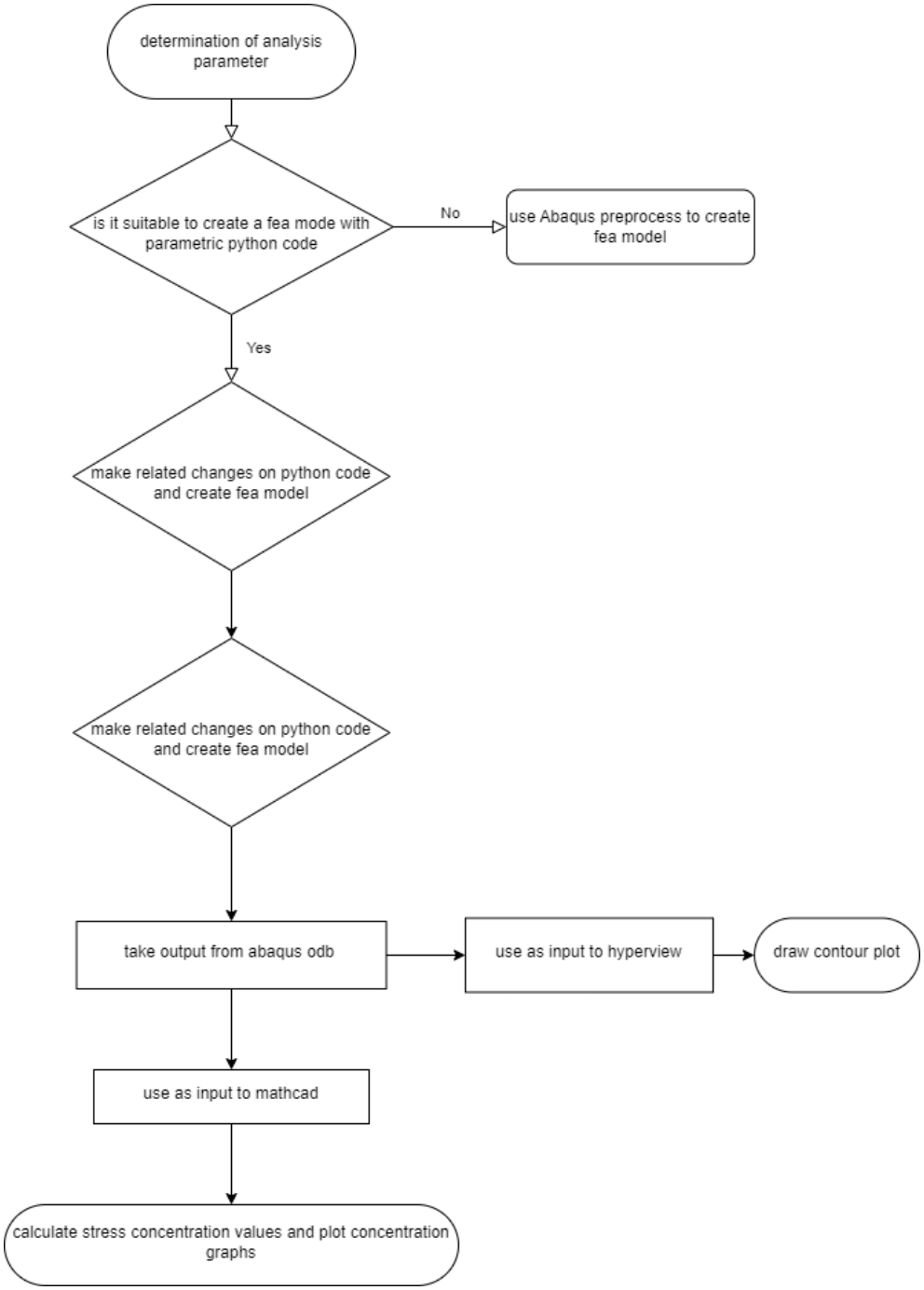

Figure 3.1 Overall research methodology representation.

3.1. Development of FEA Models

In this section, common properties of all models are stated. An important property of Abaqus is that program does not have a unit system and to work with a logical model, unit consistency must be taken into account and should be satisfied by the user. Regarding this situation unit system employed during this study is as micro-Newton for force, MPa for stress and modulus of elasticity, and micrometer for both displacement and length. Unit system employed during this study is also given in Table 3.1.

Table 3.1 Unit system used for FEA models

Quantity	Unit
Force	μN
Stress	MPa
Displacement	μm
Length	μm
Modulus Of Elasticity	MPa

During creation of models, required materials are assigned to specified regions. In this study, both homogenous composite and hybrid composite models are used. Homogenous composite models are used as a control group in evaluation stage of the results. For the models used in this thesis study, glass and carbon are used as fiber material and epoxy is used as matrix material. All of the material properties can be seen in Table 3.2 [25]. Two main RVE types used in this thesis study as Hexagonal RVE and Random RVE.

Table 3.2 Material properties used within the analysis

Glass	Epoxy	Carbon (IM-7)
$\boldsymbol{E = 72\ GPa}$	$E = 3\ GPa$	$E_L = 276\ GPa$
$\boldsymbol{\upsilon = 0.25}$	$\upsilon = 0.4$	$E_T = 10.3\ GPa$
		$G_{TT} = 3.8\ GPa$
		$G_{LT} = 27.9\ GPa$
		$\upsilon_{LT} = 0.26$

3.1.1. Hexagonal RVE Models

Stages of hexagonal RVE creation, different hexagonal RVE types created and investigated during this study will be given in this section.

Using both Python codes and Abaqus pre-process, hex RVE FEA models, , are created. If an investigated case is suitable to work with a parametric model(without radius change), then the study is conducted with a FEA model, which is created using python code, but if the investigated parameter requires a change in fiber radius value, then by re-organizing input values and arranging required changes on python code, to preserve fiber volume ratio as 0.6, hex RVE models are created. Triple hexagonal model and mini square angled models are set up using Abaqus pre-process part and fiber volume ratio is set as 0.6. Element types used with hex RVE models are set as C3D6 and C3D8R in all models.

For the models created using Python code, interface section between fiber and matrix is modeled by layering the interface region into different stages. On the other hand, for the models created with the Abaqus preprocessor module, instead of layering, an appropriate amount of FEA element is used within interface region.

In hexagonal RVE modeling, fiber materials are also changed regarding available fiber radius values. Glass fiber radius value is taken as five micrometers, carbon fiber radius value is taken as 3.5 micrometers [25]. Changes on radius values on hex RVE are applied by making related changes on Python input data files which contain geometrical information about fibers. After that, RVE sizes are derived regarding maintaining fiber volume ratio as 0.6 and a model is created and BC's are applied via Python codes. For all parametric hexagonal RVE models, base Python scripts are studied previously by Sabuncuoğlu [25]

A flow chart about hex RVE creation can be seen in Figure 3.2.

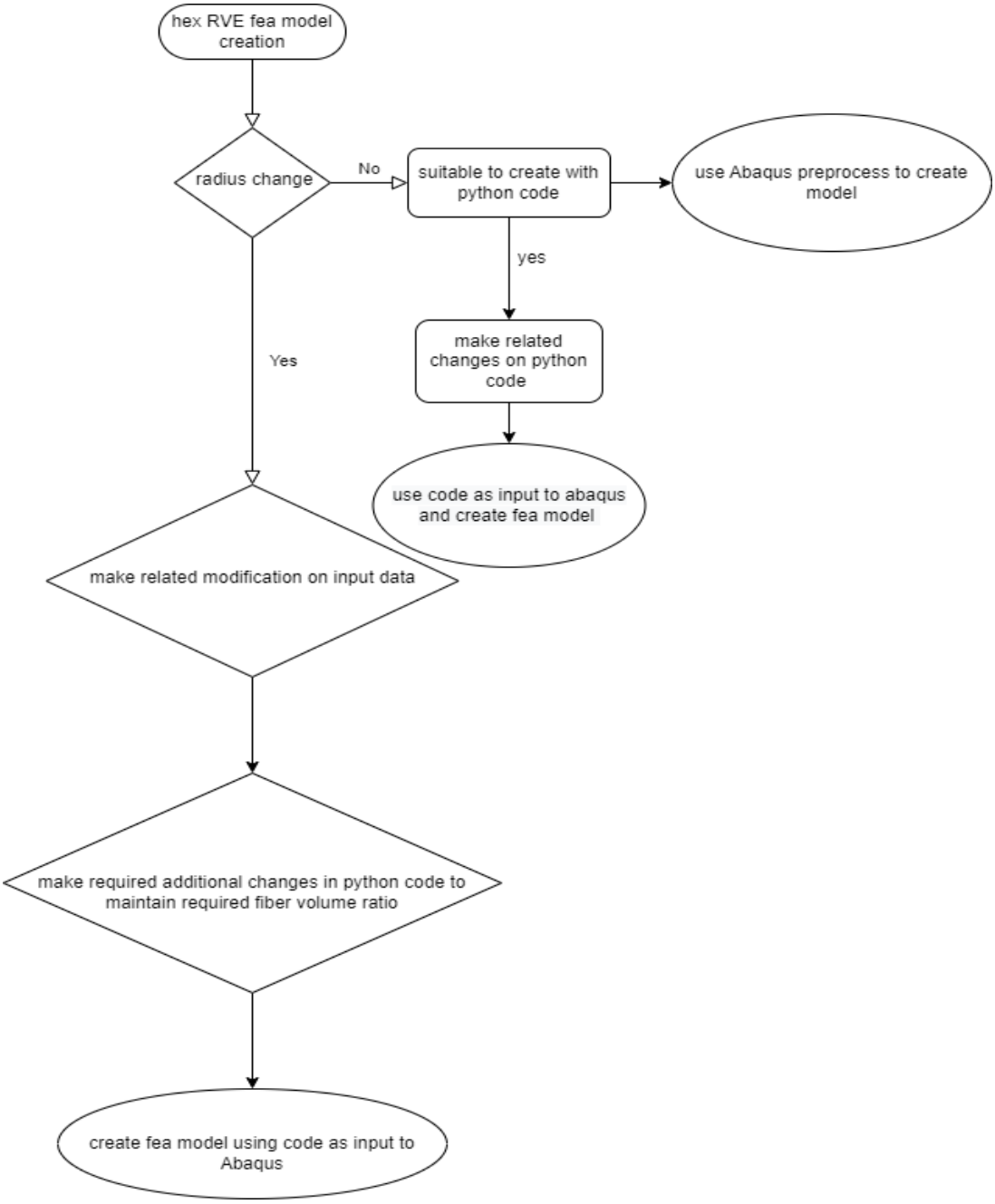

Figure 3.2 A flowchart to reveal Hex RVE FEA model creation.

3.1.1.1. Hexagonal Fiber Distribution Representative Volume Element

An overall insight about hexagonal RVE is given under this heading general properties of Hex RVE. Information about element type and meshed views is given in this section. A homogenous (in terms of geometrical parameters) hex RVE geometry with interface layers can be seen in Figure 3.3. This model is created with parametric Python code by making certain changes to satisfy the required needs. Number of elements is 14292. A representation of hexagonal RVE as a geometric and meshed view can be seen in Figure 3.3

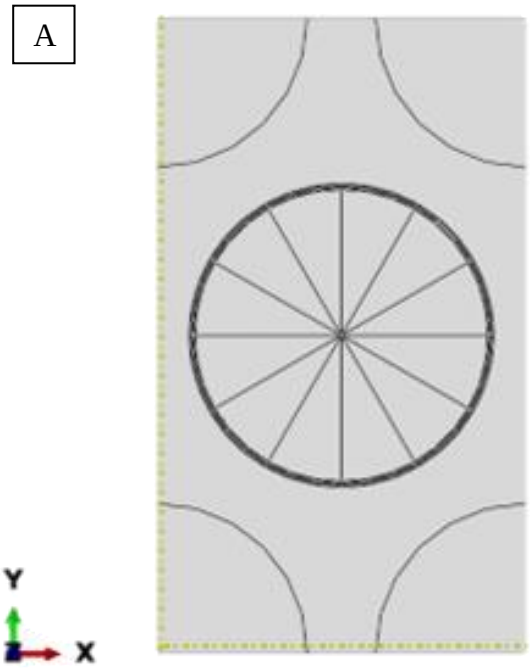

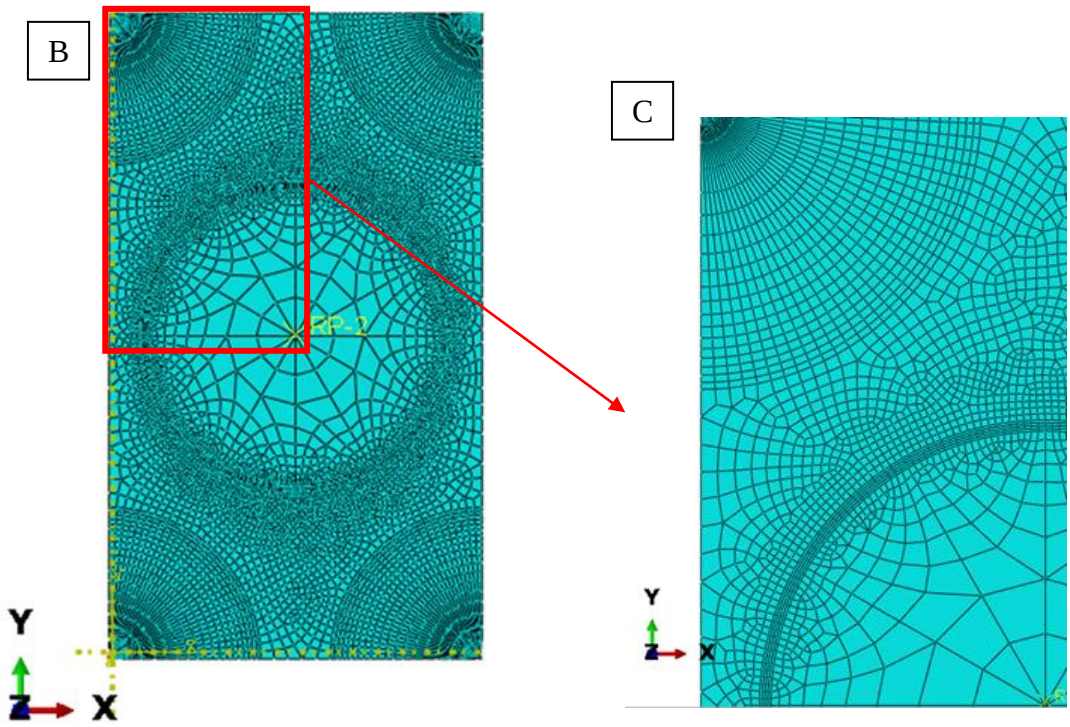

Figure 3.3 overall hexagonal RVE representatio:n (a) geometrical representation ; (b) meshed view: (c) detailed interface meshed region representation.

Both Maligno and periodic boundary conditions applied to the structure. Load applied as displacement.

3.1.1.2. Triple Hexagonal Fiber Distribution Representative Volume Element

In the RVE model there exists only one central fiber. Triple FEA model is created to examine the stresses when different type of fibers exists as the central fiber. ınstead of periodic boundary conditions, this FEA model is completely settled with Abaqus preprocessor. Fiber volume ratio is set as 0.6 and difference from other models is not applying periodic boundary conditions. Number of elements is 11916. load is applied as displacement through transverse direction. Geometric view can be seen in Figure 3.4 and meshed view is given in Figure 3.5.

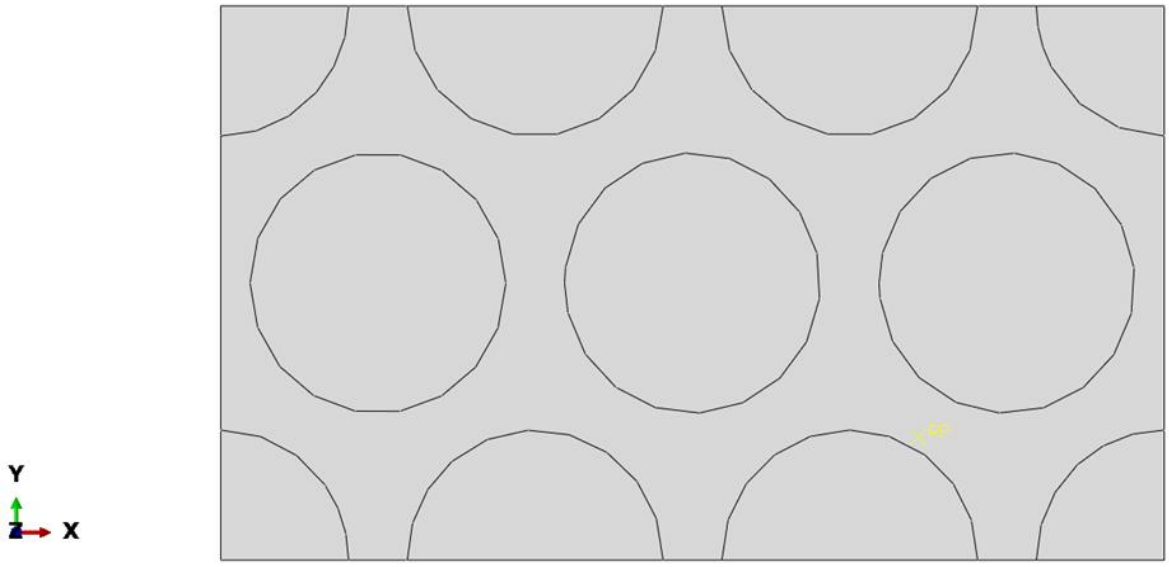

Figure 3.4 Triple hexagonal RVE geometrical representation.

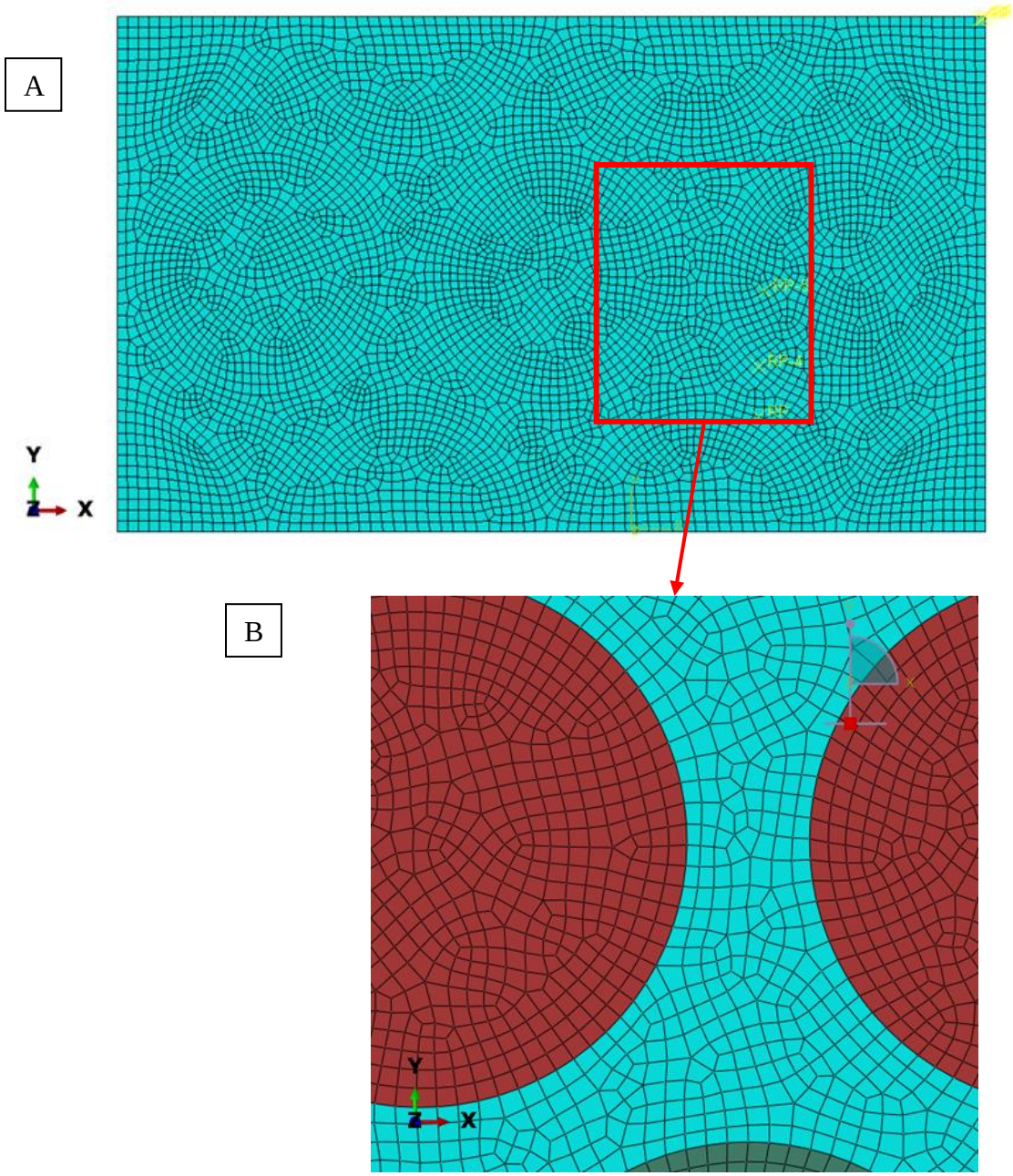

Figure 3.5 Triple hexagonal RVE meshed representation: (a) overall triple hexagonal RVE meshed view; (b) detailed interface region meshed representation.

3.1.1.3. Shear Loading Hexagonal Fiber Distribution Representative Volume Element Section

In general, stated Hex RVE that is used for transverse loading is also used in shear loading cases. Material effect, fiber radius effect and combination of these two parameters are investigated by using hexagonal RVE. To understand the behavior of the structure under different loadings, an additional model need occurred and a 45-degree angled cut quarter square RVE model is created to examine load path. Load is applied perpendicular to the angled surface in xy plane. A geometric representation of this model can be seen in Figure 3.6 and a meshed view can be seen in Figure 3.7

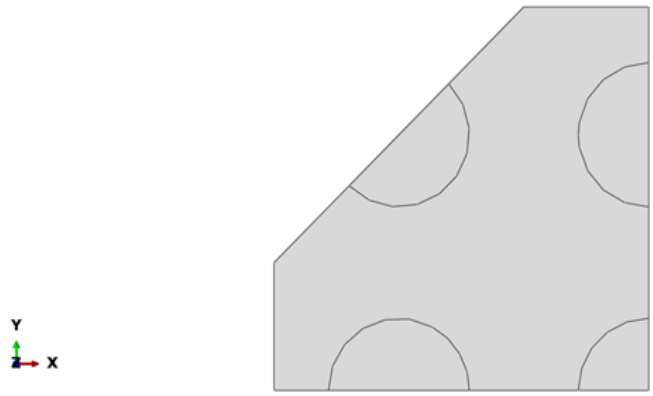

Figure 3.6 Geometrical representation of angled model.

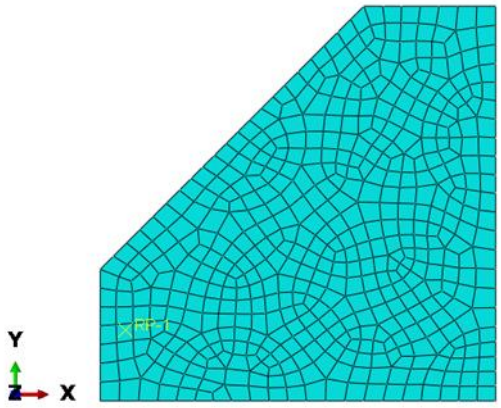

Figure 3.7 Angled model meshed view.

3.1.1.4. Hexagonal Fiber Distribution Representative Volume Element with Varying Fiber Radius

These models are created to investigate fiber radius effects. Models are created by making changes on python code input files. These input files are used for geometrical properties of fibers. These input files used in Python scripts .After that, Python codes are used as input to Abaqus program.

Fiber radius values are selected As 3.5 um and 5 um for carbon and glass fibers, respectively . Fiber volume ratio is set as 0.6. Load is applied as displacement in transverse direction. Both Maligno and periodic BCs which are explained under heading 3.2, are employed in these models.

20370 elements are used for inner 5 micrometer radii model and 23823 elements are used for inner 3.5 micrometer fiber radii model. Also, these models are used to implement material effect by combining fiber radius effect. Representation related to these models can be seen in Figure 3.8 and Figure 3.9.

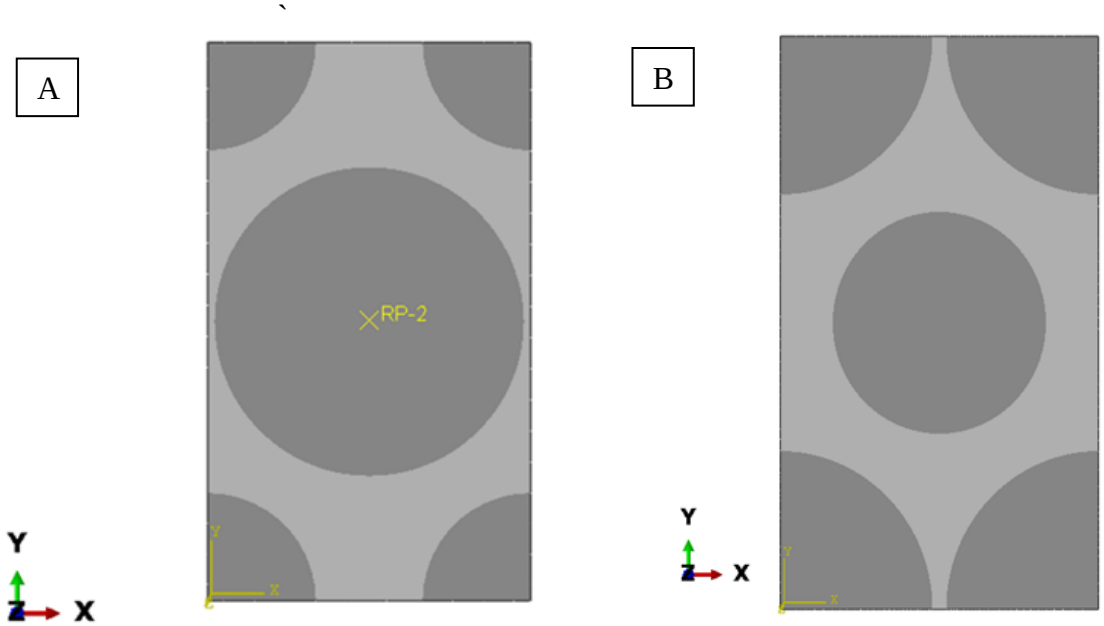

Figure 3.8 Geometrical representation of models with different fiber radius values: (a) with inner 5micrometer fiber; (b) outer 3.5 micrometer fiber.

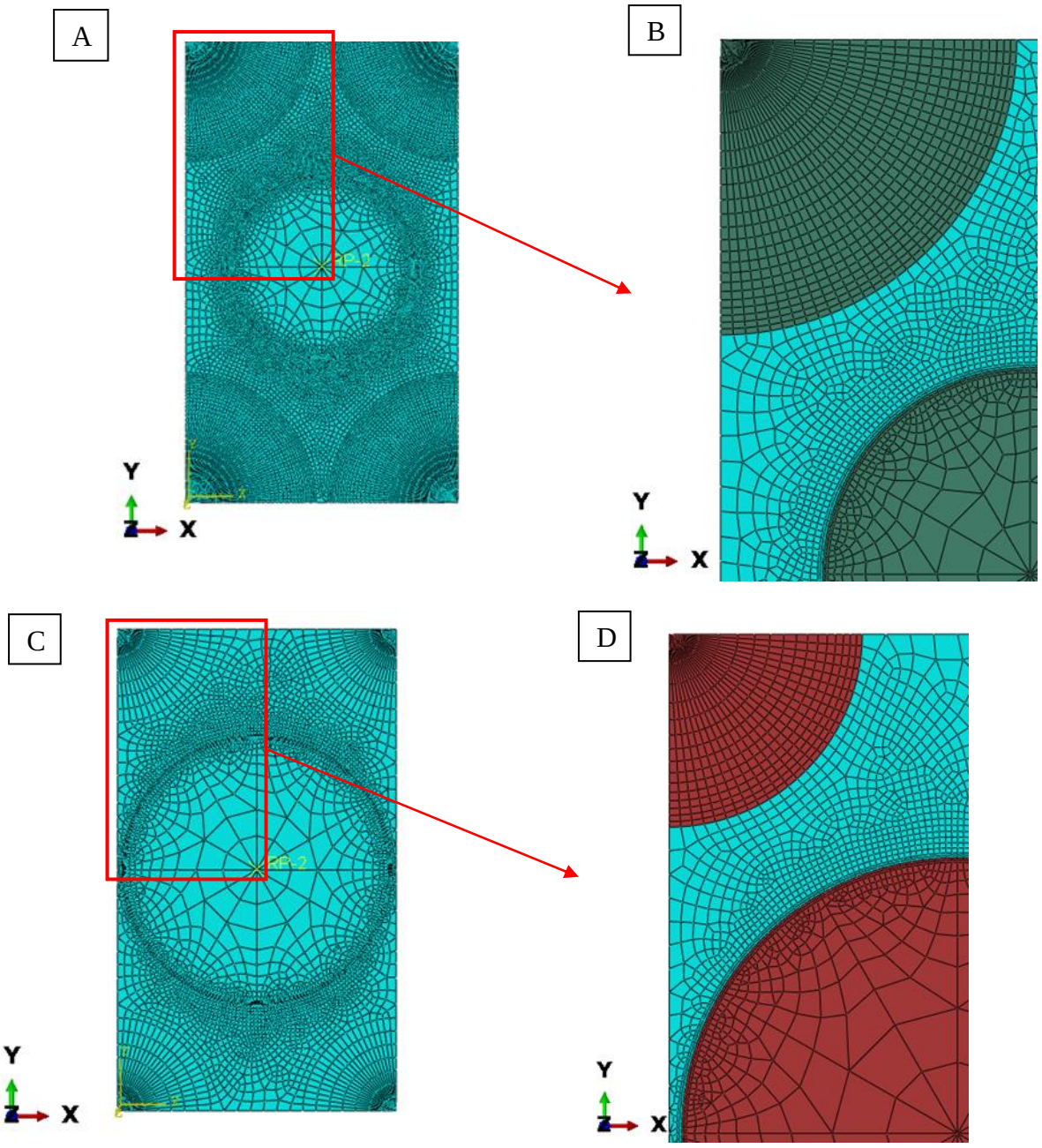

Figure 3.9 Meshed view of models with different fiber radius values: (a) 3.5 micrometer center fiber meshed view;(b) detailed view of interface region with center 3.5 micrometer fiber;(c) 5 micrometer center fiber meshed view;(d) detailed view of interface region with center 5 micrometer fiber.

3.1.2. Random RVE Creation

Random RVE is the other RVE type used in this thesis study. Random RVE creation methods and details about a variety of Random RVE models are given under this heading. Main motivation of random RVE studies is fiber distribution within a matrix in real manufacturing processes is not as in certain array instead fibers are distributed in matrix randomly.

In this thesis study, two main random RVE types are used with different material combinations. These models can be said as the one having a standard radius value and the other random model constitutes variable fiber radius. These models have different way of FEM creation method.

For the model with constant fiber radius value, Python code is used as input to Abaqus to create FEA model. On the other hand, for varying fiber radius model, another python code is used for calculating fiber locations regarding required fiber volume ratio and specified RVE dimensions; then, implementing these geometrical information about fibers into Abaqus Preprocessor FEM model is created. Input values are set regarding certain considerations such as min fiber distance, fiber volume ratio, RVE dimensions hybridization type.

For parametric modeling, without any radius variation, base python code is obtained from studies of Sabuncuoğlu [25]; for the model with varying radius, used base python code is obtained from Muyago& Guerrero [53]. After making certain changes and implementing on these codes, they are utilized for the current thesis study. some of the inputs for python script are fiber radius, RVE dimensions, inter fiber distance, fiber volume ratio etc. A representation of part of input section, output npz file, and output fiber plot of script can be seen in Figure 5.1, Figure 5.2 and Figure 5.3 in appendix. A representation of the random RVE creation flowchart is given in Figure 3.10.

In all of the models, fiber volume ratio is set as 0.6 and element type used in random models are C3D6, C3D8R and C3D8RH.

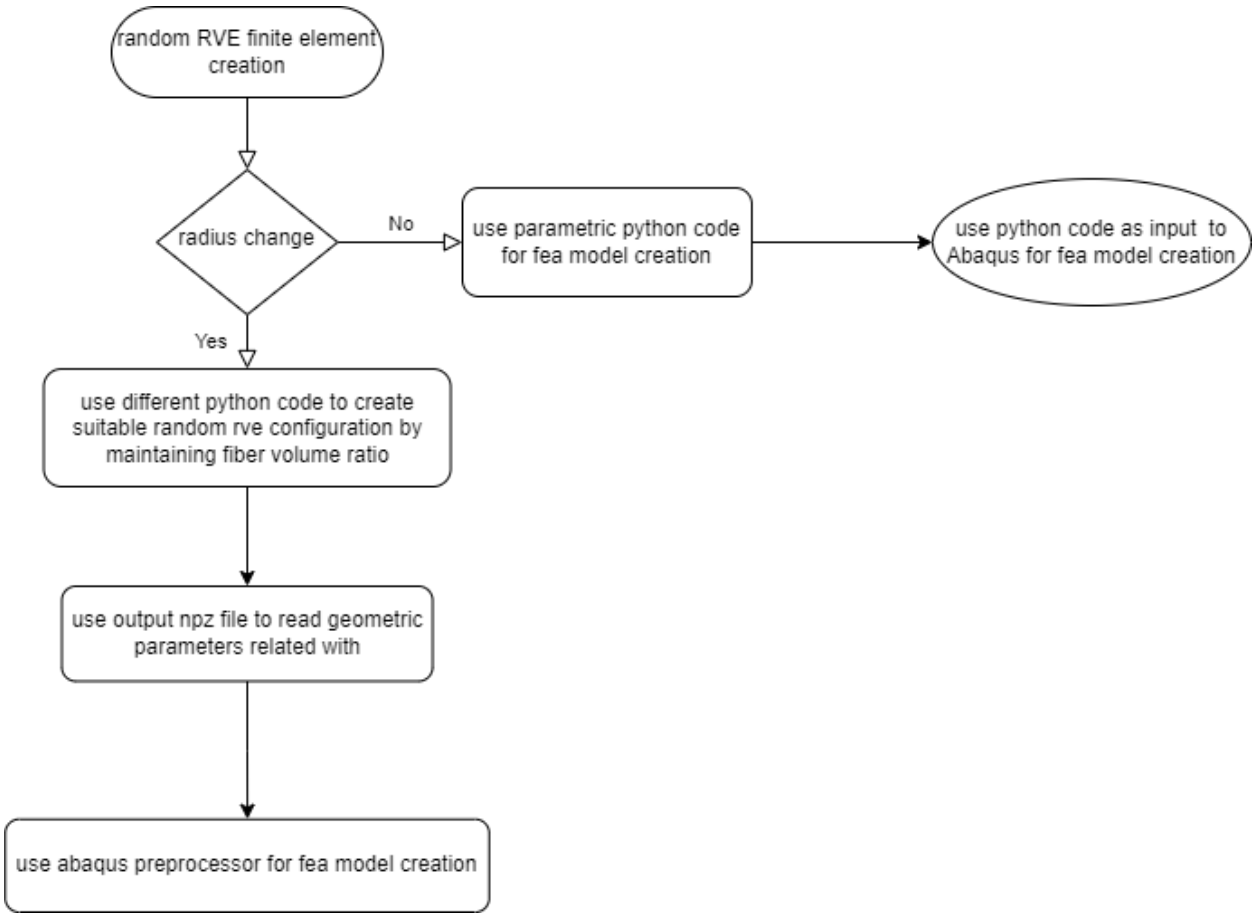

Figure 3.10 A flowchart to reveal random RVE creation.

3.1.2.1. Random Fiber Distribution Representative Volume Element

This random RVE model is used to see the effect of material change effect on Random RVE. Model created with the help of Python; parametric modeling achieved. A variety of different fiber arrangements with carbon and glass fiber materials are created. Fiber volume ratio is set as 0.6. and total number of elements is 24014. Maligno and periodic boundary conditions applied as BC's as explained in heading 3.2. Load is applied as displacement. A representation of model in terms of geometrical and meshed view can be seen in Figure 3.11 and Figure 3.12.

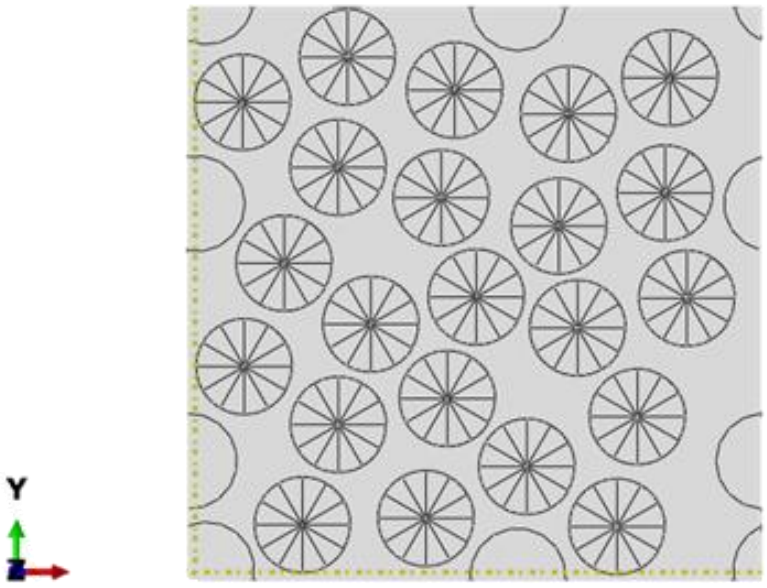

Figure 3.11 Geometrical representation of random RVE with constant fiber radius.

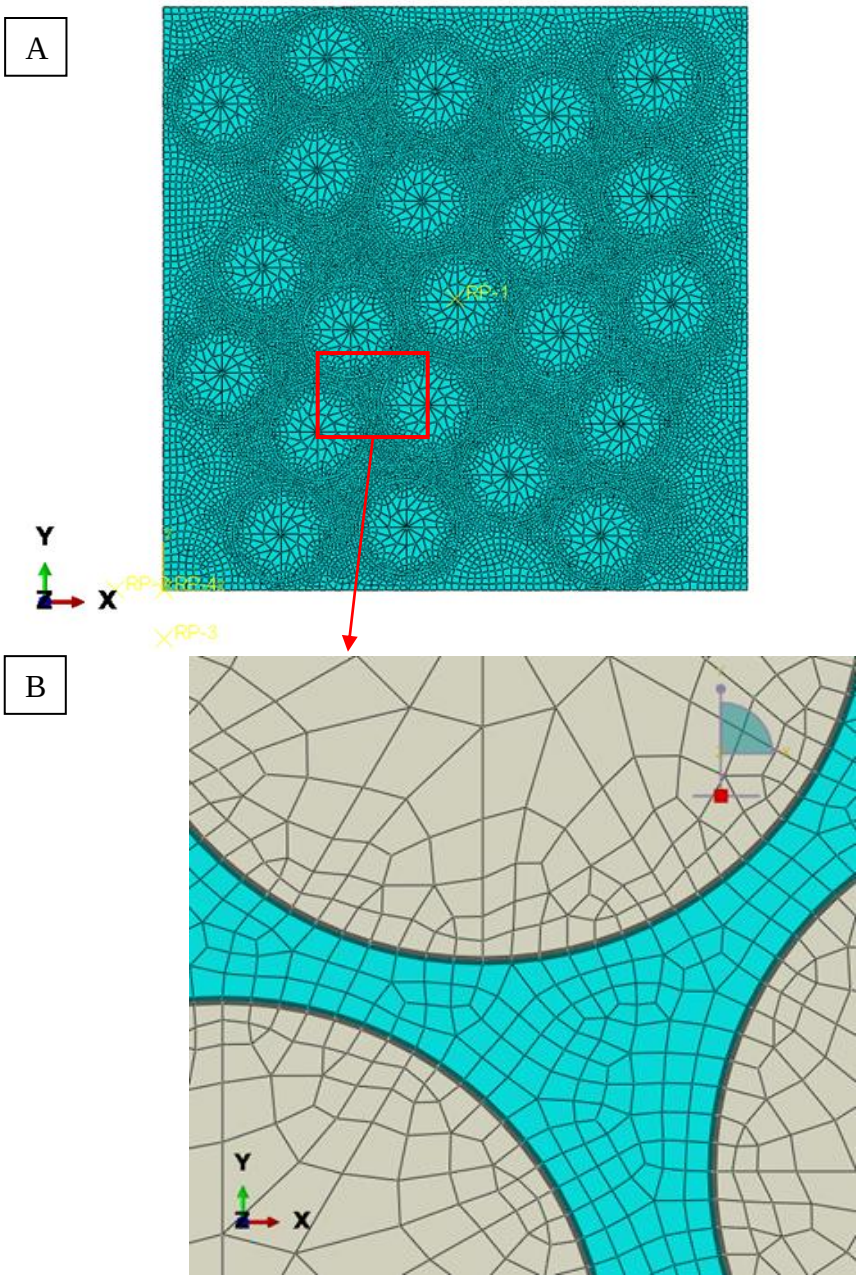

Figure 3.12 Meshed view of random RVE with constant fiber radius: (a) whole random RVE meshed view;(b) detailed view of fiber interface.

3.1.2.2. Random Fiber Distribution Representative Volume Element with Varying Fiber Radius

Random RVE with varying fiber radius model is explained under this heading. This random model is used to see the effect of variable fiber radius on stress distribution and concentration. Fiber radius values are set as 5 micrometers for glass and 3.5 micrometers for carbon. Also, these models are used to see combination of material and fiber radius effects. Model is created using Abaqus preprocessor. Input values for fiber geometry and fiber distribution are calculated by using Python script. Certain changes are made on Python script to maintain fiber volume ratio as 0.6, inter-fiber distance is set by regarding to settle appropriate value for substantiative amount of elements in interface region. Total number of elements is 83476. A representation of geometrical and meshed view can be seen in Figure 3.13 and Figure 3.14.

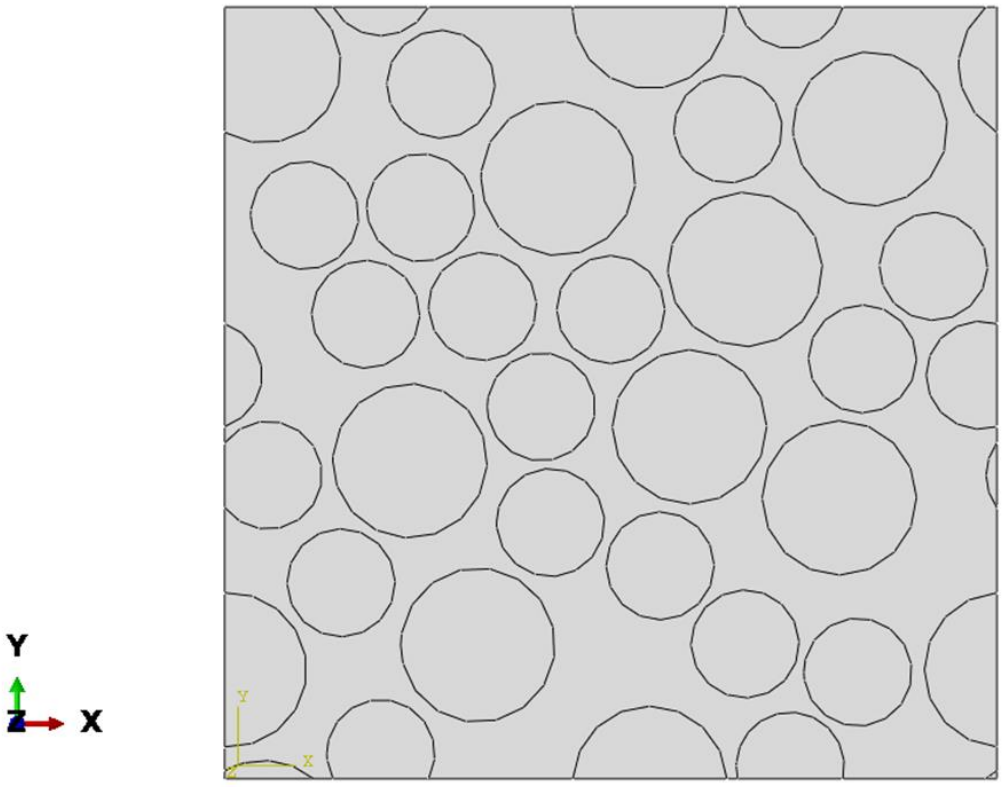

Figure 3.13 Geometrical representation of random RVE with varying fiber radius value.

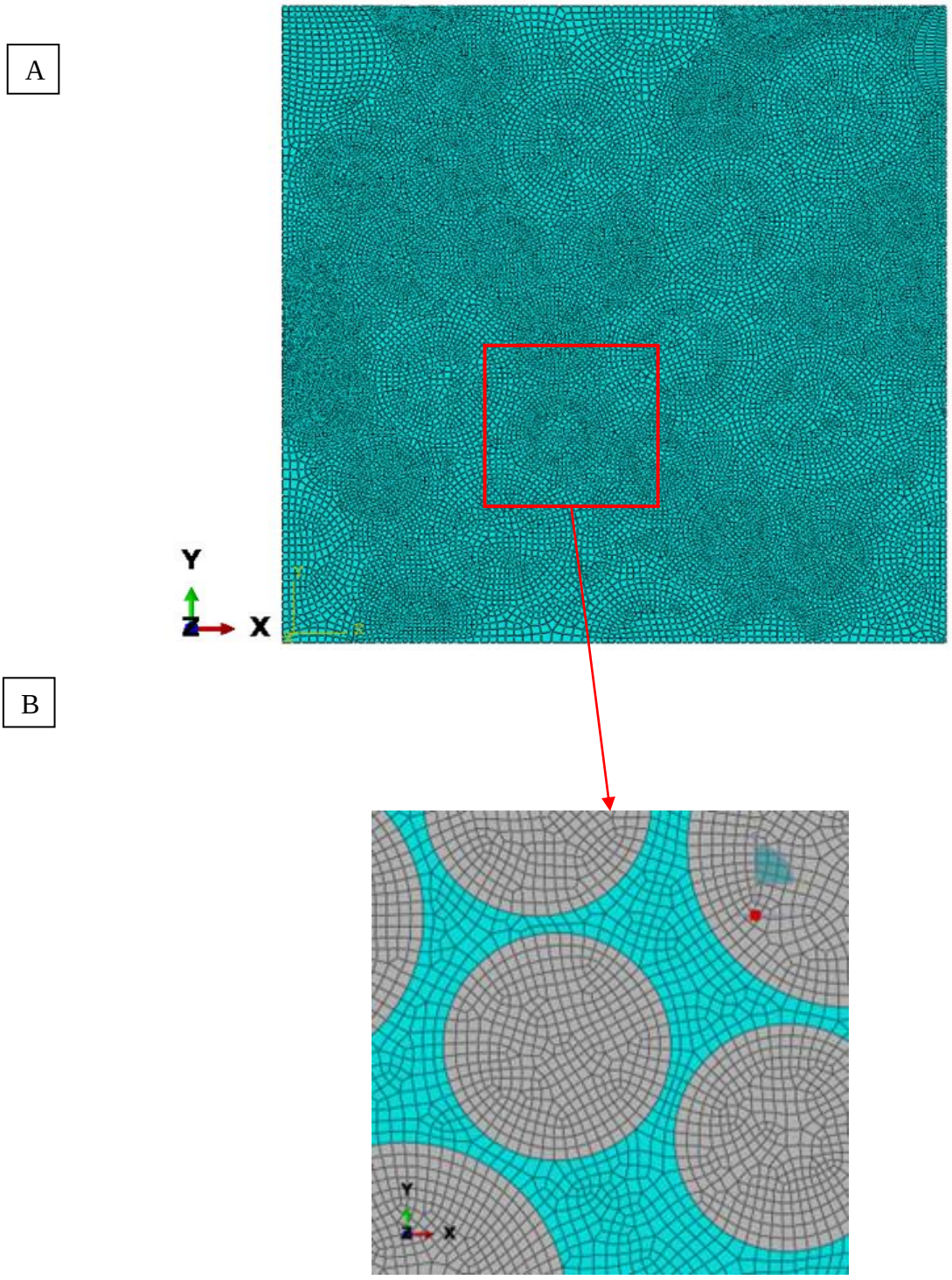

Figure 3.14 A meshed representation of random RVE with varying fiber radius: (a) a whole random RVE with varying fiber radius; (b) detailed view of interface region .

3.2. Boundary Conditions

An important point in finite element analysis modeling is employing correct boundary conditions to get realistic results which converge with experimental results and to evaluate real loading conditions better.

During finite element model creation stage of this thesis study, mostly two main boundary condition states are employed. These boundary conditions are periodic boundary conditions and Maligno boundary conditions.

Periodic boundary conditions (PBC);

In this thesis study, representative volume elements are employed by assuming these representative elements repeat themselves through the structure. This assumption requires creating an appropriate constraint through the intersection nodes with neighboring representative elements.

Nodes that have the same location coordinate value in y and z directions on each side of RVE (assuming x direction as surface normal, at left and right sides of RVE), bounded together by using tie constrain. By employing PBC, each side of RVE moves together and the results will have periodic structure

For periodic boundary condition applications following displacement procedures are employed.

$$u_i^{x+} - u_i^{x-} = \varepsilon_x (x_i^{x+} - x_i^{x-})$$
$$v_i^{y+} - v_i^{y-} = \varepsilon_y (y_i^{y+} - y_i^{y-})$$

In the equations given above u_i^{x+} and u_i^{x-} represents max and min displacement of each node in x direction. x coordinate locations of each node are represented with x x_i^{x+} and x_i^{x-}, v_i^{y+}ve v_i^{y-} represents max and min displacement of each node in y direction; y_i^{y+} and y_i^{y-}, represents node locations in terms of y coordinate; $\varepsilon_x$ve ε_y represents elongation values in x and y directions. Deformed shape when these boundary conditions employed are given in Figure 3.16.

Maligno Boundary Conditions;

Maligno [33] studied and employed these boundary conditions in his own studies. These boundary conditions are used to reveal the Poisson's contraction effect as allowing the structure to extend in one direction but creating a contraction effect on the other direction. In general, a translational constraint is applied to nodes on each surface in the surface's normal direction, and nodes on opposite surface are bounded together with tie constraint. Regarding this boundary condition, nodes on back surface of representative volume element are constrained in z-direction by setting displacement in z direction is as zero. Nodes on the front surface are bounded with tie constraint to move together. Nodes on lower surface of representative volume element are constrained in y direction by applying zero displacement in y direction. On the contrary, nodes on opposite surface (upper surface) are tied together to move as a whole surface. Nodes on side surface of representative volume element are constrained as zero. A representation of Maligno BC's can be seen in Figure 3.15.

Load Application.

Load is applied to the side surface (opposite of the constrained surface) whose surface normal is in x direction, as displacement in transverse direction (in x direction).A FEM model representation of boundary conditions can be seen in Figure 3.16.

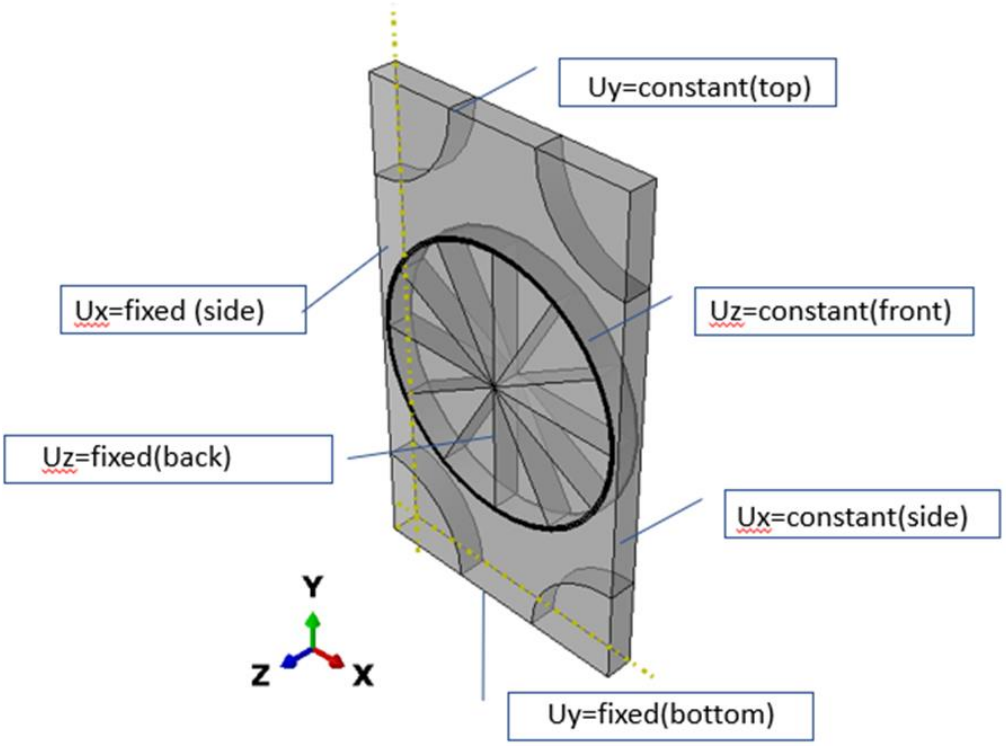

Figure 3.15 Representation of Maligno BC's.

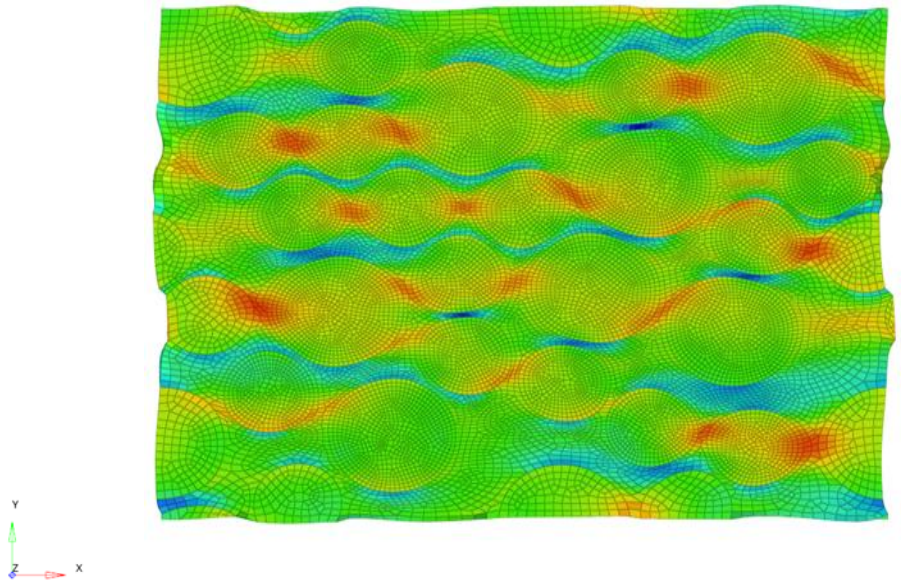

Figure 3.16 Representation of all PBC's on deformed fem.

Exceptionally for the angled and triple hex RVE models, periodic boundary conditions are not applied to the structure. Main aim of the angled part is to reveal load localization in stiffer regions . For the triple hex model, periodic boundary conditions are not needed since two neighboring elements are also modeled. A representative view of boundary conditions applied on triple Hex model can be seen in Figure 3.17 and a representation of angled model boundary conditions can be seen in Figure 3.18

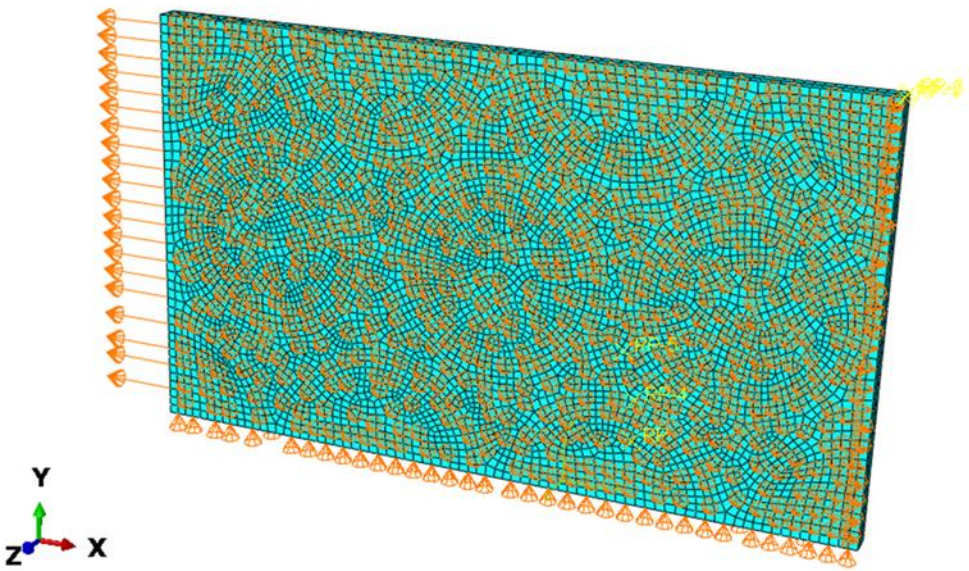

Figure 3.17 Triple hex RVE BC's representation.

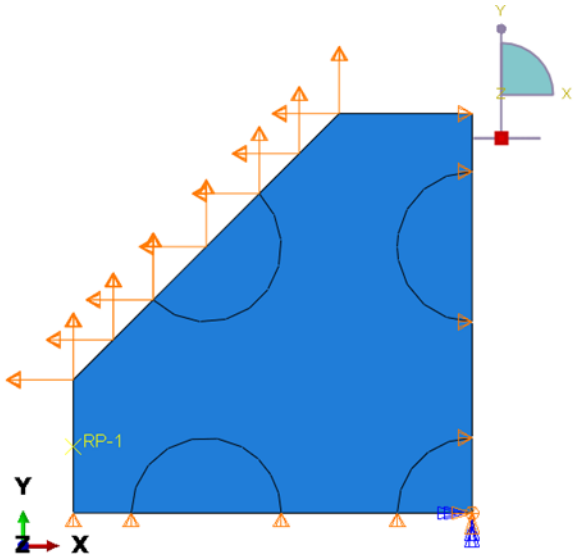

Figure 3.18 Angled square RVE BC's representation.

3.3. Results & Data Analysis Method

FEA models created using Python and Abaqus pre-process are run and solved with the help of Abaqus solver stated within Abaqus program.

For each model, average strain value and average stress value are taken as output data. Stress values extracted at the interface around center fiber in each model by tracking a path. A demonstration of path can be seen in Figure 3.19.

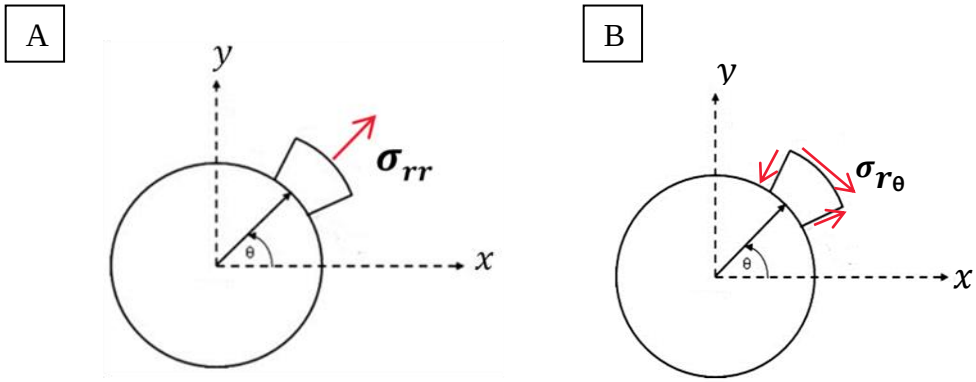

Figure 3.19 Stress extraction path representation: plot (a) radial(normal) distribution representation; (b) tangential(shear) distribution representation.

These values are used as input to Mathcad. Each stress value is normalized by dividing with average values and stress concentration value around the center fiber calculated.
Stress concentration values are calculated by based on the following mathematical equations.

$$K_{RR} = \frac{\sigma_{RR}}{\sigma_{avex}} \quad \textbf{(4)}$$

$$K_{R\theta} = \frac{\sigma_{R\theta}}{\sigma_{avex}} \quad \textbf{(5)}$$

Where K_{RR} represents the normal stress concentrations and $K_{R\Theta}$ represents the shear stress ones. σ_{avex} represents average stress value. On the other hand, Abaqus .odb files are used as an input to the Hyperview program to draw contour plots of stress distribution concentration on matrix.

In results section within the study radial stress distribution K_{RR} and $K_{R\theta}$ values will be demonstrated as S_norm in stress concentration plots and tables. Same stress concentration calculation procedure employed, only representation of concentration value differs in plots as S_norm .

3.4. Studied Parameters

Before starting to study on the subject, with the help of literature survey, parameters that are subjected to lower amount of studies than others, are selected to work on within the scope of this thesis study. Parameters that are selected to work on this study are given in Table 3.3.

Table 3.3 Overall representation of studied parameters

Parameter	Hex RVE	Random RVE
Fiber material effect		
Homogenous glass fiber	✓	✓
Homogenous carbon fiber	✓	✓
Center glass fiber	✓	✓
Center carbon fiber	✓	✓
Fiber volume ratio effect		
Vf=0.6	✓	✓
Vf=0.4	✓	✓
Fiber radius effect		
Without material effect by protecting fiber volume ratio	✓	✓
With material effect by protecting fiber volume ratio	✓	✓
RVE shape change(90 degree turned)	✓	
Shear loading	✓	

4. RESULTS AND EVALUATIONS

4.1. Hexagonal RVE

4.1.1. General Information about HEX RVE Modeling & Results

In this section, results of the studies which are made with a variety of Hex RVE models have been revealed. In each section, normalized stress concentration plots and contour graphs are represented. In all of the studies represented here, stress concentration around center fiber is employed, fiber configurations for each model given within the symbolic representation of each plot.

Homogenous hex RVE with glass and carbon fiber comparison is given in this section. The normalized stress concentration plot can be seen in Figure 4.1 plot (c), and contour plot for each configuration can be seen in Figure 4.1 plot (a) and plot (b). In general, load carried by glass fiber under transverse loading is higher(modulus of glass in transverse direction is higher than that of the carbon) and this situation creates higher amount of concentration on 0 and 180 degree around fiber.

These homogenous RVE results will be used as a control group to compare with each hybrid composite analysis result.

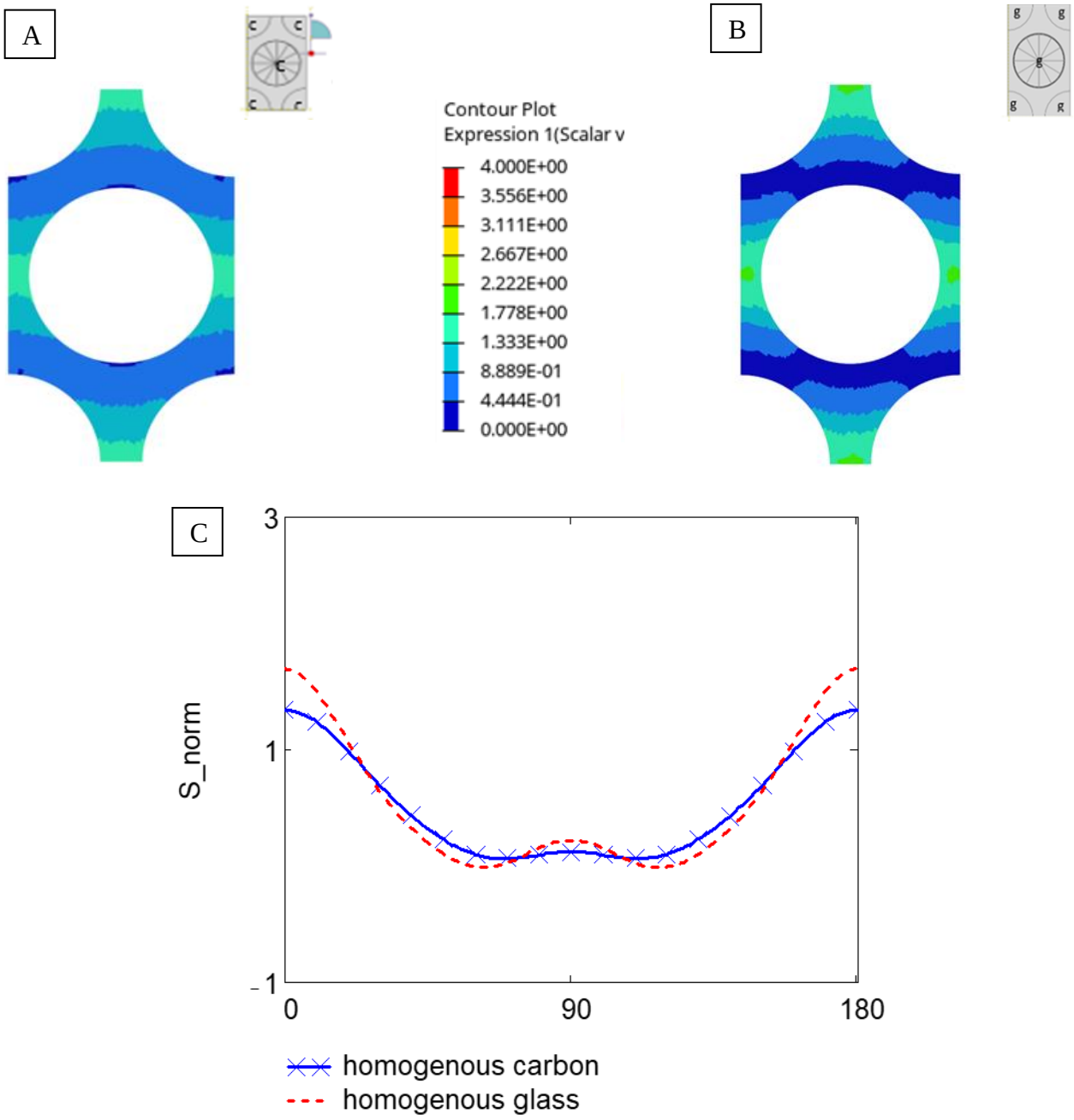

Figure 4.1 Hexagonal RVE homogenous fiber and glass composite materials results: (a) homogenous carbon stress concentration contour graph; (b) homogenous glass stress concentration contour graph; (c) normalized stress concentration plot.

4.1.2. Material Effect

In order to see the material effect, stress concentrations around the central fiber/matrix interface results and the contour plots for normalized stress distribution are shown in Figure 4.2 plot a and Figure 4.3. Plot a. Stress concentration distribution plots are shown in in Figure 4.2 plot b and Figure 4.3 plot b. Figure 4.3 plots a and b were drawn to show the hybridization effect with center fiber carbon and Figure 4.2 with center fiber glass. Fiber materials were assigned as stated in representative RVEs.

From these results, it can be observed that the presence of glass fiber decreases the amount of stress concentration around (carbon) fiber by taking up the load on the carbon fiber as it has a higher stiffness value in the transverse direction. According to Figure 4.3, the opposite situation takes place when carbon fibers are present around the glass fiber. The stress concentrations around the glass fiber increased considerably due to carbon fibers around them. These carbon fibers have less stiffness in the transverse direction, causing the central glass fiber to carry more load than the case when it is surrounded by the same glass fibers.

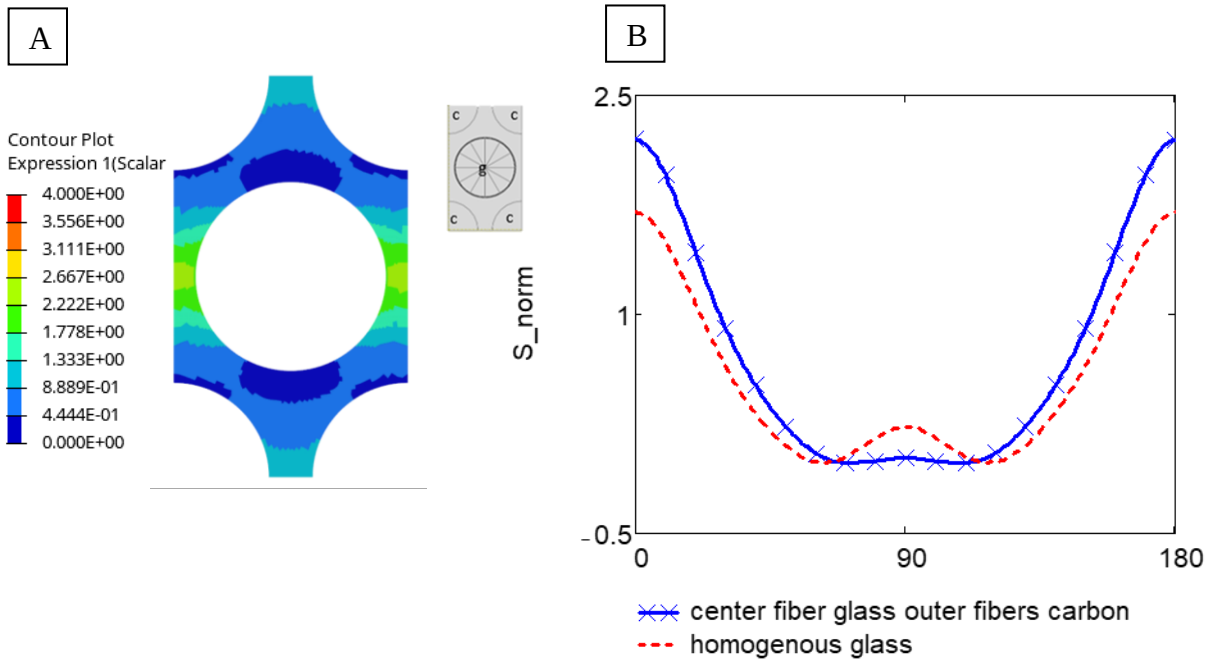

Figure 4.2 Hexagonal RVE center glass fiber hybrid composite results: (a) center fiber glass stress concentration contour graph; (b) normalized stress concentration plot.

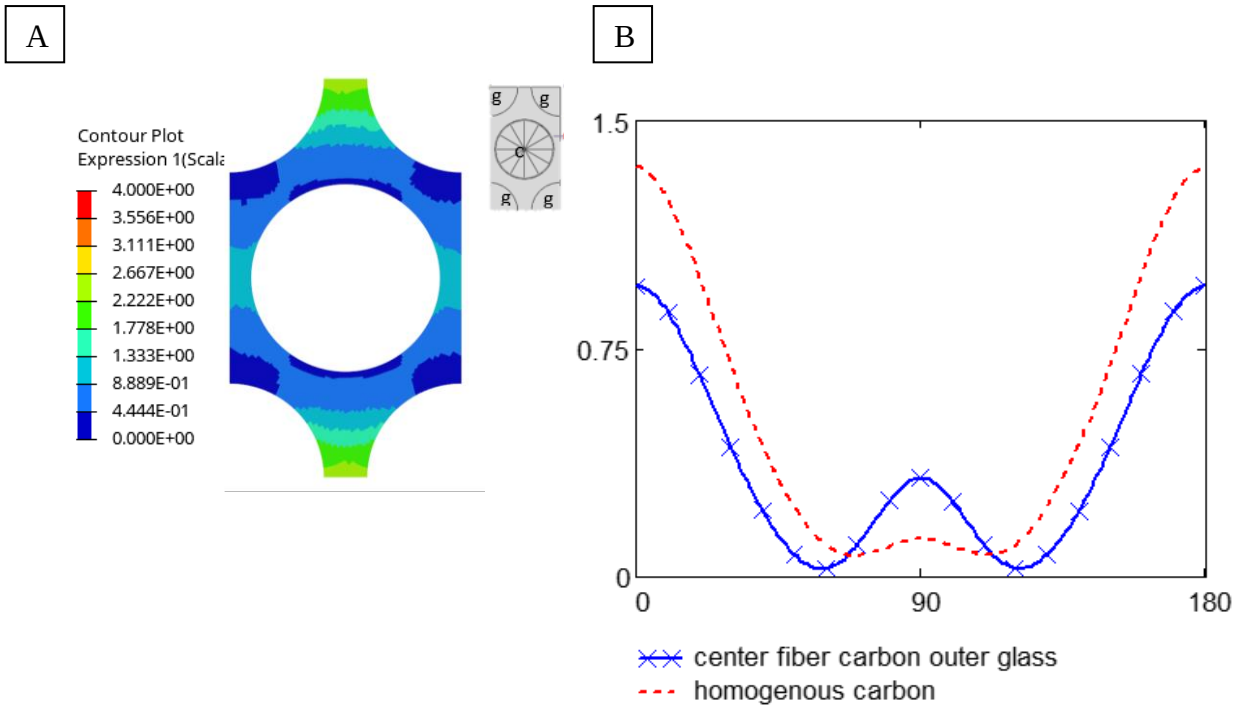

Figure 4.3 Hexagonal RVE center carbon fiber hybrid composite results: (a) center fiber carbon stress concentration contour graph; (b) normalized stress concentration plot.

Comparing the distribution results of the hybrid composite models with homogenous models in Figure 4.2 and Figure 4.3, higher stresses are observed between the corner fibers. In addition, we can easily observe the decrease in stresses around the central fiber. Comparing the distribution in in Figure 4.2 and Figure 4.3 when the corner glass fibers are replaced by carbon fibers, a significant increase in the stresses is observed near the central fiber (especially when theta=0 and 180). Also, the stresses between the corner fibers were decreased. As the corner fibers are replaced by less stiff carbon fibers, central fiber must carry more load to compensate for the lack of stiffness. Therefore, these findings are in accordance with the findings of in Figure 4.2.

4.1.3. Fiber Volume Effect

In order to observe the effect of fiber volume ratio, graphs and plots are obtained for $vf = 0.4$ and $vf = 0.6$. Results are shown in Figure 4.4 for homogenous RVE , Figure 4.5 for center fiber glass and Figure 4.6 for center fiber carbon. For a detailed analysis, maximum SC values are depicted in Table 4.1.

A

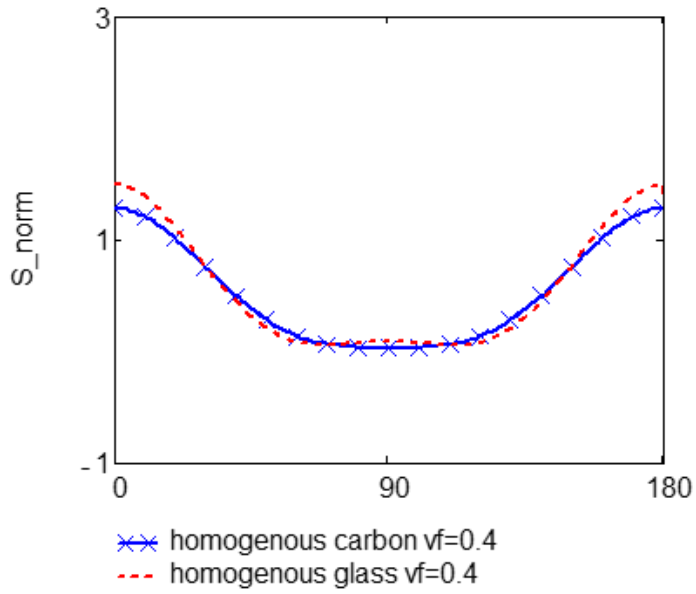

B

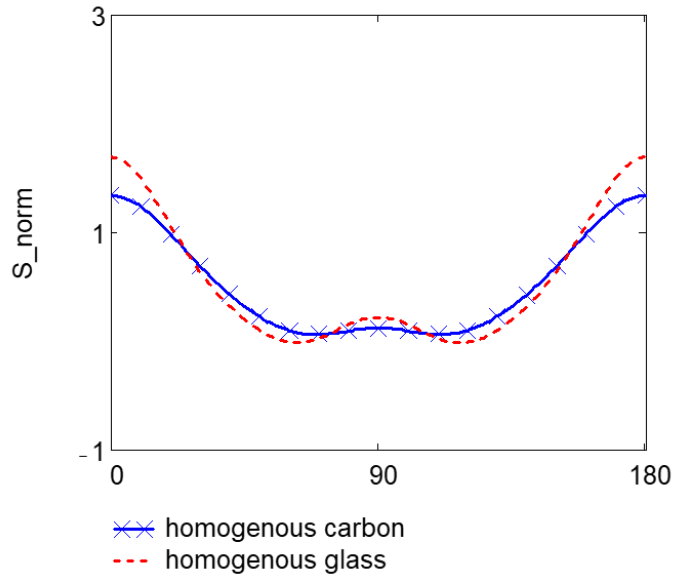

Figure 4.4 Hexagonal RVE homogenous composite results: (a) fiber volume ratio 0.4 normalized stress concentration plot; (b) fiber volume ratio 0.6 normalized stress concentration plot.

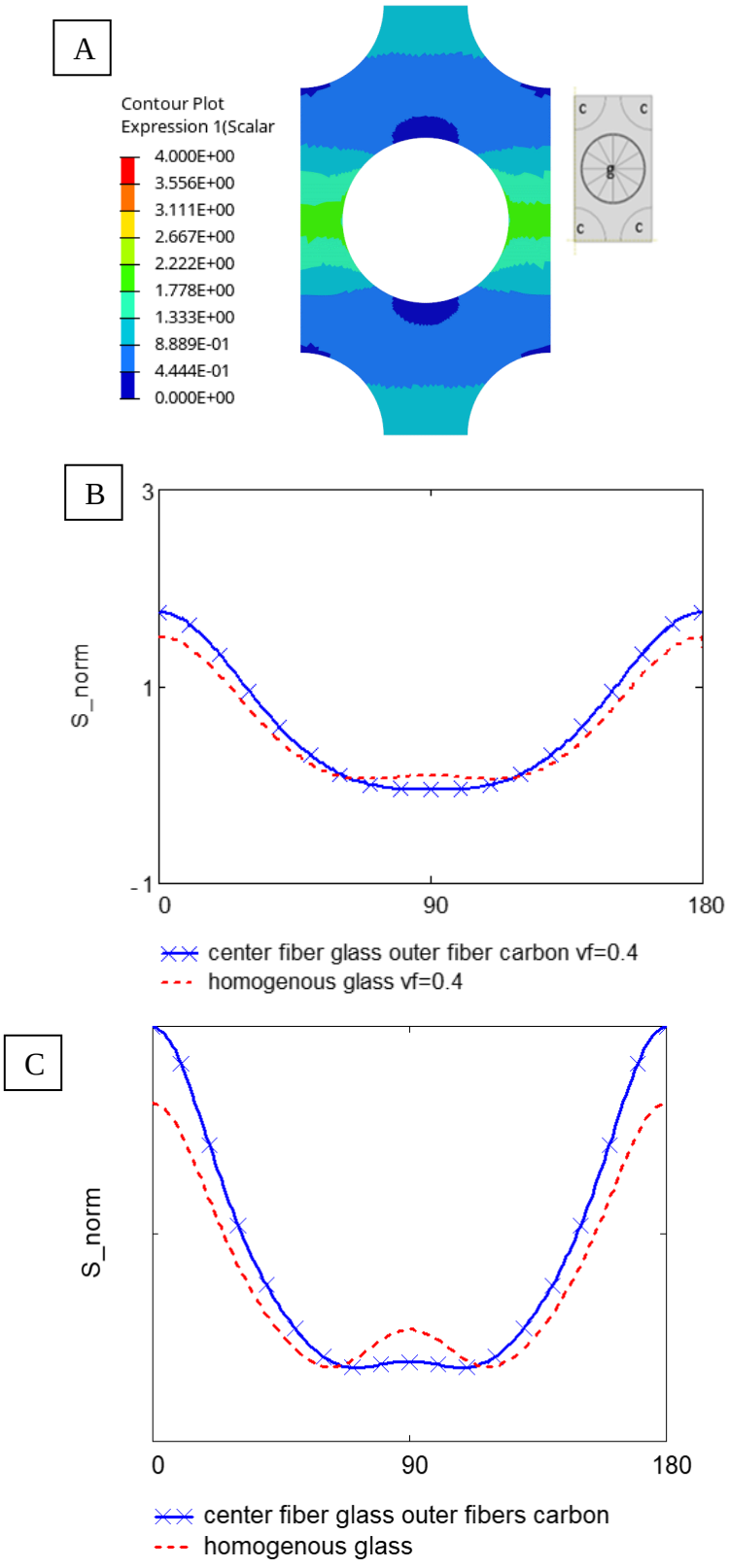

Figure 4.5 Hexagonal RVE hybrid composite results with glass center fiber: (a) carbon center fiber,

fiber volume ratio 0.4 contour graph (b) fiber volume ratio 0.4 homogenous hexagonal RVE normalized stress concentration plot; (c) fiber volume ratio 0.6 normalized stress concentration plot.

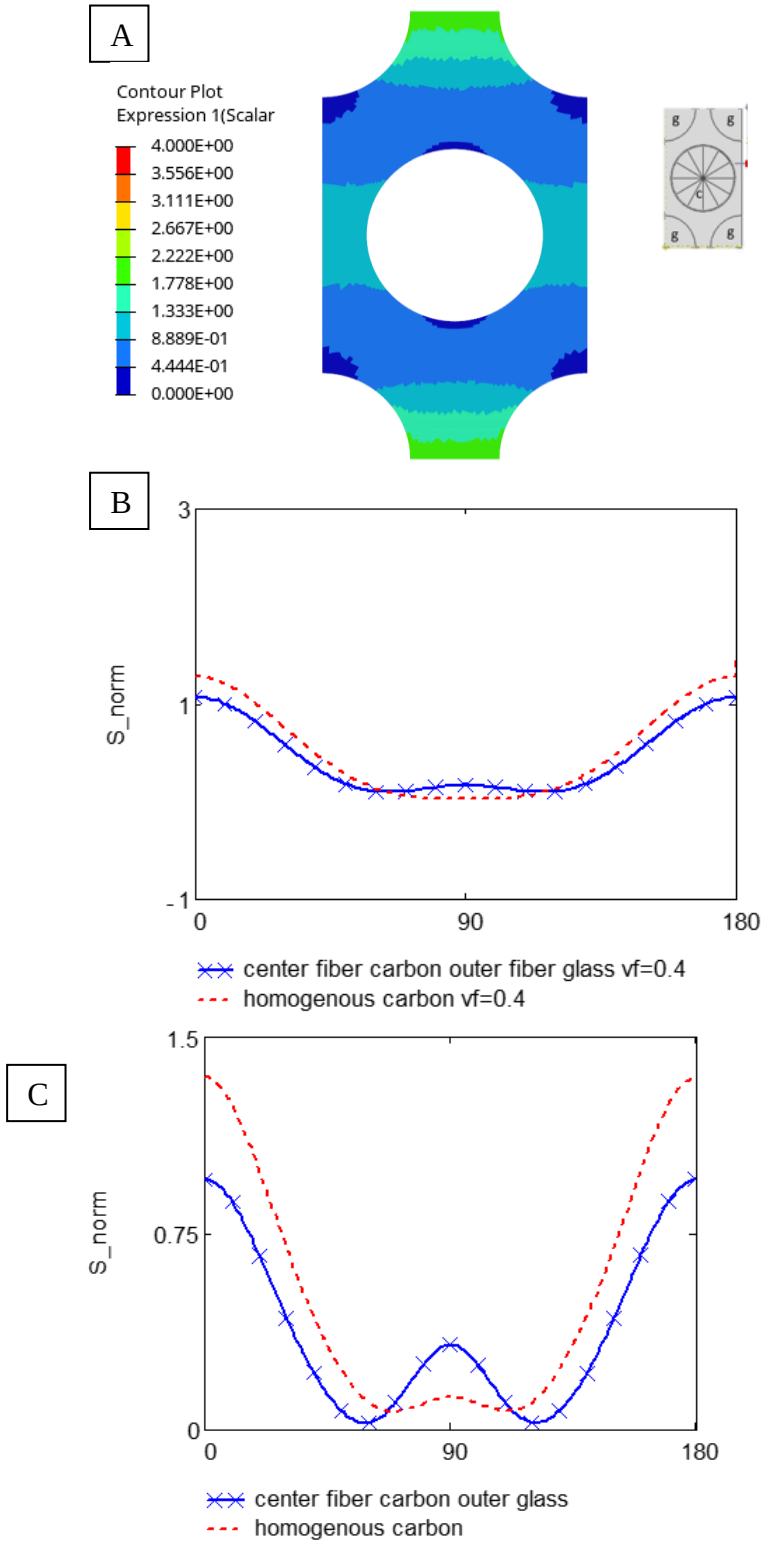

Figure 4.6 Hexagonal RVE hybrid composite results with carbon center fiber: (a) glass center fiber, fiber volume ratio 0.4 contour graph (b) fiber volume ratio 0.4 homogenous hexagonal RVE normalized stress concentration plot; (c) fiber volume ratio 0.6 normalized stress concentration plot.

Regarding results stated in Figure 4.4, Figure 4.5 and Figure 4.6 it is observed that stress distributions show similar behavior with the models constructed with higher fiber volume ratio, but the difference is stress concentration becomes higher when the fiber volume ratio increases as expected in accordance to the findings in [25] . Also, comparison results can be seen in Table 4.1.

Table 4.1 S_norm values of vf=0.4 and vf=0.6

	All carbon (Homogenous RVE)	Inner carbon (Hybrid RVE)	Ratio	All glass (Homogenous RVE)	Inner glass (Hybrid RVE)	Ratio
Vf=0.4	1.285	1.069	1.202	1.503	1.755	0.856
Vf=0.6	1.347	0.955	1.41	1.697	2.193	0.774

For the RVE in which the fiber volume ratio is 0.4, the hybridization effect can be seen clearly regarding stress concentration values stated in Table 4.1. For the RVE constructed with carbon fiber and inner carbon fiber with $vf = 0.4$, stress concentration around central fiber is found as 1.285 for homogenous RVE and 1.069 for hybrid RVE, and the ratio of these concentration values is found as 1.202. On the other hand, the ratio of the stress concentration values for the RVE constructed with $vf = 0.6$ is found as 1.41. Comparing these values, it can be stated that the hybridization effect increases as the fiber volume ratio increases. The same situation can be observed by comparing RVE constructed with glass fiber and inner glass fiber. As the corner fibers are changed with carbon fibers, the load carried by the central fiber increases. On the contrary, stress concentration value around central fiber is found as 1.755 for $vf = 0.4$ and 2.193 for $vf = 0.6$, and these results can be explained by the situation stated as ‘hybridization effect increases with increased fiber volume ratio.

4.1.4. RVE Loading Side Change Effect

In order to see the effect of loading side on the stress concentration, RVE is rotated and while keeping the load in horizontal direction. Model configurations are shown in representative RVEs. Loading direction, Stress concentration results are given in Figure4.7 for center fiber carbon and Figure 4.8 for center fiber glass.

A

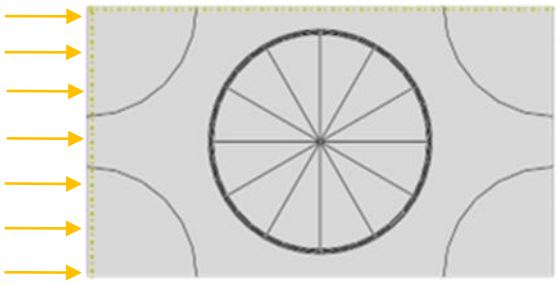

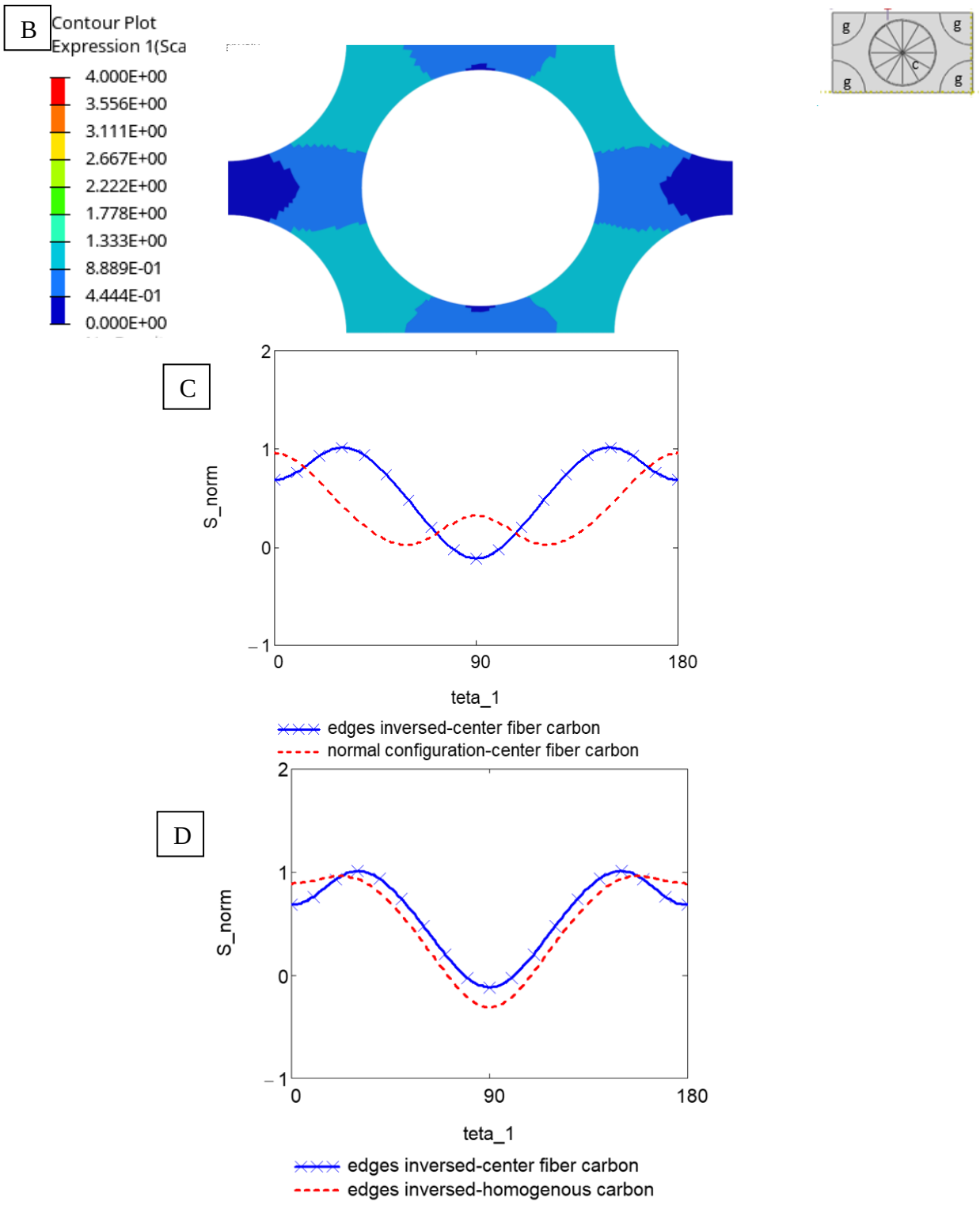

Figure4.7 Hexagonal RVE edge change hybrid composite results with carbon center fiber:(a) loading direction representation; (b) edges inversed, center fiber carbon stress concentration contour graph; (c) center fiber carbon, edge changed, and normal configuration stress concentration; plot (d) center fiber carbon, edge changed homogenous and hybrid normalized stress concentration plots.

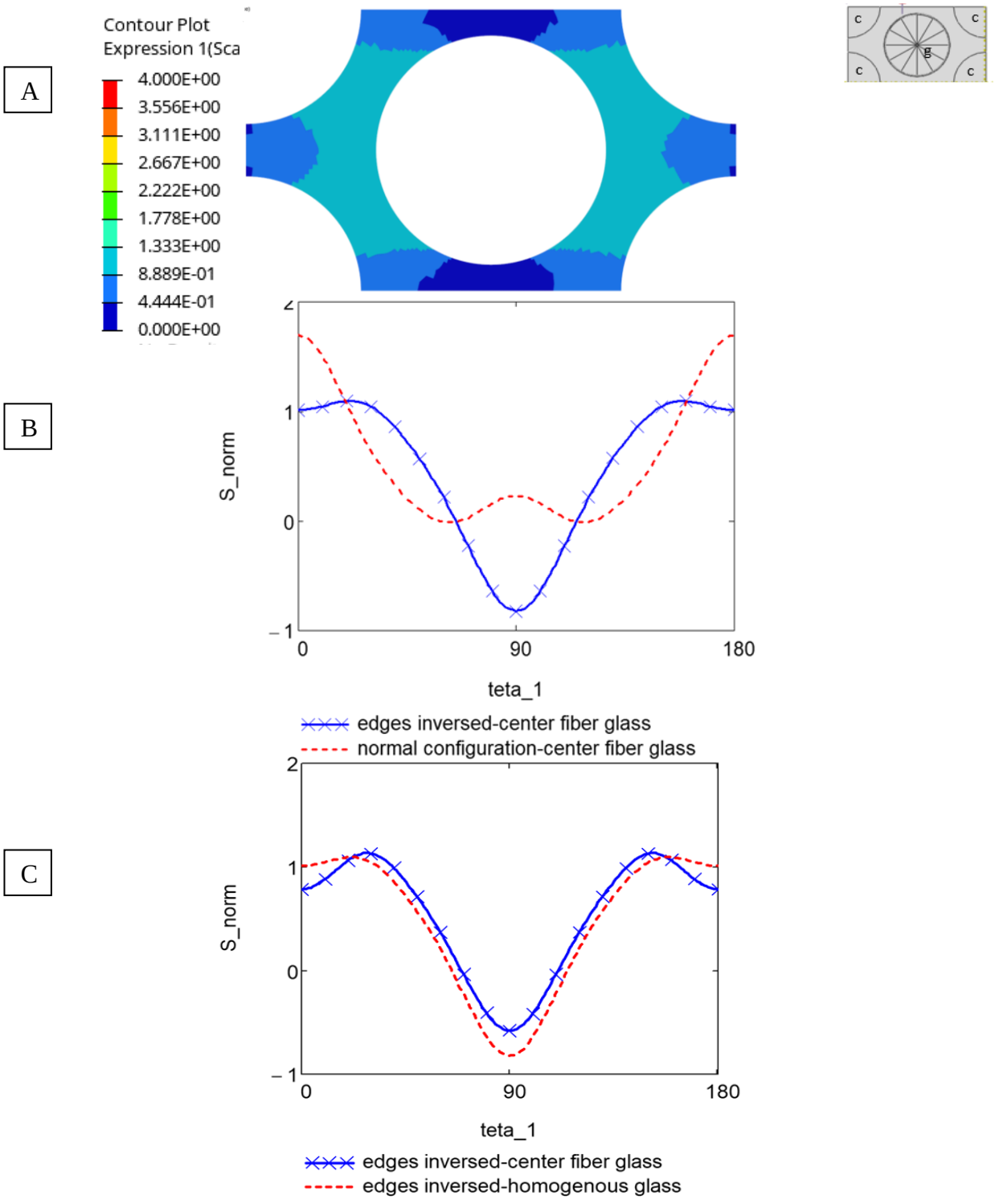

Figure 4.8 Hexagonal RVE edge change hybrid composite results with glass center fiber: (a) edges inversed, center fiber glass stress concentration contour graph; plot (b) center fiber glass, edge changed, and normal configuration stress concentration; plot (c) center fiber glass, edge changed homogenous and hybrid normalized stress concentration plots

Table 4.2 S_norm values of rotated and regular RVE

	All carbon	Inner carbon	Ratio	All glass	Inner glass	Ratio
Regular RVE	1.347	0.955	1.41	1.697	2.193	0.774
Rotated RVE	0.887	0.682	1.3	0.787	1.013	0.776

Rotated and regular type RVEs, results can be found in Table 4.2 . For rotated RVE, maximum stress concentration value for hybrid RVEs is found as 0.682 with inner fiber modeled as carbon and 1.013 with inner fiber modeled as glass. Hybridization effect can be observed as stress concentration around central fiber decreases in RVE with inner carbon outer glass fiber. Also, regarding RVE constructed with all glass fibers and inner glass outer carbon fiber, load carried with central fiber increases as the hybridization effect takes place. On the contrary, ratio values for both regular and rotated RVEs with all carbon fibers and inner carbon outer glass fiber are calculated as 1.41 and 1.3, respectively and with all glass and inner glass outer carbon fiber, calculated as 0.774 and 0.776, respectively. Regarding these ratio values, it can be stated that the stiffness of RVEs in loading direction has an important effect. In the rotated RVE, there is more matrix material in the loading direction. This provides the stresses to distribute in the matrix more evenly. Thus, the stress concentrations decrease together with the decrease of the hybridization effect. This shows that the direction of loading also affects the concentrations.

4.1.5. Fiber Radius Effect

Generally, glass fibers are manufactured with a larger radius than carbon fibers. In this section, the effect of different fiber radii on stress concentration is investigated. Stress concentration results are shown in Figure 4.9 and Figure 4.10 are shown using homogenous results as the control group, where RVE was generated by setting all fibers with a 5 micrometer radius and with 3.5 micrometer radius. Effect of hybridization was studied by comparing hybridized RVE results with these. In all of the homogenous RVEs, stiffness of all fibers are set same in order to prevent the contribution of stiffness. The radii of some of the fibers in the RVE are changed, and the RVE size is adjusted to keep the fiber volume ratio constant. According to Figure 4.9 plot b, it can be stated that with a smaller fiber radius at the center, the stress concentrations decrease around the fiber/matrix interface of this fiber. This shows a positive hybridization effect when smaller fibers are surrounded by larger fibers. The opposite is valid from the observation of Figure 4.10. When a large fiber is surrounded by relatively smaller fibers, the stress concentration around the larger fiber decreases even with the same fiber volume ratio. This is an expected result. Smaller fibers take up less load, and larger fibers become responsible to carry the stresses due to the lack of material.

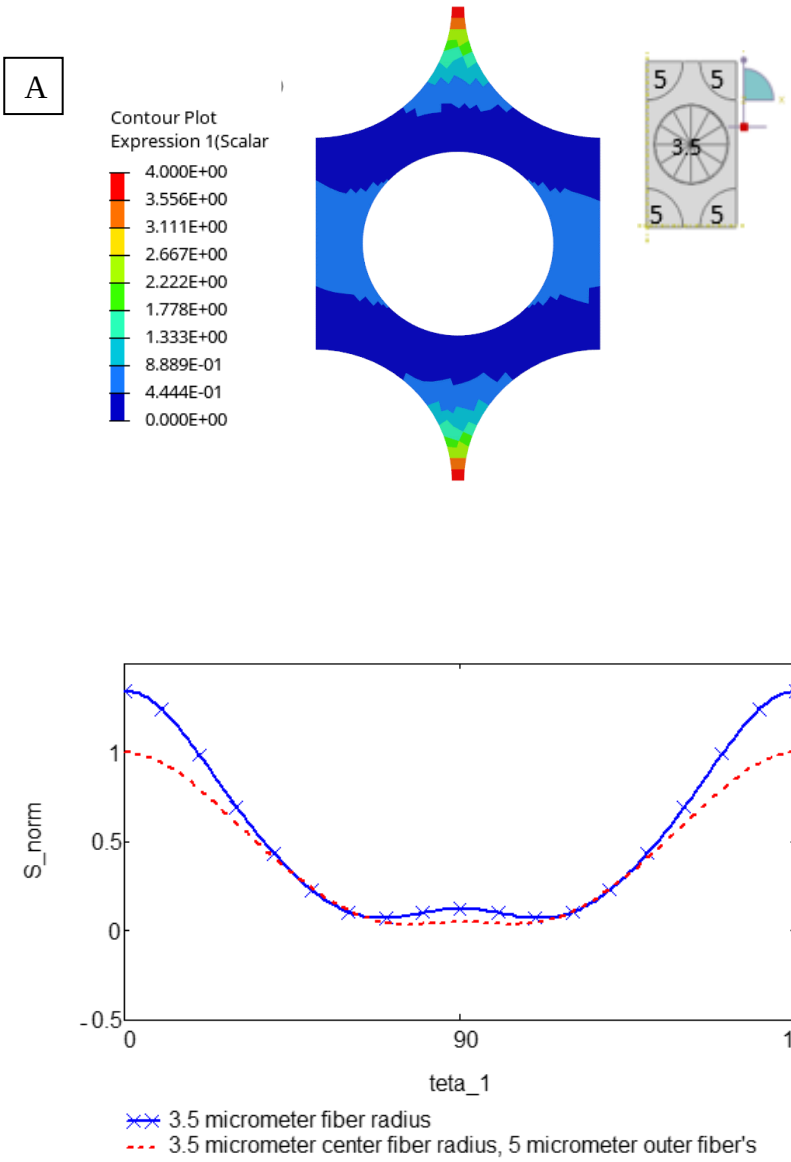

Figure 4.9 Stress concentration distribution:(a) contour plot regarding different radius values as center fiber r=3.5micrometer and outer fiber r=5micrometer;(b) comparison of normalized stress concentration plots with RVE's all radius values are r=3.5micrometer and inner radius value is 3.5micrometer outer radius value is 5 micrometer.

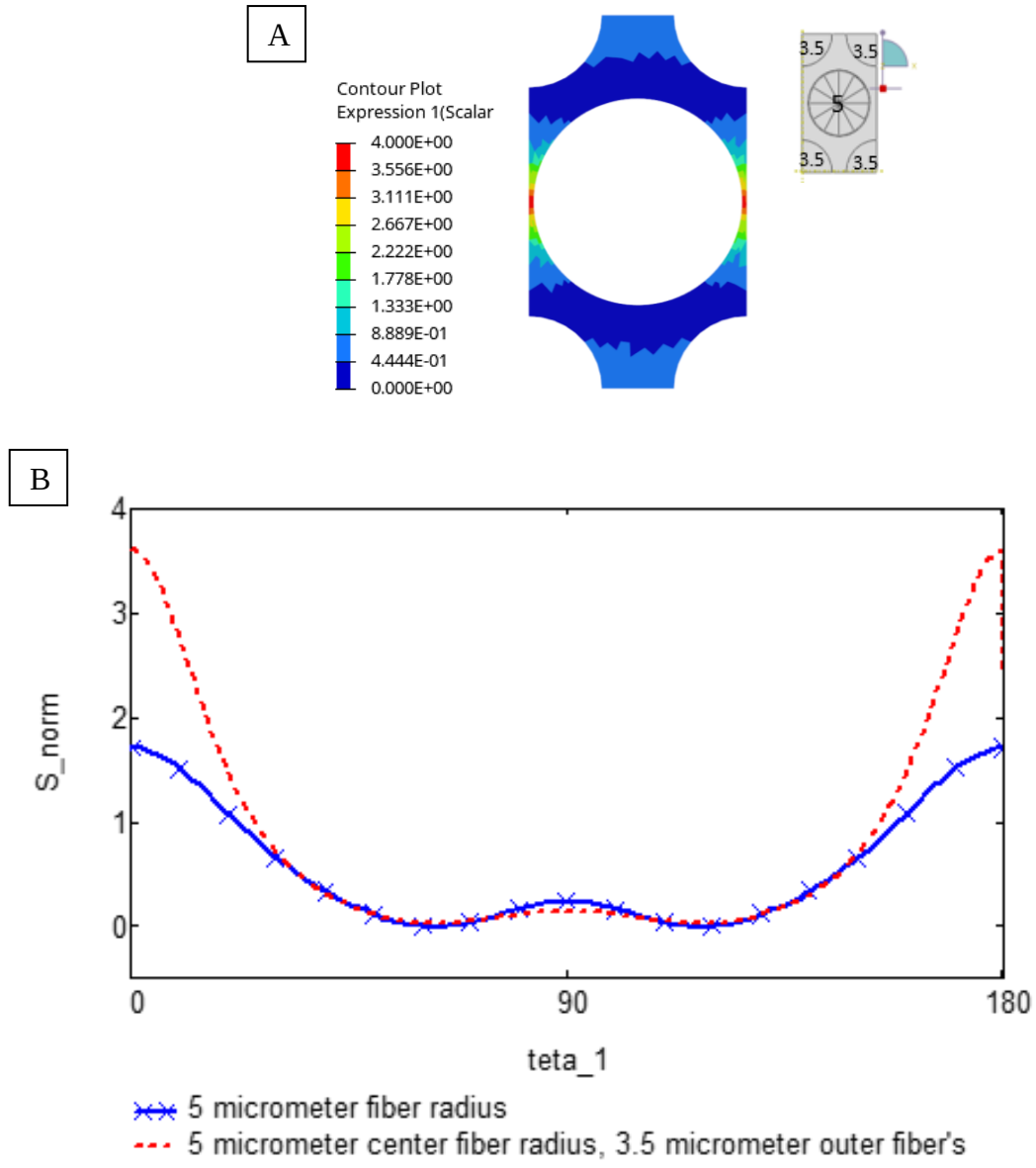

Figure 4.10 Stress concentration distribution:(a) contour plot regarding different radius values as center fiber r= 5micrometer and outer fiber r=3.5micrometer;(b) comparison of normalized stress concentration plots with RVE's all radius values are r=5micrometer and inner radius value is 5micrometer outer radius value is 3.5 micrometer.

Stress concentration distribution on matrix can be seen in Figure 4.9 plot b and Figure 4.10 plot b. stress concentration at 0 and 180 degrees is lower in Figure 4.9 b than in Figure 4.10 figure b. As matrix material is very small in this region, they need to stretch more to compensate for the transverse load. Similar behavior can be seen between the corner fibers for the model having the smaller fiber at the center.

4.1.6. Fiber Radius and Material Combined Effect

In order to study these effects, 4 different analysis results are compared by dividing them wrt center fiber radii. These RVE's constructed by keeping fiber volume ratio fixed as $vf = 0.6$. Graphs that are drawn for these analyses and plots used as control group can be seen in Figure 4.1. Each case is designated with a letter which can be seen in Table 4.3 and Table 4.4. Results for different combinations are shown in Figure 4.11-Figure 4.14

Table 4.3 S_norm values for varying fiber radius p1

	All carbon r=3.5	Inner carbon, outer glass r=3.5	All carbon r=3.5, outer r=5	Inner carbon, r=3.5, outer glass r=5
Max. Stress Concentration	1.347	0.955	1	0.406(A)
Ratio to All carbon	1	1.41	1.347	3.318

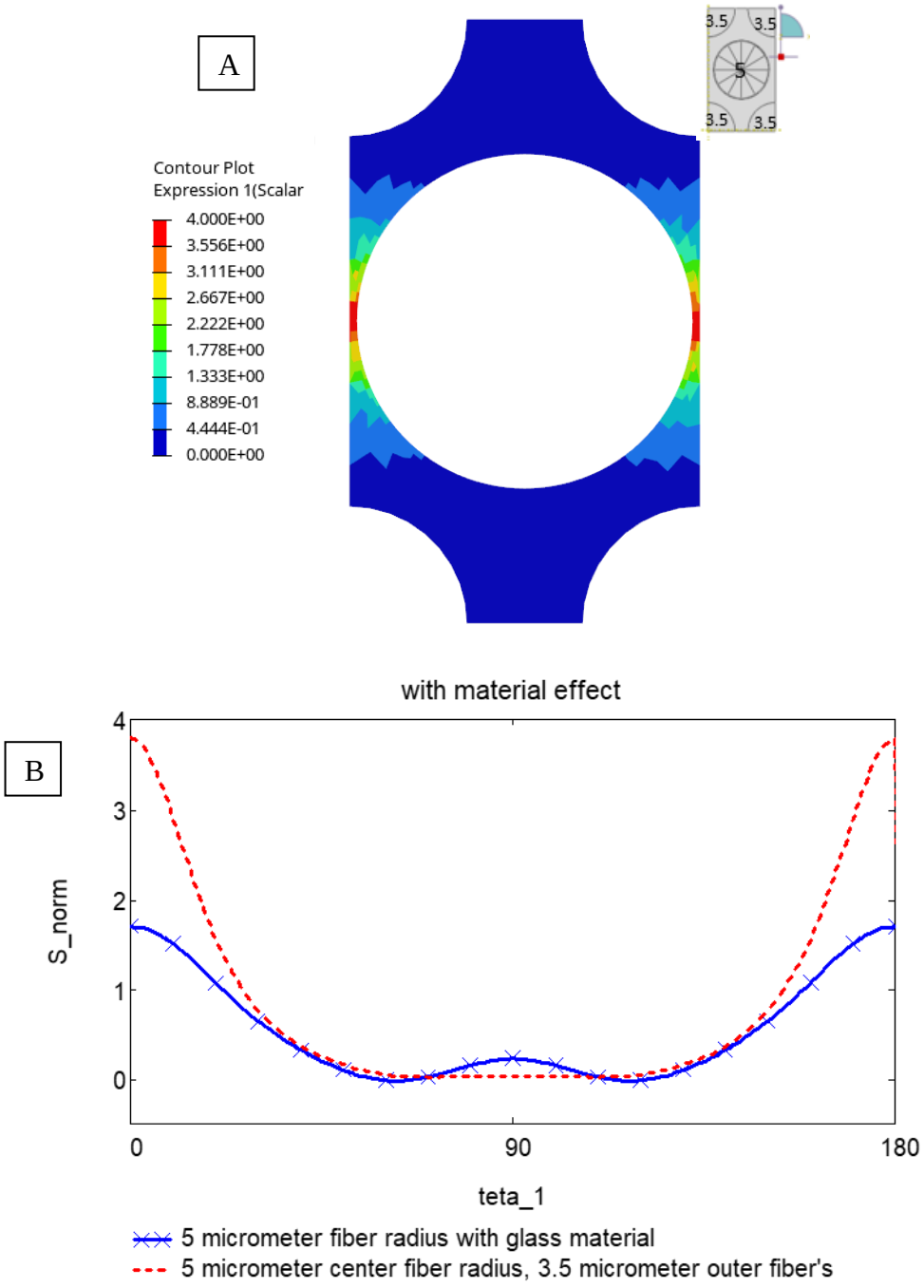

Figure 4.11 Stress concentration distribution with material effect :(a) contour plot regarding different radius values as center fiber r= 5micrometer&glass material and outer fiber r=3.5micrometer& carbon material ;(b) comparison of normalized stress concentration plots with RVE's properties are all fibers with r=5micrometer&glass, and inner radius value is 5 micrometer& glass outer radius value is 3.5 micrometer&carbon.

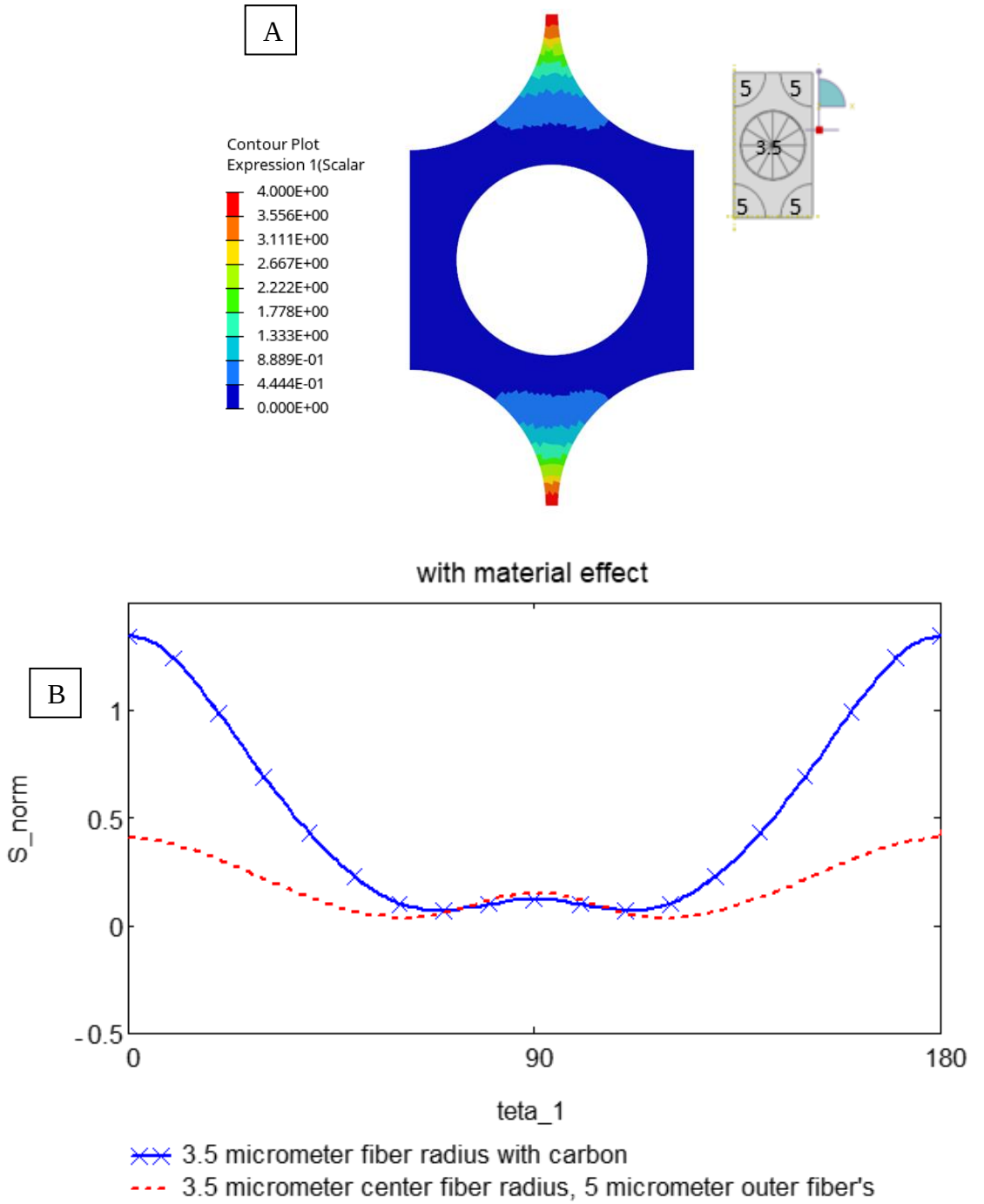

Figure 4.12 Stress concentration distribution with material effect :(a) contour plot regarding different radius values as center fiber r= 5micrometer&glass material and outer fiber r=3.5micrometer& carbon material ;(b) comparison of normalized stress concentration plots with RVE's properties are all fibers with r=5micrometer&glass, and inner radius value is 5 micrometer& glass outer radius value is 3.5 micrometer&carbon.

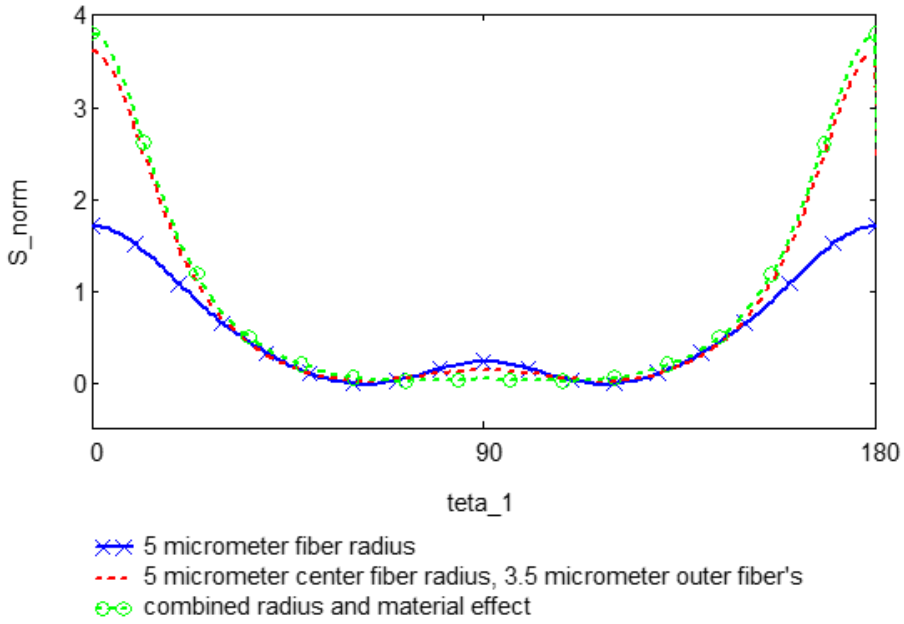

Figure 4.13 Comparison of all stress concentration distributions regarding inner glass fiber variations

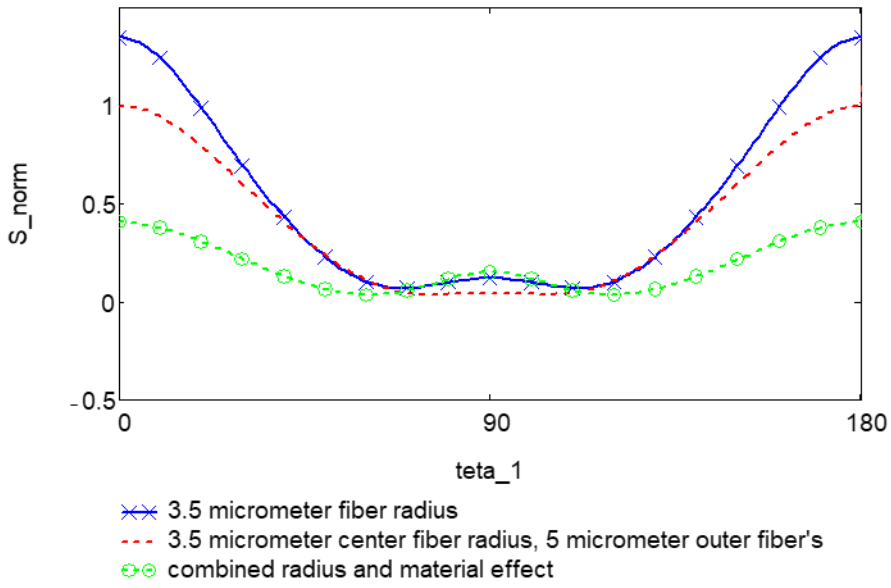

Figure 4.14 Comparison of all stress concentration distributions regarding inner carbon fiber variations

Table 4.4 S_norm values for varyin fiber radius p2

	All glass r=5	Inner glass, outer carbon r=5	All glass r=5, outer r=3.5	Inner glass, r=5, outer carbon r=3.5
Max. Stress Concentration	1.697	2.193	3.598	3.771(B)
Ratio to All glass	1	0.774	0.472	0.45

Stress concentration values designated with letters A and B reveal combined results of both radii and material change. Stress concentration values found in case A (0.406) are lower than other stress concentration cases, which are revealed in Table 4.3. It can be stated that the amount of decrease in stress concentration achieved with material change is slightly higher than the decrease found with radius change for glass and carbon fibers. Highest amount of decrease in stress concentration is achieved by combining these effects.

On the other hand, by regarding values stated in Table 4.4. It can be stated that amount of change in stress concentration found with radius change is higher than the value found with material change. Highest change is found with the combination of these effects, as shown in case B. This result strengthens the previous explanation as the highest increase is caused by both material effects as changing outer fibers with less stiff fiber and decreasing the radii of outer fibers.

Regarding these results, by setting outer fibers as glass fiber and central fiber as carbon fiber, a decrease in the stress concentrations can be achieved with the combined effect of a larger radius and higher stiffness on the outer and higher strength at the center.

4.1.7. Shear Loading

In this part shear load result of an hexagonal RVE wrt different materials is represented.
First, the model is verified. For the verification of the model all components are set as epoxy and shear modulus value is calculated by dividing average stress to average strain value found using fea models, these values are tabulated in Table 4.5. After that, shear modulus value is computed using equation **(6)** by setting elastic modulus and poisons ratio values as stated in Table 3.2 and results obtained from fea study is compared with the result of simple solid mechanics formulae and both of the results are found is agreement.

$$G = \frac{E}{2 * (1 + \vartheta)} \quad \textbf{(7)}$$

G, E and ϑ refers to shear modulus, elastic modulus and poisons ratio respectively. The calculated shear modulus value is compared with a referenced value. FEA data and results are given in Table 4.5

Table 4.5 modulus values found using fea outputs

Ave_E(micrometer/micrometer)	Ave_S(Mpa)	Shear Modulus(Mpa)
4.41E-06	0.004725677	1.07E+03

4.1.7.1. Material Effect

To examine material effect, stress concentration plots of homogenous glass RVE and hybrid RVE with center glass and homogenous carbon RVE with center carbon fiber are given in Figure 4.16 and Figure 4.18. 2 different model results are represented in plots; stress concentration distributions represent the radial stress result. Homogenous model results represented in Figure 4.15 are used as a control group. Figure 4.16 and Figure 4.18 were used to reveal the hybridization effect regarding radial stress concentration distribution and Figure 4.17 Figure 4.19 are given for shear stress concentration distribution. Assigned fiber materials are stated within small RVE shapes.

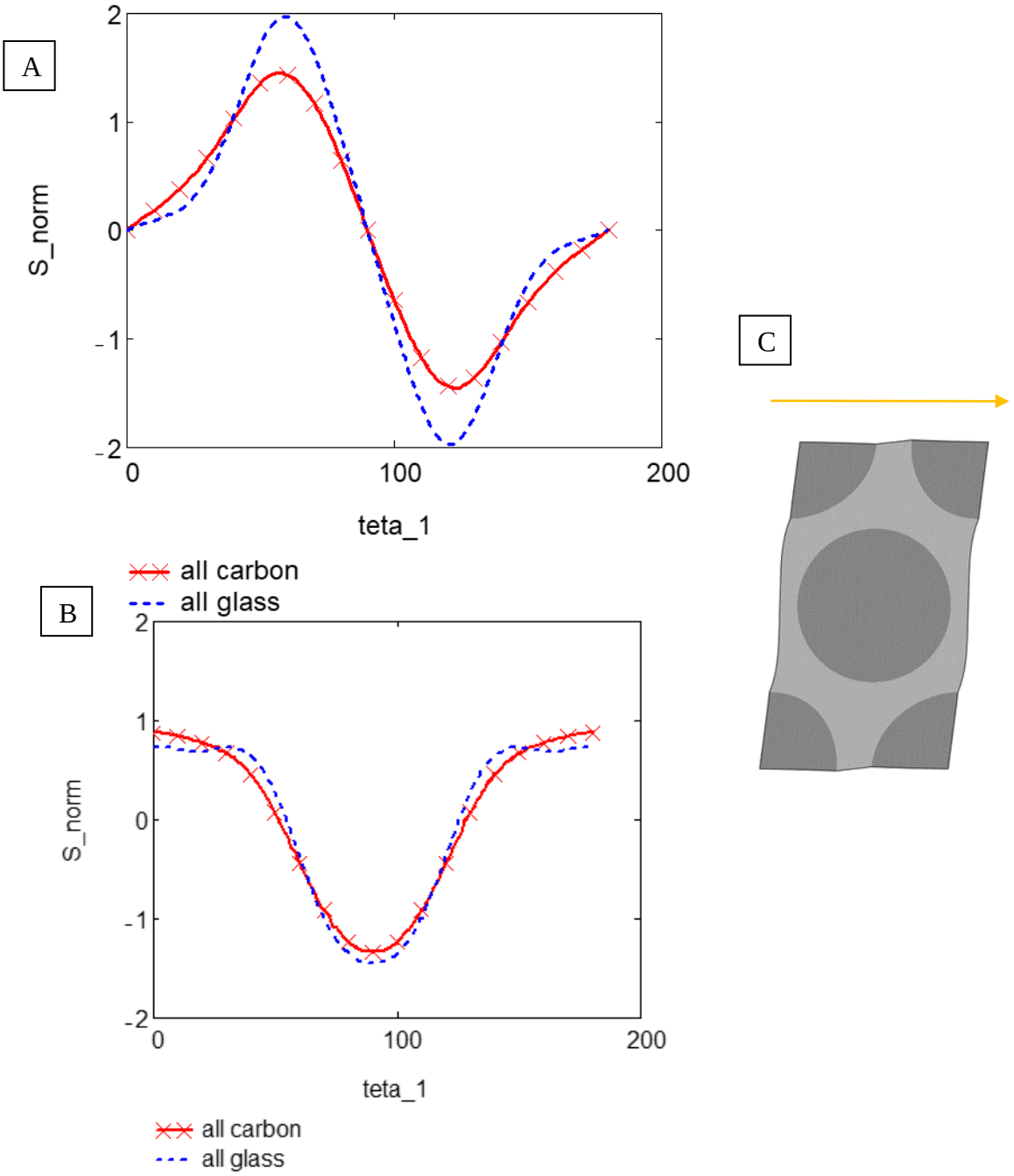

Figure 4.15 Comparison of stress concentration distributions regarding homogenous hexagonal RVE under shear loading: (a) radial stress distibution ; (b) shear stress distribution; (c) loading representation .

Results revealed in this section are totally different from the results stated in material effect under transverse loading. In this section, it is observed that the presence of glass fiber

increases the stress concentration around center (carbon) fiber. On the contrary opposite situation occurs when carbon fibers are set around center glass fiber. The stress concentration around the glass fiber decreases. Localization of stress concentration occurs around 60 degrees instead of 0 and 180 degrees around center fiber .

A

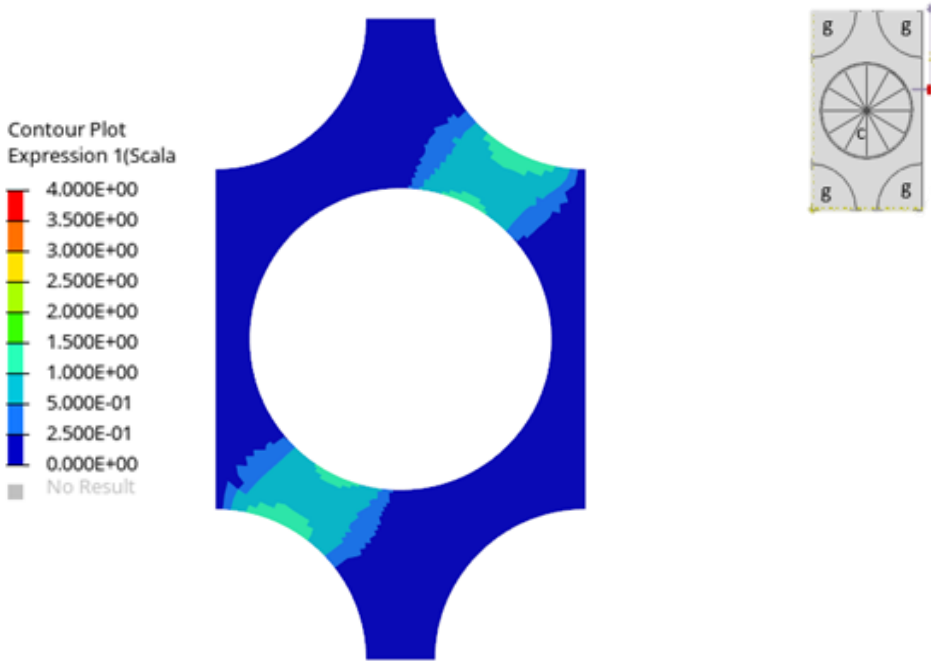

B

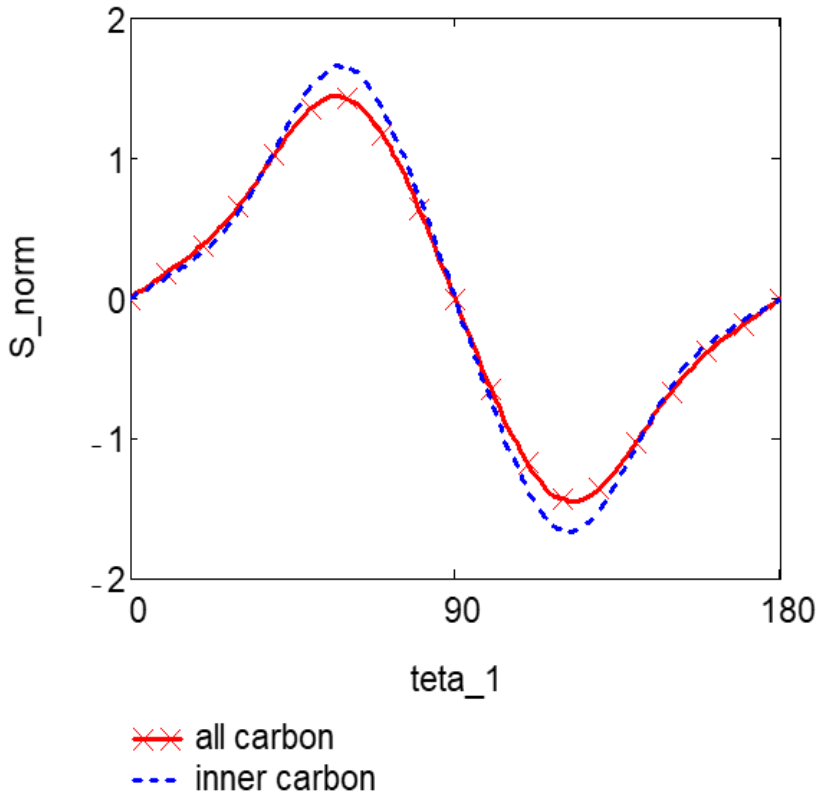

Figure 4.16 Hexagonal RVE, shear loading center carbon fiber hybrid composite results radial stress distribution : (a) center fiber carbon stress concentration contour graph; (b) normalized stress concentration plot.

A

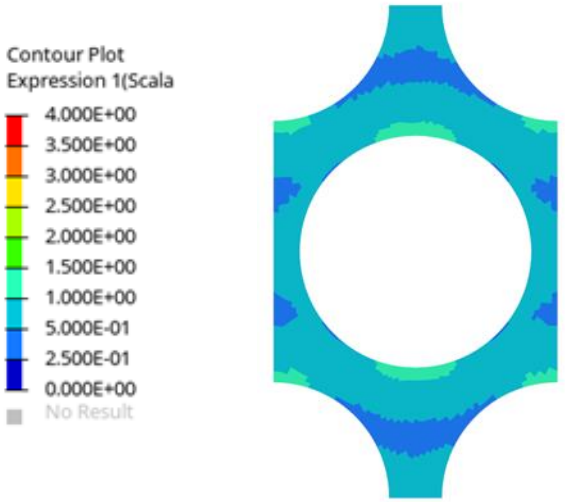

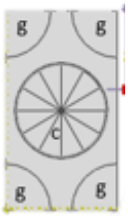

B

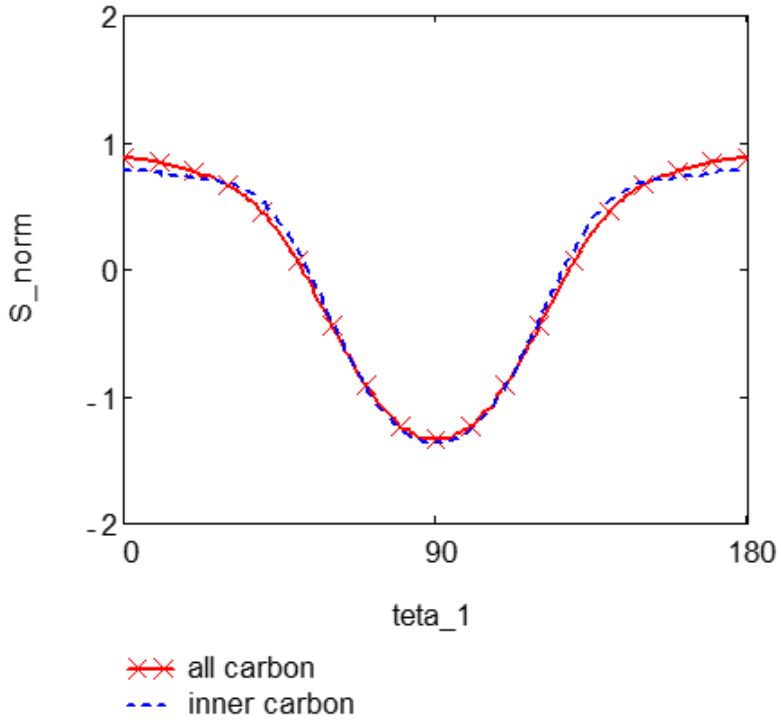

Figure 4.17 Hexagonal RVE, shear loading center carbon fiber hybrid composite results shear stress distribution : (a) center fiber carbon stress concentration contour graph; (b) normalized stress concentration plot.

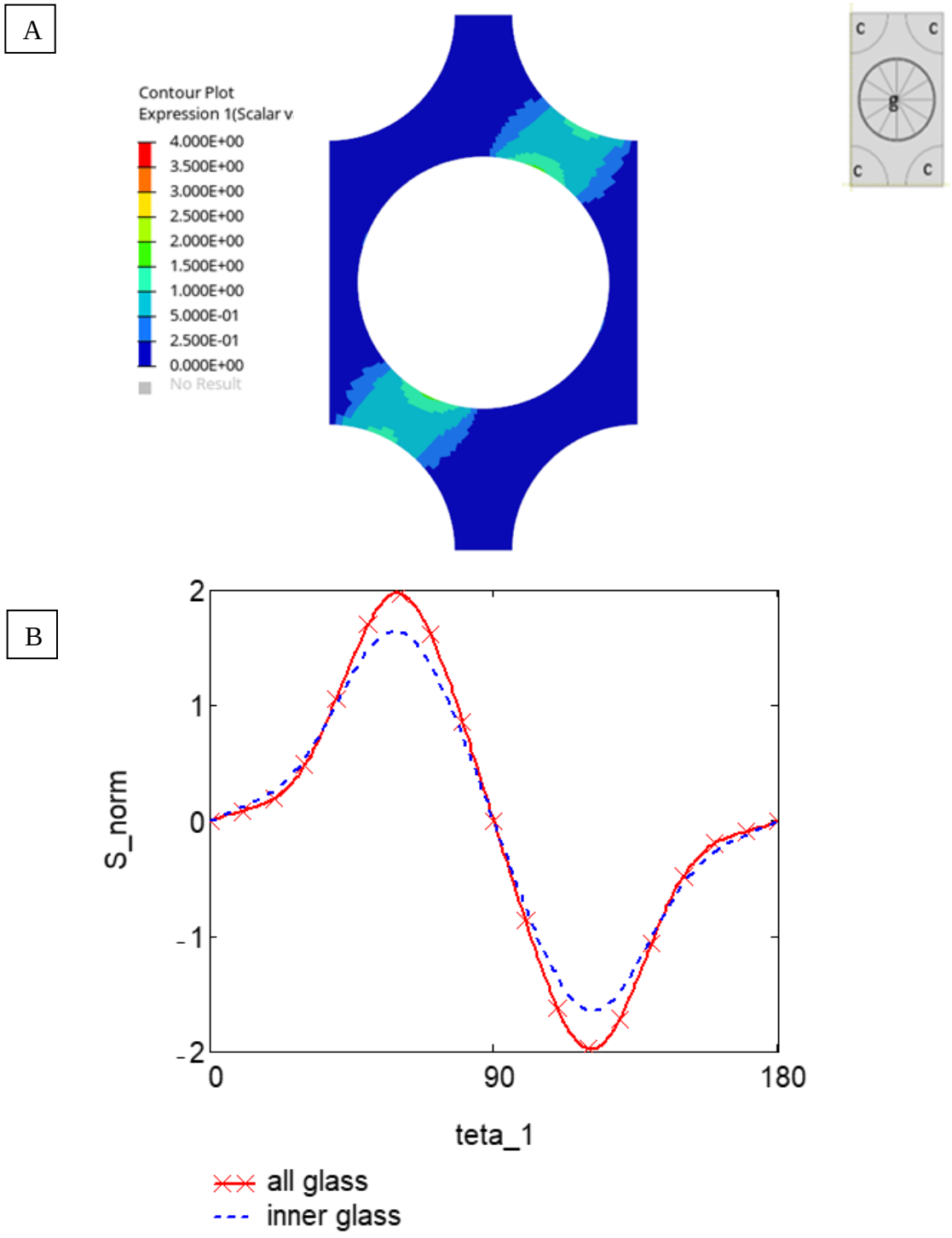

Figure 4.18 Hexagonal RVE, shear loading center glass fiber hybrid composite results radial stress distribution: (a) center fiber glass stress concentration contour graph; (b) normalized stress concentration plot.

A

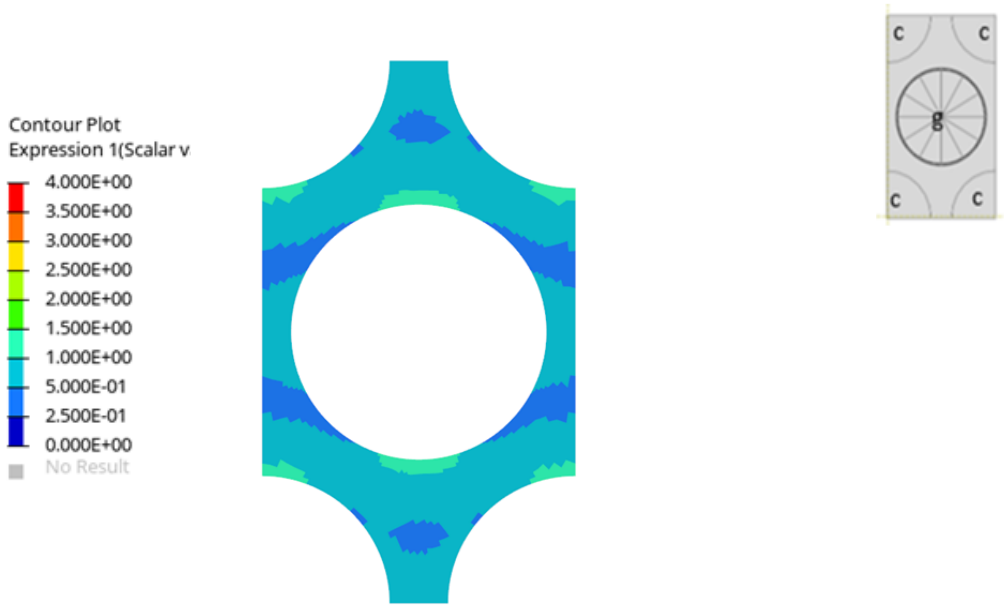

B

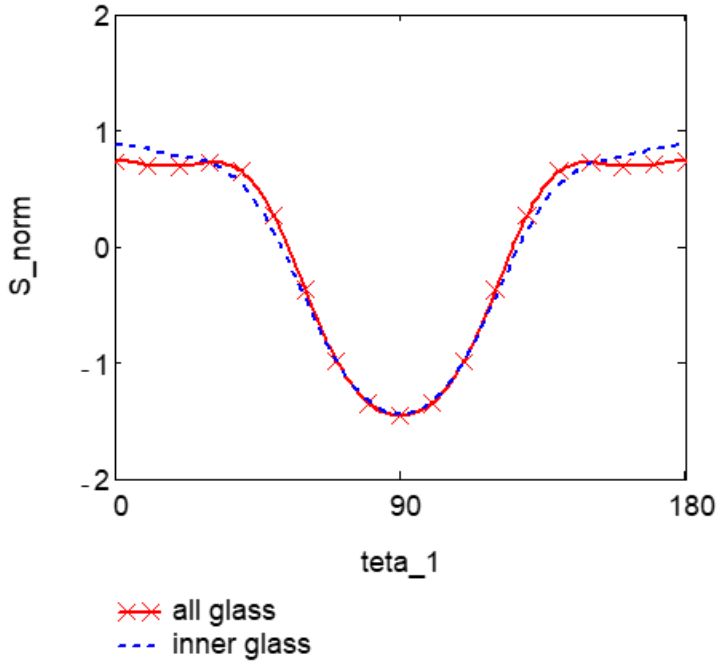

Figure 4.19 Hexagonal RVE, shear loading center glass fiber hybrid shear stress distribution: (a) center fiber glass stress concentration contour graph; (b) normalized stress concentration plot.

Regarding radial stress distribution Figure 4.16, when outer fibers changed with glass fiber, stress concentration around center fiber at 60 degrees increases since load carried by center fiber increases due to stiffness increase in loading direction opposite situation occurs in center glass outer carbon configuration that is shown in Figure 4.18. Shear stress concentration distribution results are given in Figure 4.17and Figure 4.19 these results shows similar behavior with transverse loading radial distribution as a slight decrease in concentration values when outer fibers changed with stiffer fibers and vice versa.

4.1.7.2. Fiber Radius Effect

In this section effect of variable fiber, radius results are given. Stress concentration distribution results are shown in Figure 4.20 and Figure 4.21 and shear data results are revealed in Figure 4.22Figure 4.23

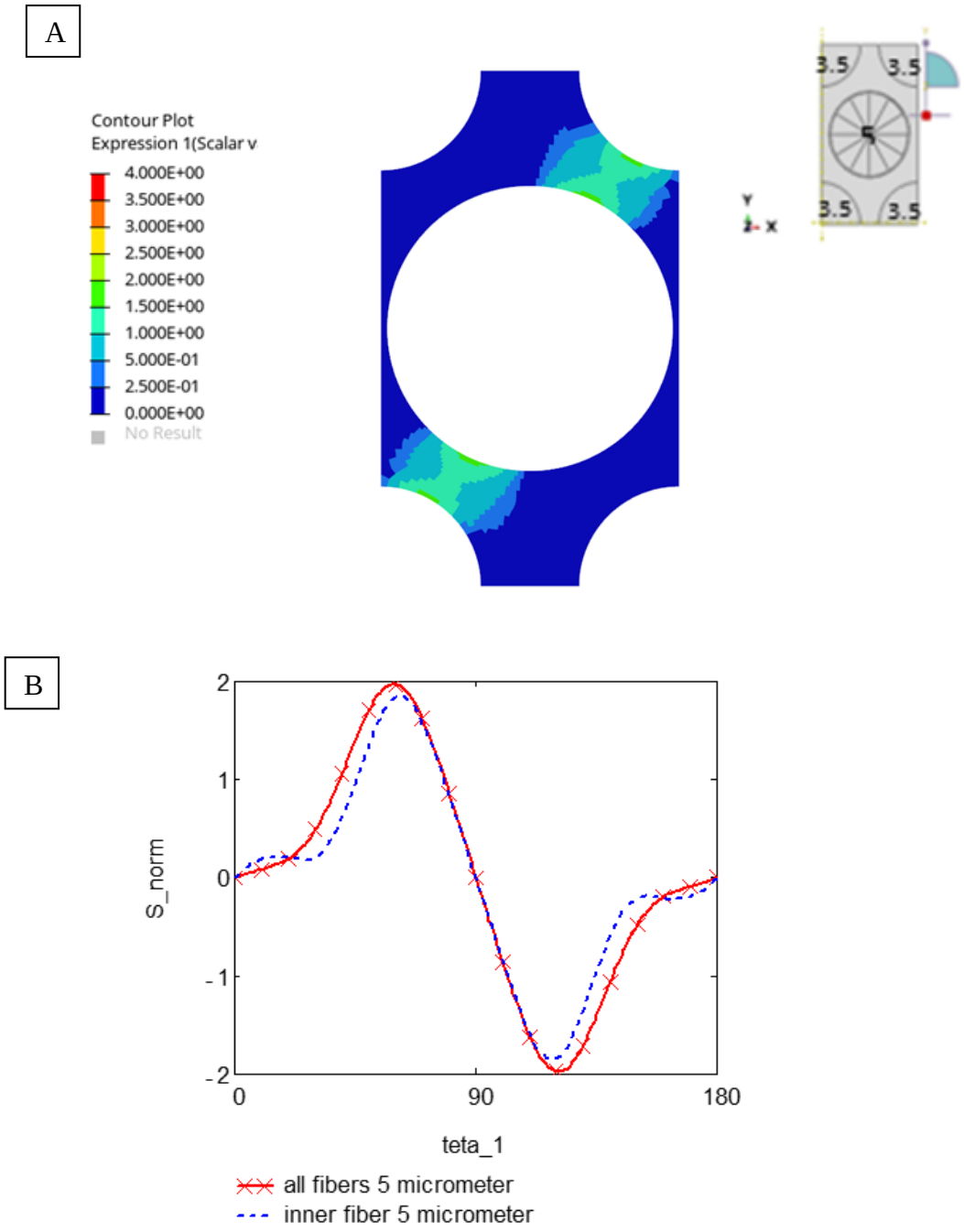

Figure 4.20 Stress concentration distribution under shear loading radial stress distribution :(a) contour plot regarding different radius values as center fiber r= 5micrometer and outer fiber r=3.5micrometer;(b) comparison of normalized stress concentration plots with RVE's all radius values are r=5micrometer and inner radius value is 5 micrometer outer radius value is 3.5 micrometer.

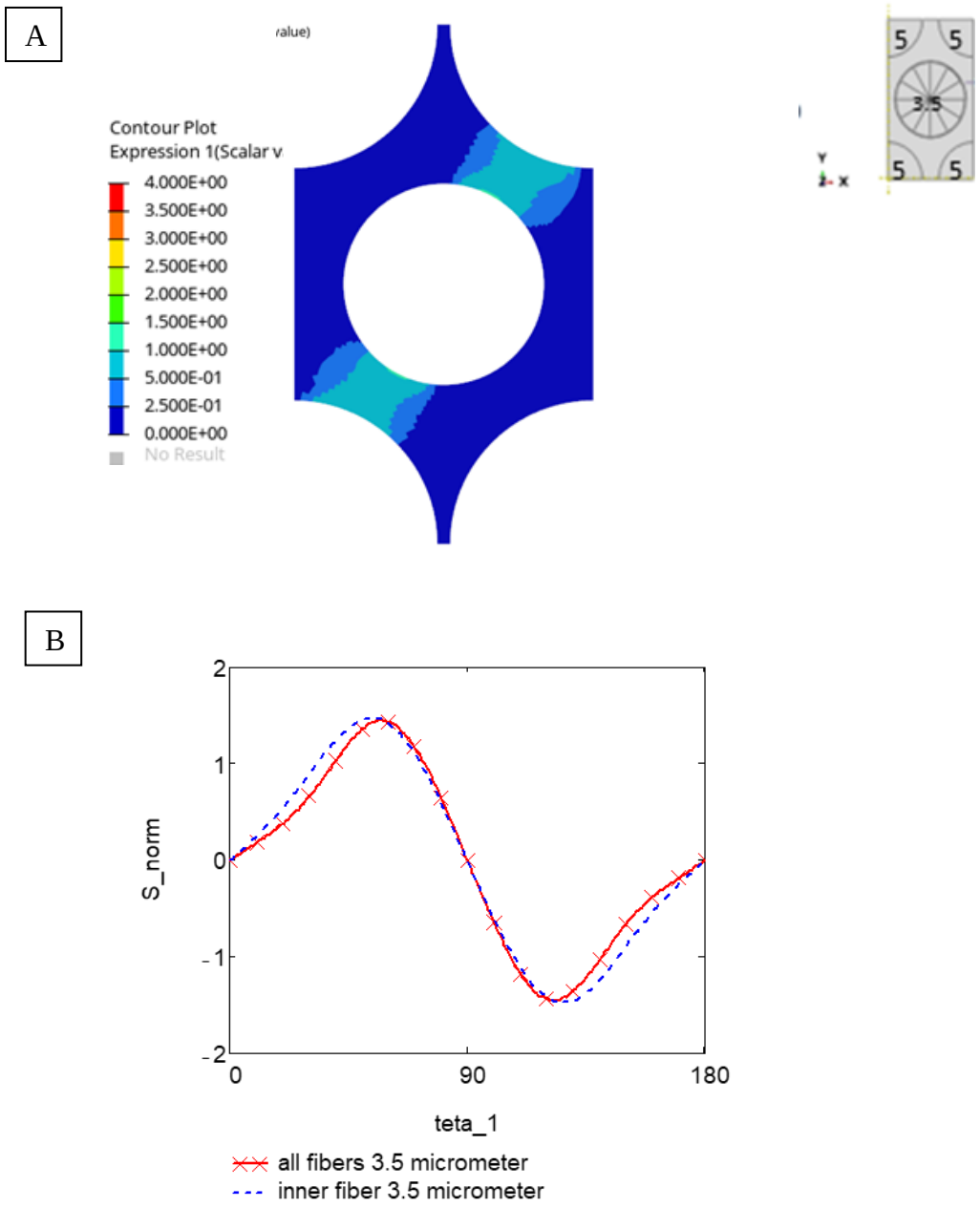

Figure 4.21 Stress concentration distribution under shear loading radial stress distribution:(a) contour plot regarding different radius values as center fiber r=3.5micrometer and outer fiber r=5micrometer;(b) comparison of normalized stress concentration plots with RVE's all radius values are r=3.5micrometer and inner radius value is 3.5micrometer outer radius value is 5 micrometer.

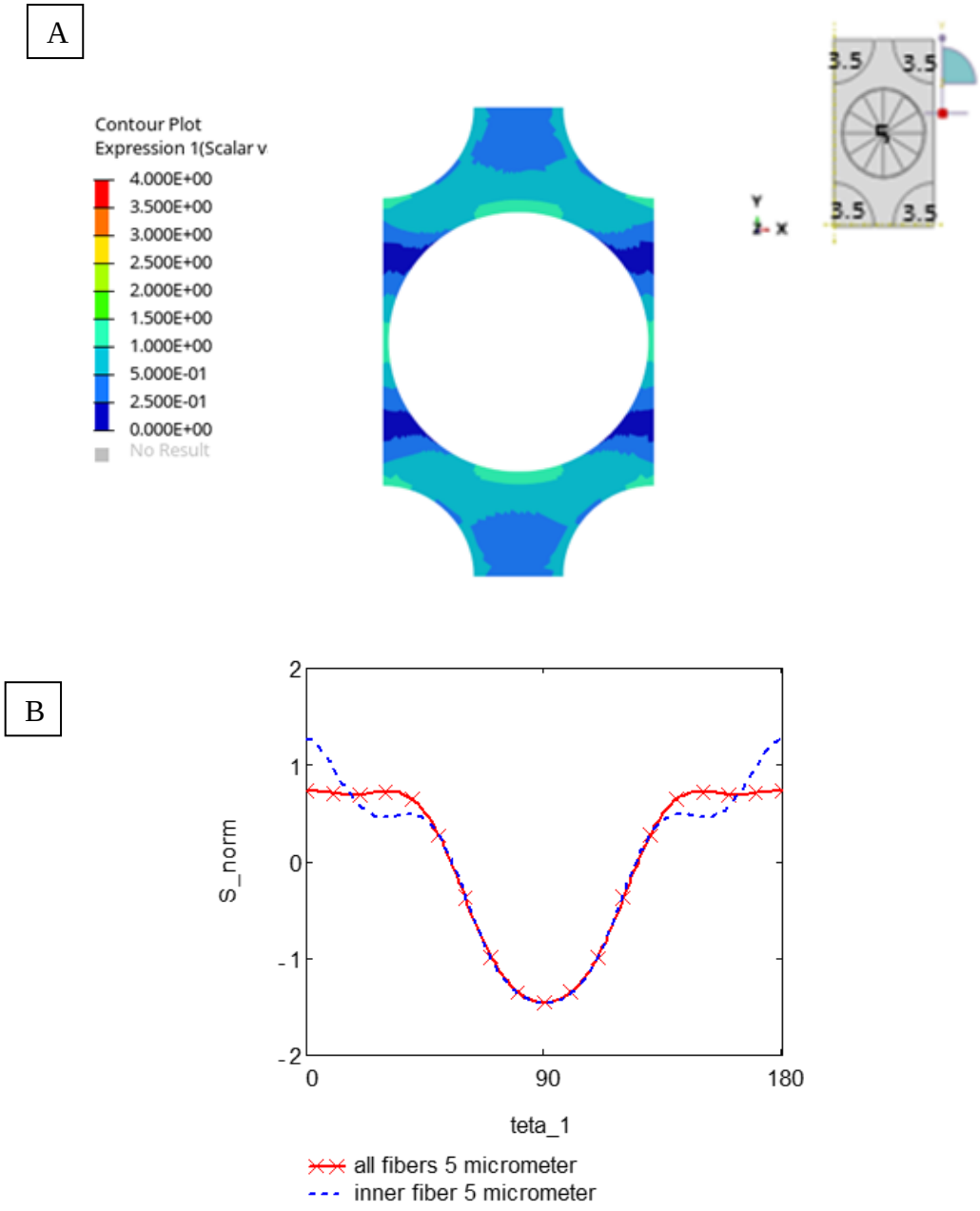

Figure 4.22 Stress concentration distribution under shear loading, shear stress distribution :(a) contour plot regarding different radius values as center fiber r= 5micrometer and outer fiber r=3.5micrometer;(b) comparison of normalized stress concentration plots with RVE's all radius values are r=5micrometer and inner radius value is 5 micrometer outer radius value is 3.5 micrometer.

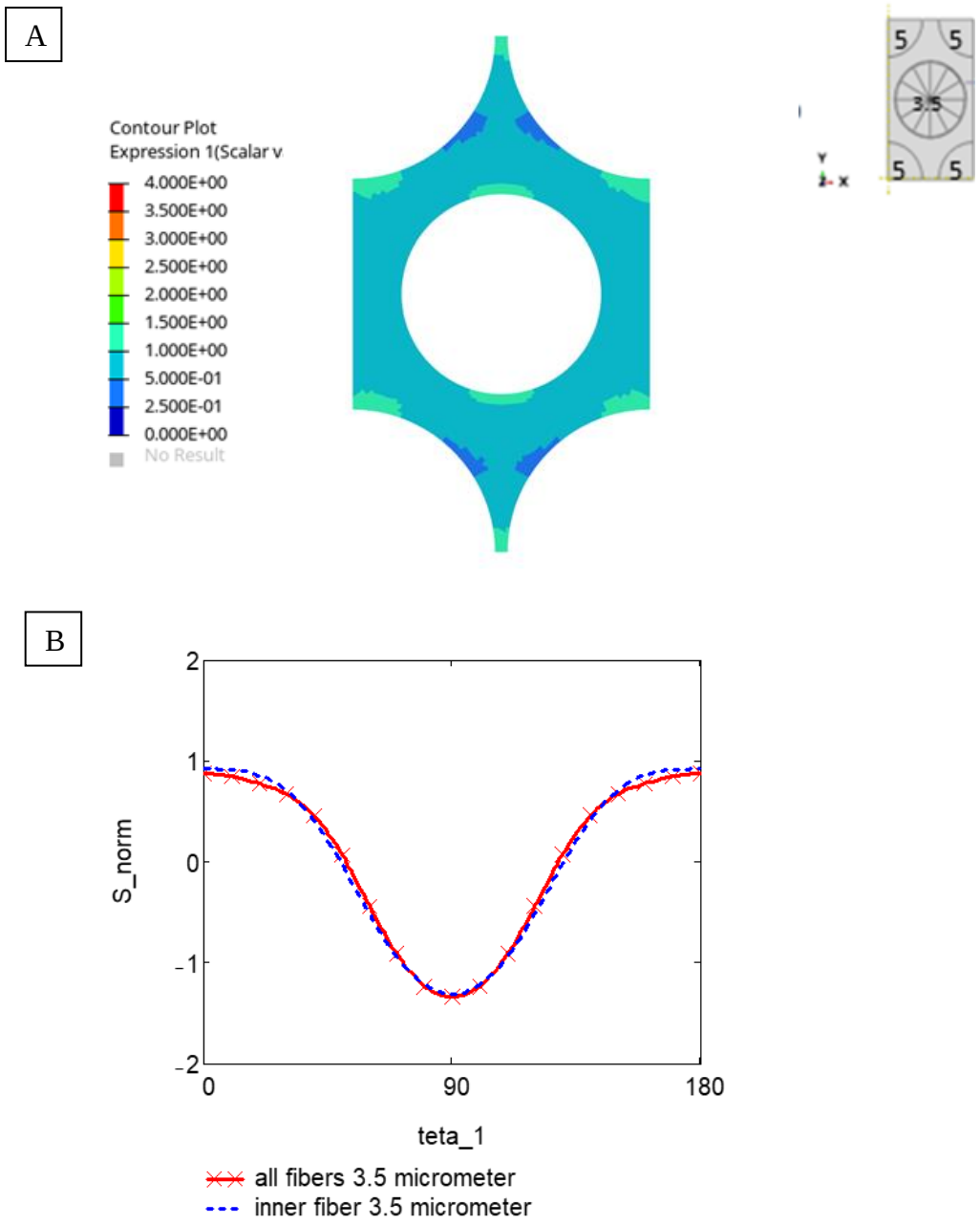

Figure 4.23 Stress concentration distribution under shear loading, shear stress distribution:(a) contour plot regarding different radius values as center fiber r=3.5micrometer and outer fiber r=5micrometer;(b) comparison of normalized stress concentration plots with RVE's all radius values are r=3.5micrometer and inner radius value is 3.5micrometer outer radius value is 5 micrometer.

Regarding plot (b) radial stress data, it can be stated that stress concentration localizes around 60 degrees, and a slight decrease in stress concentration can be observed.

Radial stress data reveal that stress concentration around 0 degrees wrt shear loading results does not differ but around 60 degrees wrt radial stress distribution data plots shows similar behaviour when inner smaller & and outer bigger fibers and all 3.5 micrometer fibers are compared. On the other hand, when inner bigger & and outer smaller fibers and all 5 micrometer fibers are compared it can be said that stress concentration decreases, main reason behind this situation is change in amount of load carried by these fibers. As the outer fibers changed with smaller fibers load carried in these stiffer regions decreases and stress concentration values in loading direction decreases and vice versa.

4.1.7.3. Fiber Radius and Material Combined Effect

A combination of varying fiber radius and material effect results are revealed under this heading, and homogenous RVE plots used as control group. Results for different combinations are shown in Figure 4.24-Figure 4.31

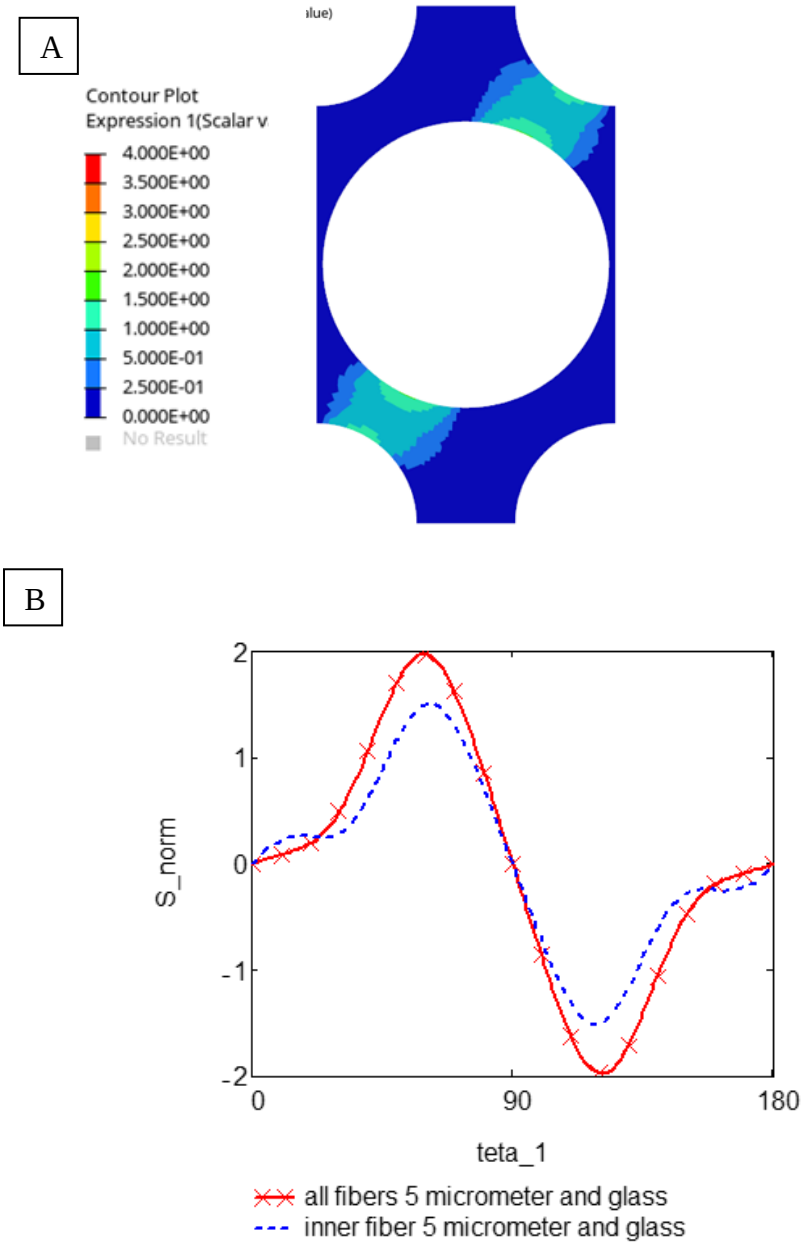

Figure 4.24 Stress concentration distribution with material effect under shear loading :(a) contour plot regarding different radius values as center fiber r= 5micrometer&glass material and outer fiber r=3.5micrometer& carbon material ;(b) comparison of normalized stress concentration plots with RVE's properties are all fibers with r=5micrometer&glass, and inner radius value is 5 micrometer& glass outer radius value is 3.5 micrometer&carbon.

A

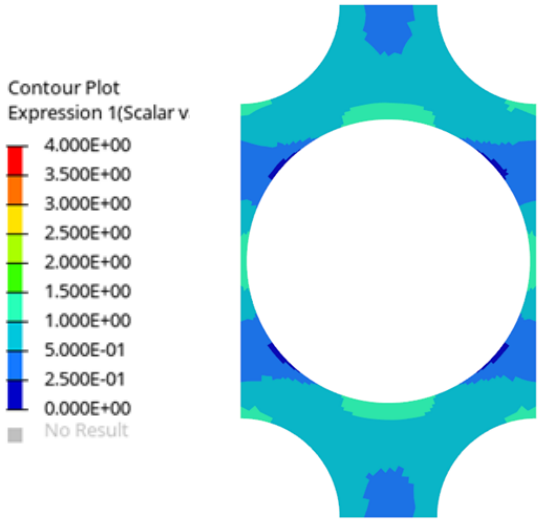

B

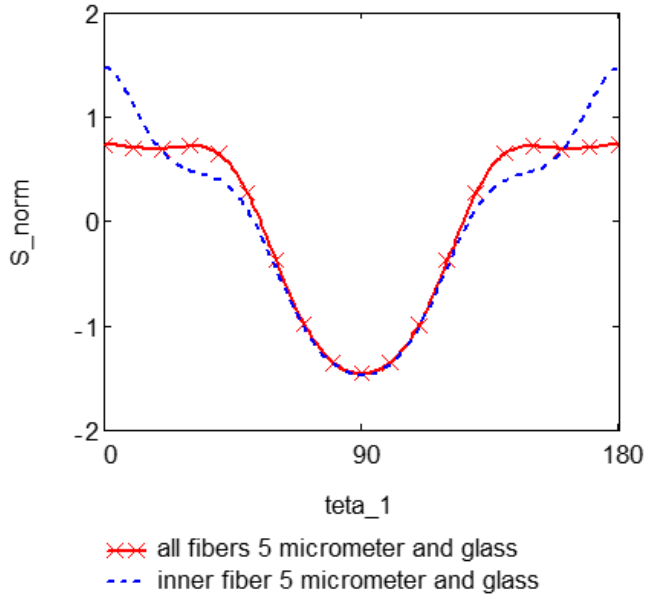

Figure 4.25 Stress concentration distribution with material effect under shear loading :(a) contour plot regarding different radius values as center fiber r= 5micrometer&glass material and outer fiber r=3.5micrometer& carbon material ;(b) comparison of normalized stress concentration plots with RVE's properties are all fibers with r=5micrometer&glass, and inner radius value is 5 micrometer& glass outer radius value is 3.5 micrometer&carbon.

A

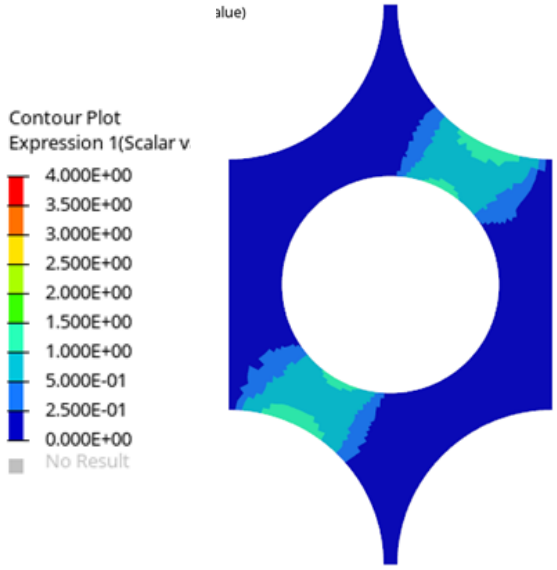

B

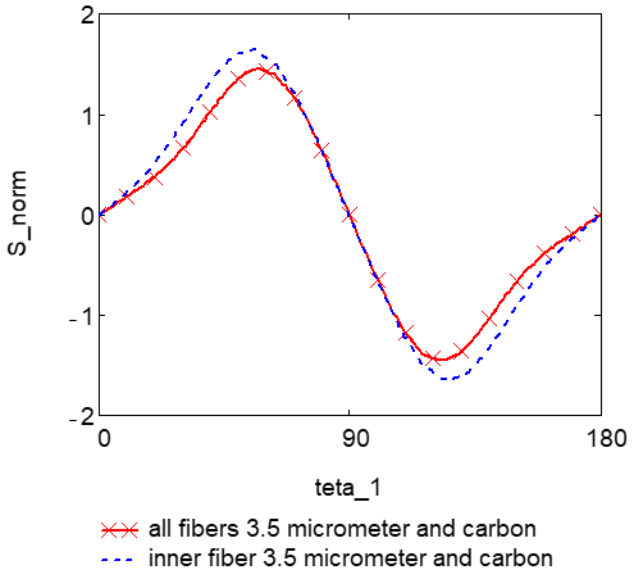

Figure 4.26 Stress concentration distribution with material effect under shear loading :(a) contour plot regarding different radius values as center fiber r= 5micrometer&glass material and outer fiber r=3.5micrometer& carbon material ;(b) comparison of normalized stress concentration plots with RVE's properties are all fibers with r=5micrometer&glass, and inner radius value is 5 micrometer& glass outer radius value is 3.5 micrometer&carbon.

A

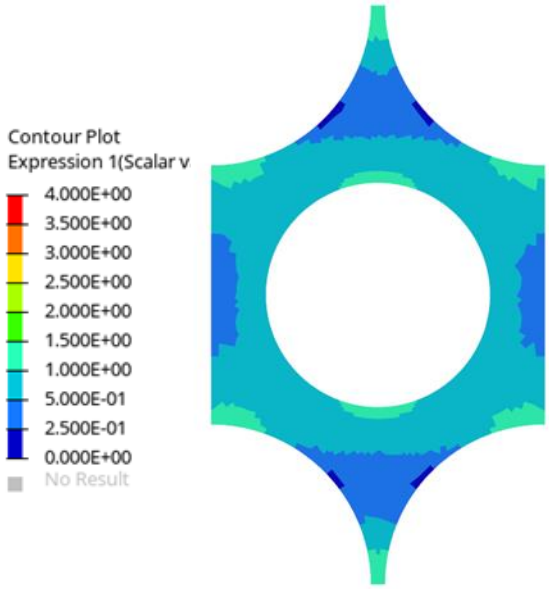

B

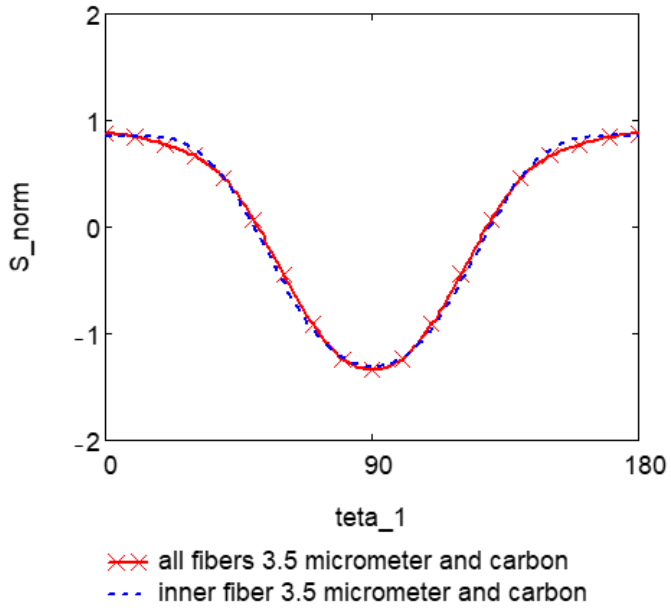

Figure 4.27 Stress concentration distribution with material effect under shear loading :(a) contour plot regarding different radius values as center fiber r= 5micrometer&glass material and outer fiber r=3.5micrometer& carbon material ;(b) comparison of normalized stress concentration plots with RVE's properties are all fibers with r=5micrometer&glass, and inner radius value is 5 micrometer& glass outer radius value is 3.5 micrometer&carbon.

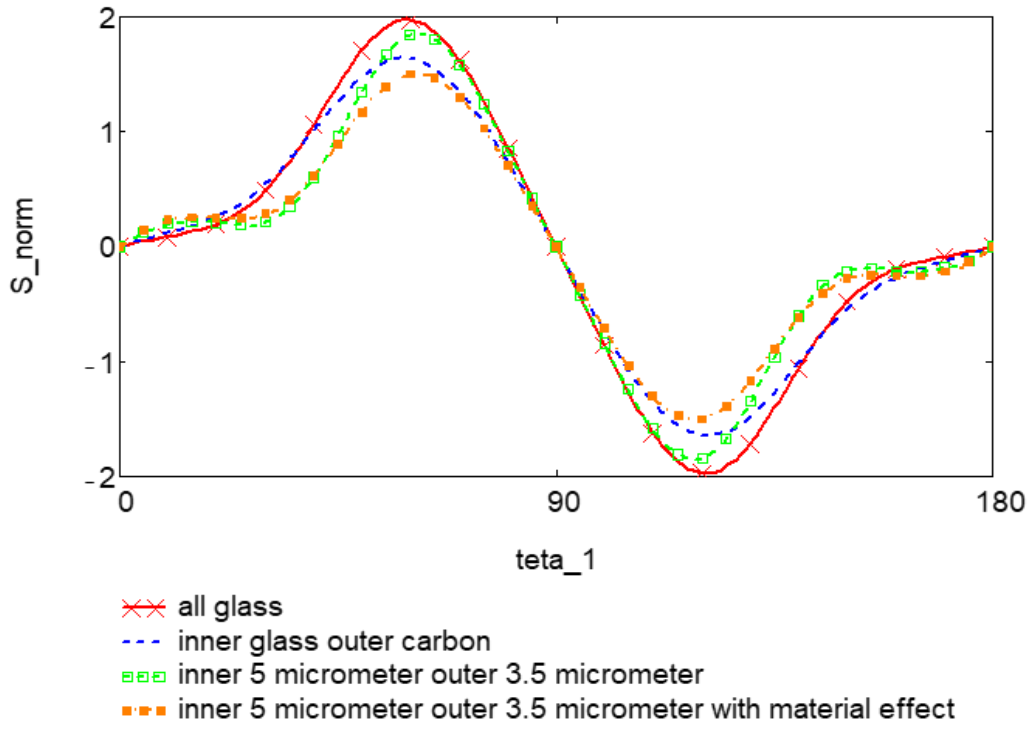

Figure 4.28 Comparison of all stress concentration distributions regarding inner glass fiber variations

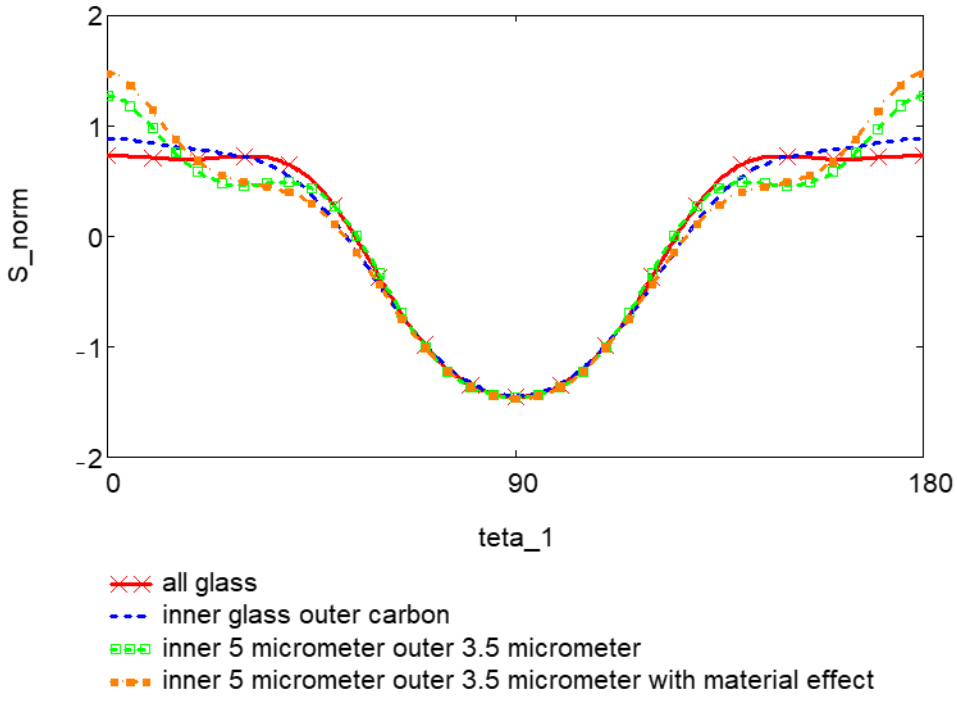

Figure 4.29 Comparison of all stress concentration distributions regarding inner glass fiber variations

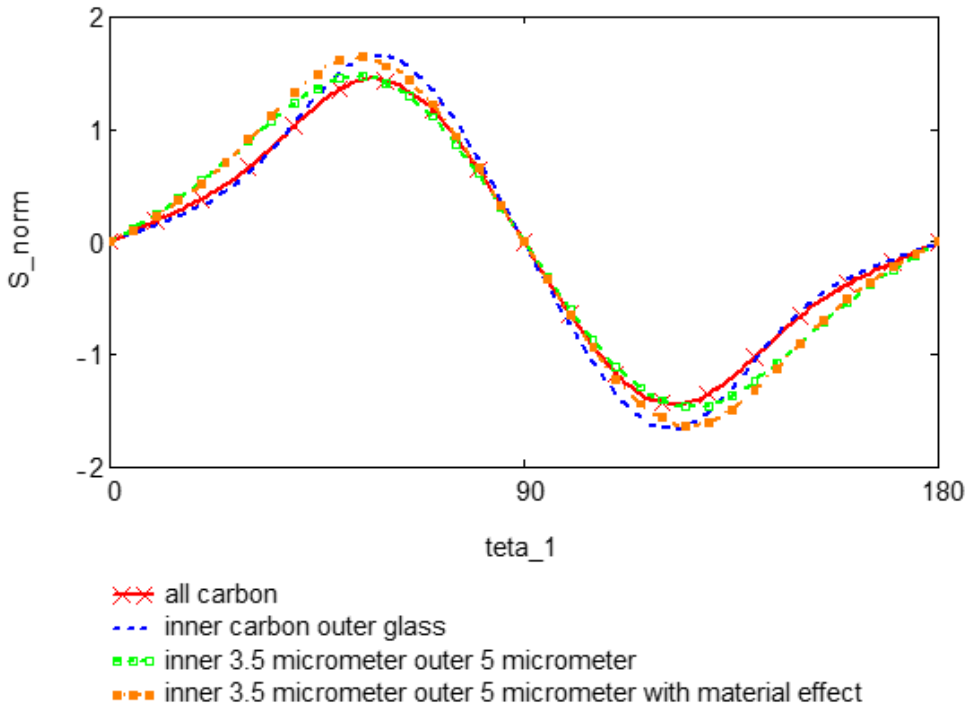

Figure 4.30 Comparison of all stress concentration distributions regarding inner carbon fiber variations

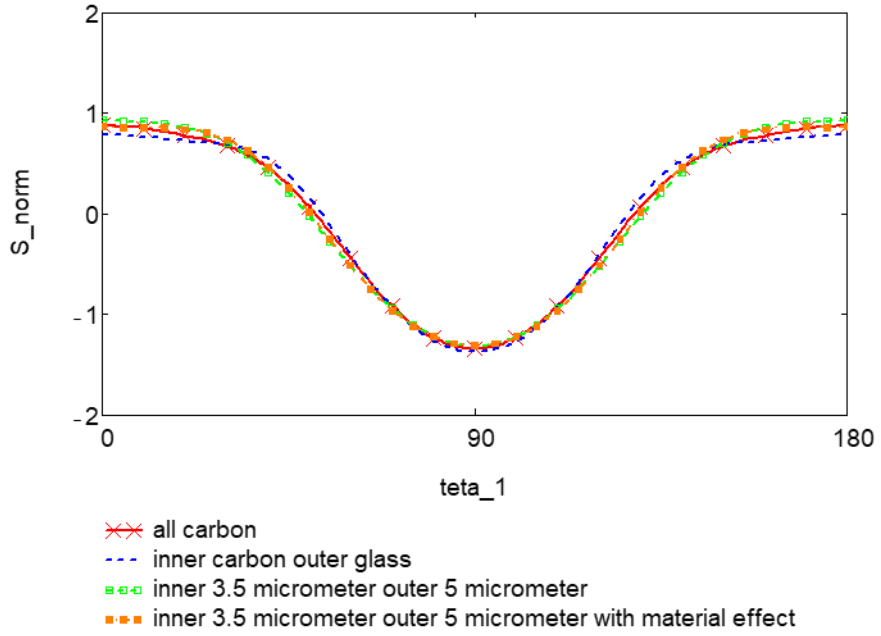

Figure 4.31 Comparison of all stress concentration distributions regarding inner carbon fiber variations

Results shown in Figure 4.28 and Figure 4.30 strengthen the observations of general shear loading results trends. With inner bigger fiber and glass material: radial stress concentration of around 60 degrees decreases. On the contrary, With smaller inner fiber and carbon material: shear stress concentration of around 0 degrees is similar to that of all carbon fiber and 3.5 micrometer radii fiber.

To see the load path under shear loading, trials made with angled square RVEs can be seen in Figure 4.32 and Figure 4.33. In general, stress localizes around stiffer regions.

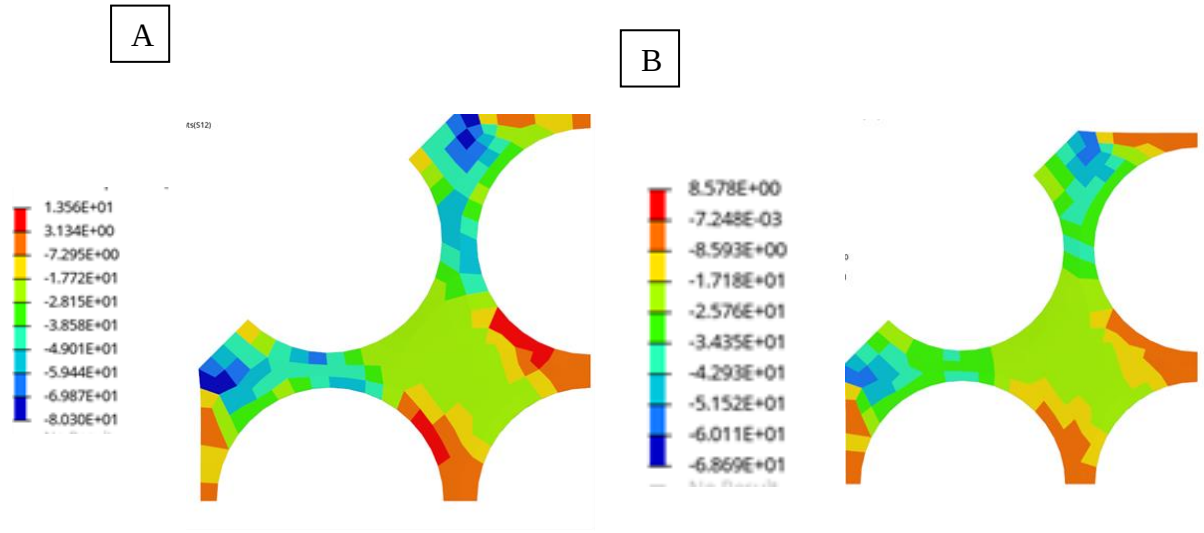

Figure 4.32 S12 stress distribution on the matrix: (a) all glass material; (b) inner glass material.

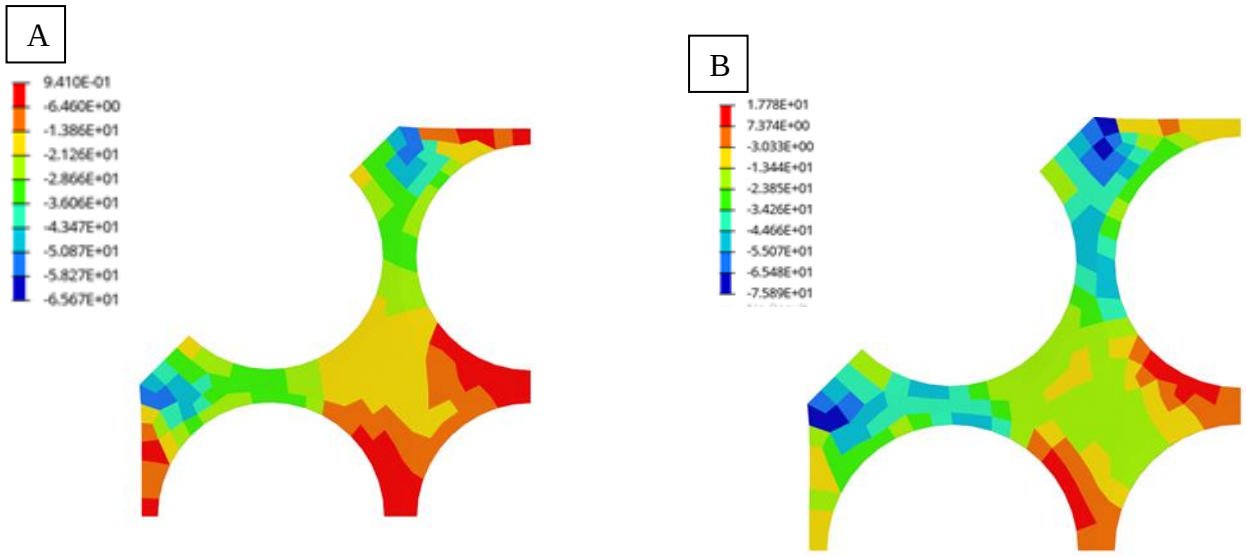

Figure 4.33 S12 stress distribution on the matrix: (a) all carbon material; (b) inner carbon material.

Table 4.6 S_norm values under shear loading with varying radius p1

	All carbon r=3.5	Inner carbon, outer glass r=3.5	All carbon r=3.5, outer r=5	Inner carbon, r=3.5, outer glass r=5
Max. Stress Concentration	1.45	1.67	1.47	1.64

Table 4.7 S_norm values under shear loading with varying radius p2

	All glass r=5	Inner glass, outer carbon r=5	All glass r=5, outer r=3.5	Inner glass, r=5, outer carbon r=3.5
Max. Stress Concentration	1.972	1.641	1.855	1.506

When results stated in Table 4.6 and Table 4.7 opposite effect of stress concentration distribution value can be seen for the hybridization achieved by material variance. On the contrary for fiber radius change, hybridization effect becomes minimal in terms of small center fiber but for center bigger fiber results follows same trend with transverse loading.

Results of shear loading draws a different picture, results do not completely differ from transverse load when smaller inner radius results employed but do not converges with transverse loading results when material hybridization results considered.

4.1.8. Triple Hex RVE

Triple Hex RVE results are given under this heading. One of the considerations of the triple hex study is to reveal the effect of different neighboring fibers on center fiber, since a distinguish between transverse and shear loading observed. All of the results stated under this heading are the collection of stress data around the center fiber at the middle row. Fiber volume ratio is set as $vf = 0.6$. Each model material configuration is given with a colored small RVE stated in each analysis set. Figure 4.34 reveals results of homogenous RVE and used as a control group. Results for different combinations are shown in Figure 4.34-Figure 4.40

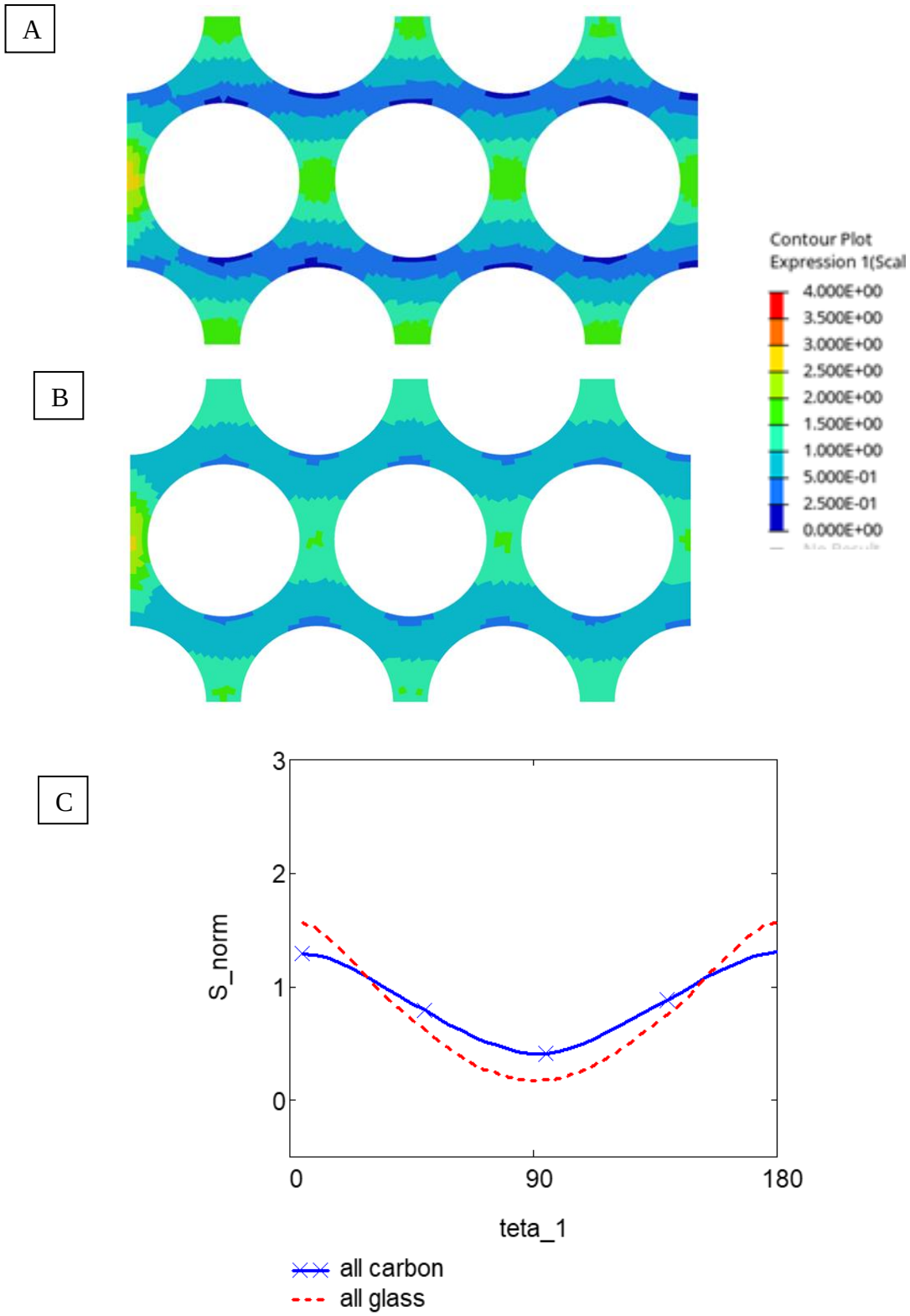

Figure 4.34 Triple hex homogenous composite results; (a)normalized contour plot of all glass material ;(b) normalized contour plot of all carbon material;(c) stress concentration distribution regarding homogenous cases

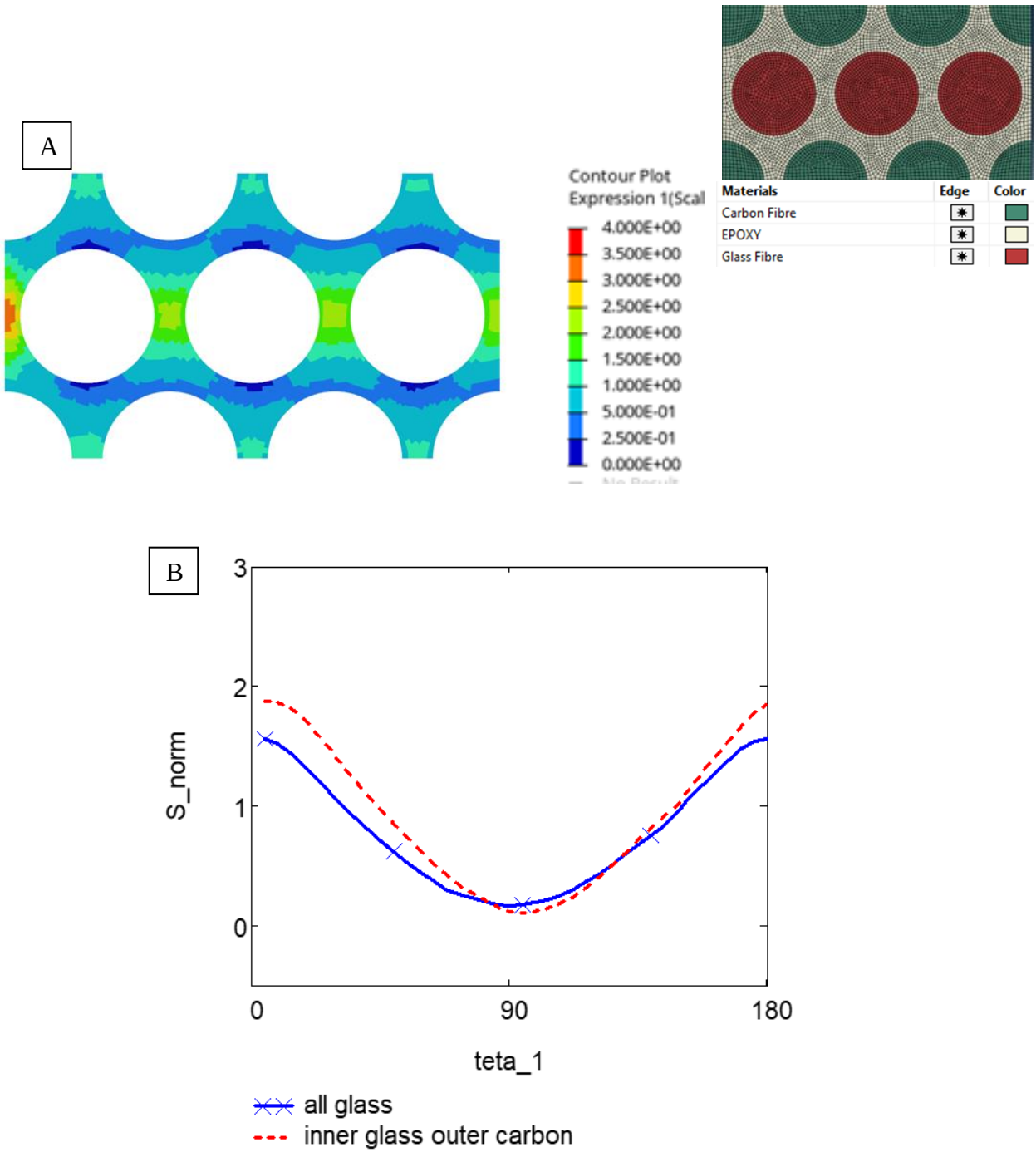

Figure 4.35 Triple hex hybrid composite results; (a)normalized contour plot for inner glass material ;(b) stress concentration distribution regarding homogenous all glass and hybrid inner row glass cases

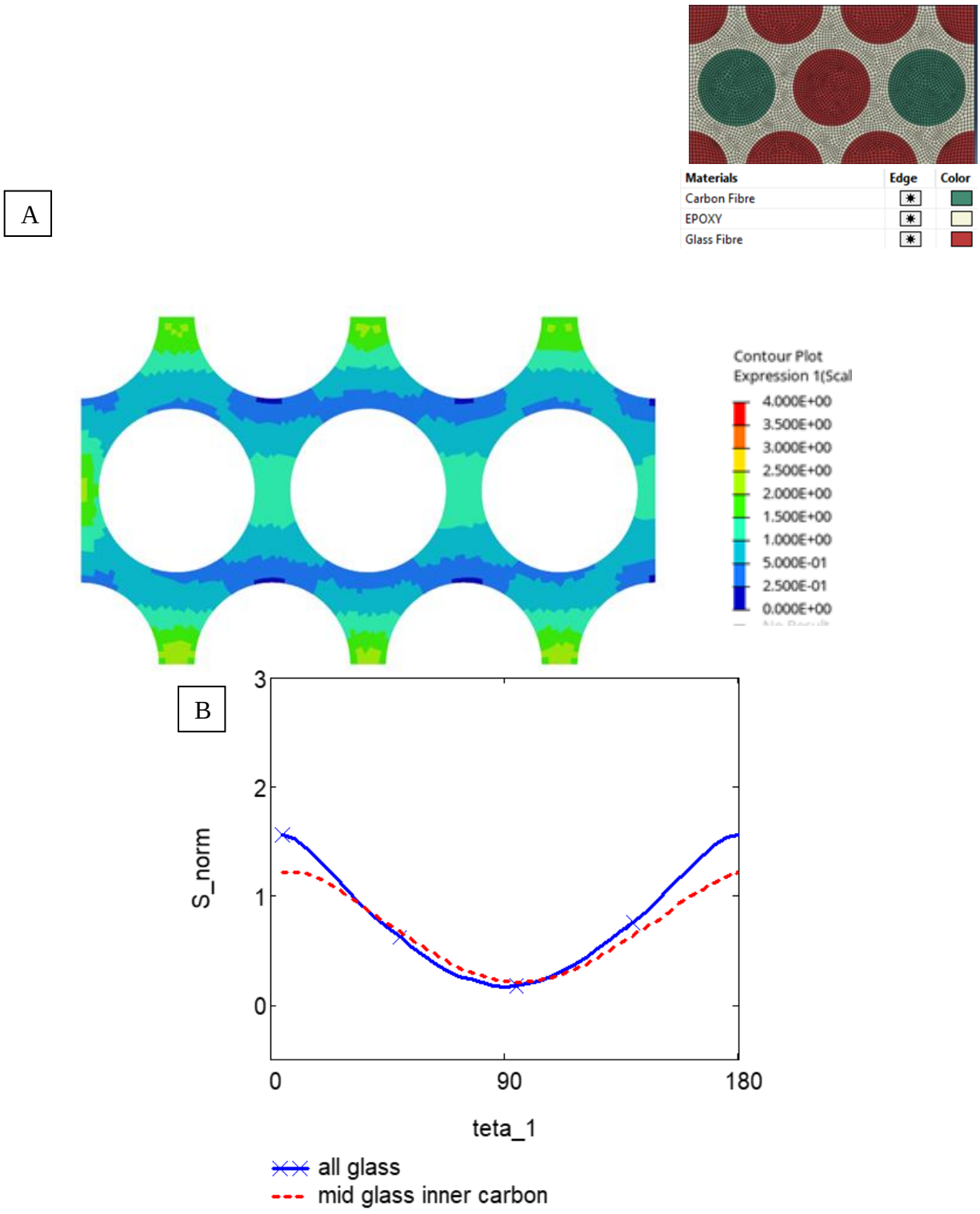

Figure 4.36 Triple hex hybrid composite results; (a)normalized contour plot for inner row carbon and center fiber glass material configuration ;(b) stress concentration distribution regarding homogenous all glass and hybrid inner row carbon and center fiber glass material configuration cases

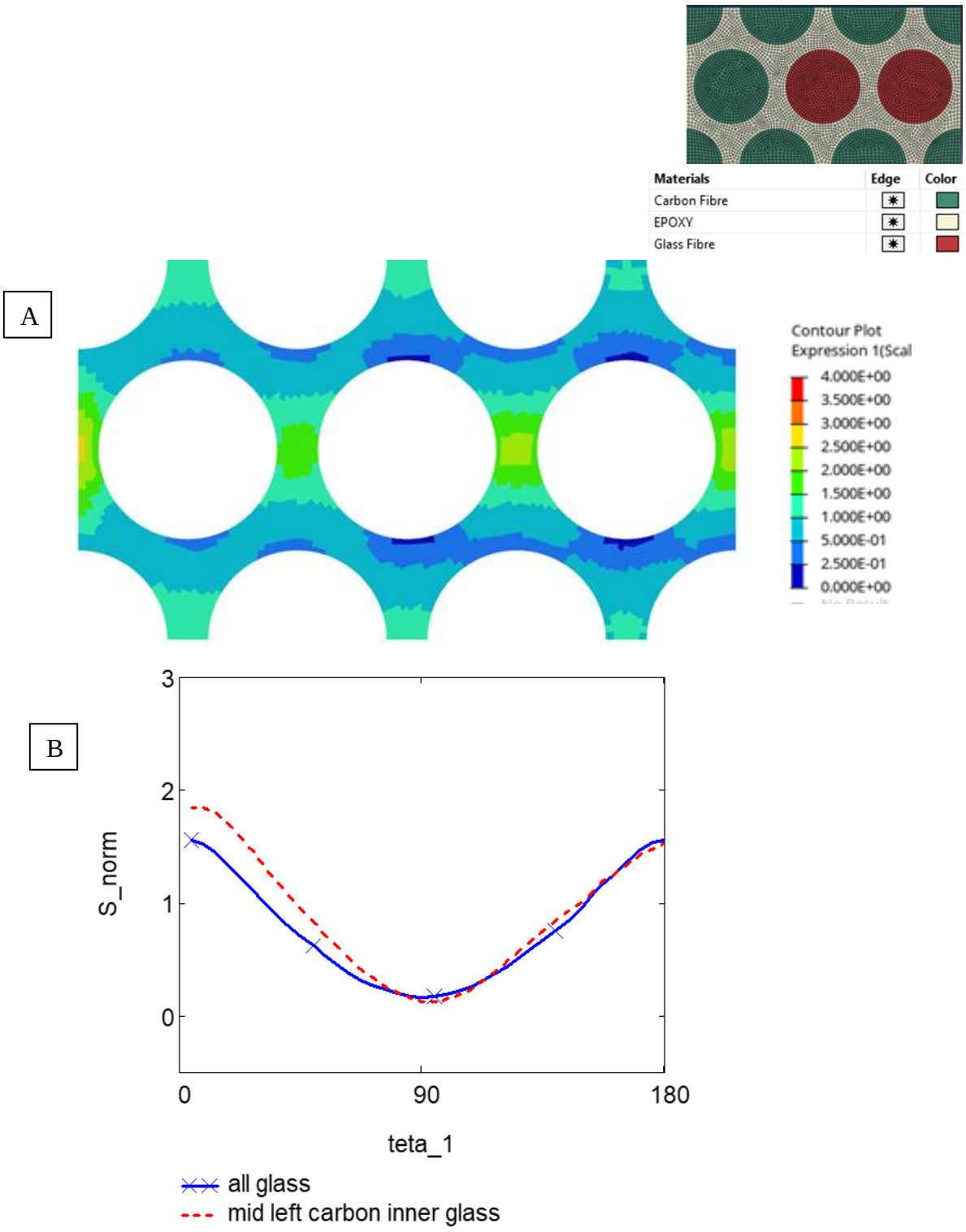

Figure 4.37 Triple hex hybrid composite results; (a)normalized contour plot for inner row 1 carbon and 2 glass fiber with glass center fiber material configuration ;(b) stress concentration distribution regarding homogenous all glass and hybrid inner row 1 carbon and 2 glass fiber with glass center fiber material configuration cases

According to the results, it can be said that stiffer rows experience a higher amount of load and stress concentration around center fiber changes regarding load carrying capability of fiber row. When the inner row is set as glass, load carried by the middle row increases and stress concentration around the center fiber increases. On the contrary, when the upper and lower rows are set as glass fiber and inner row is set as carbon fiber as in Figure 4.36 , load carried by middle row decreases and stress concentration around the middle fiber decrease. When two fibers in the middle row are set as glass as in Figure 4.37, load carried by that row increases, and due to the different fiber material, a difference around the center fiber occurs, and an increase in stress concentration value can be observed. On the contrary when inner row set as glass an increase on stress concentration distribution can be seen in as in Figure 4.35.

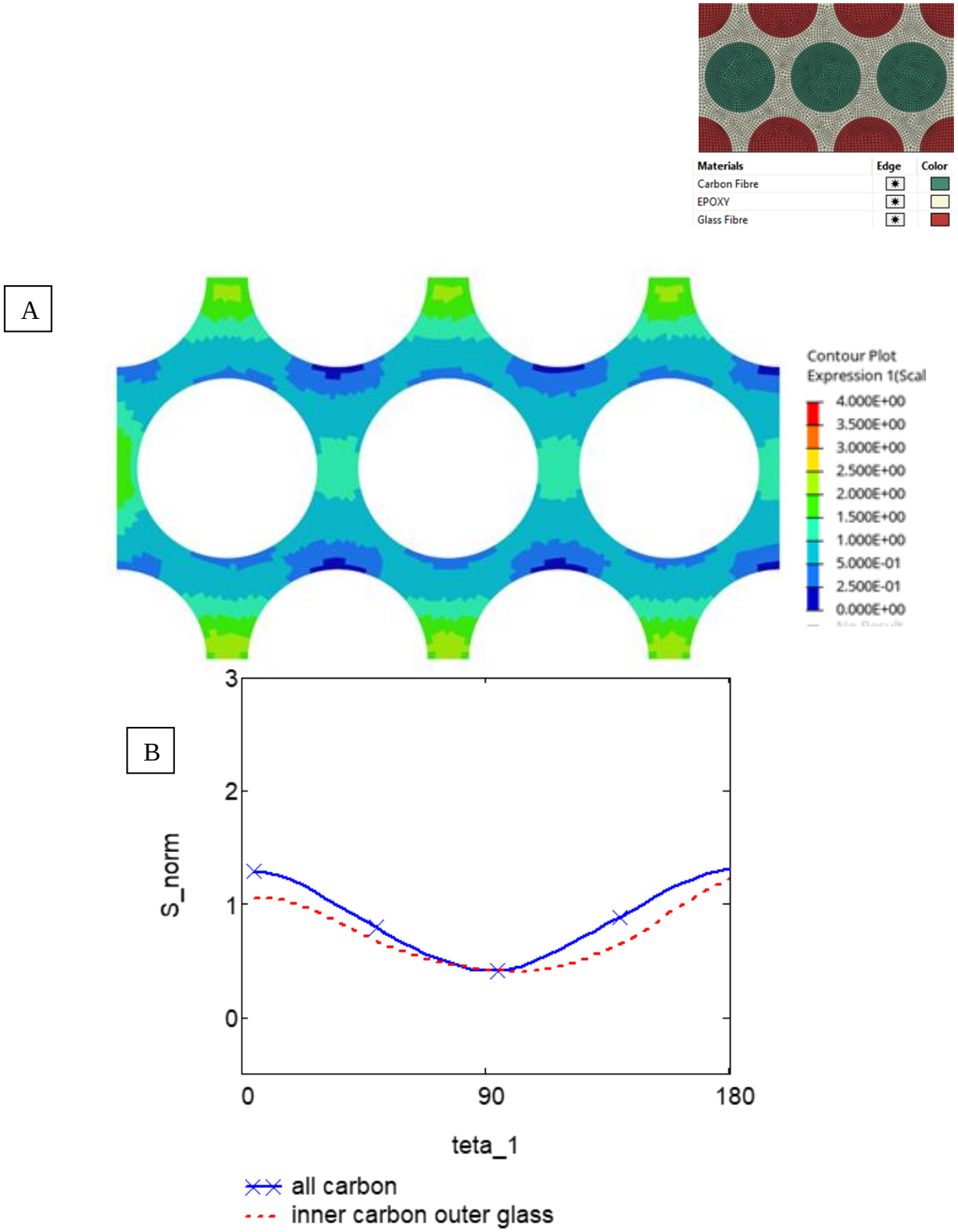

Figure 4.38 Triple hex hybrid composite results; (a)normalized contour plot for inner carbon material ;(b) stress concentration distribution regarding homogenous all carbon and hybrid inner row carbon cases

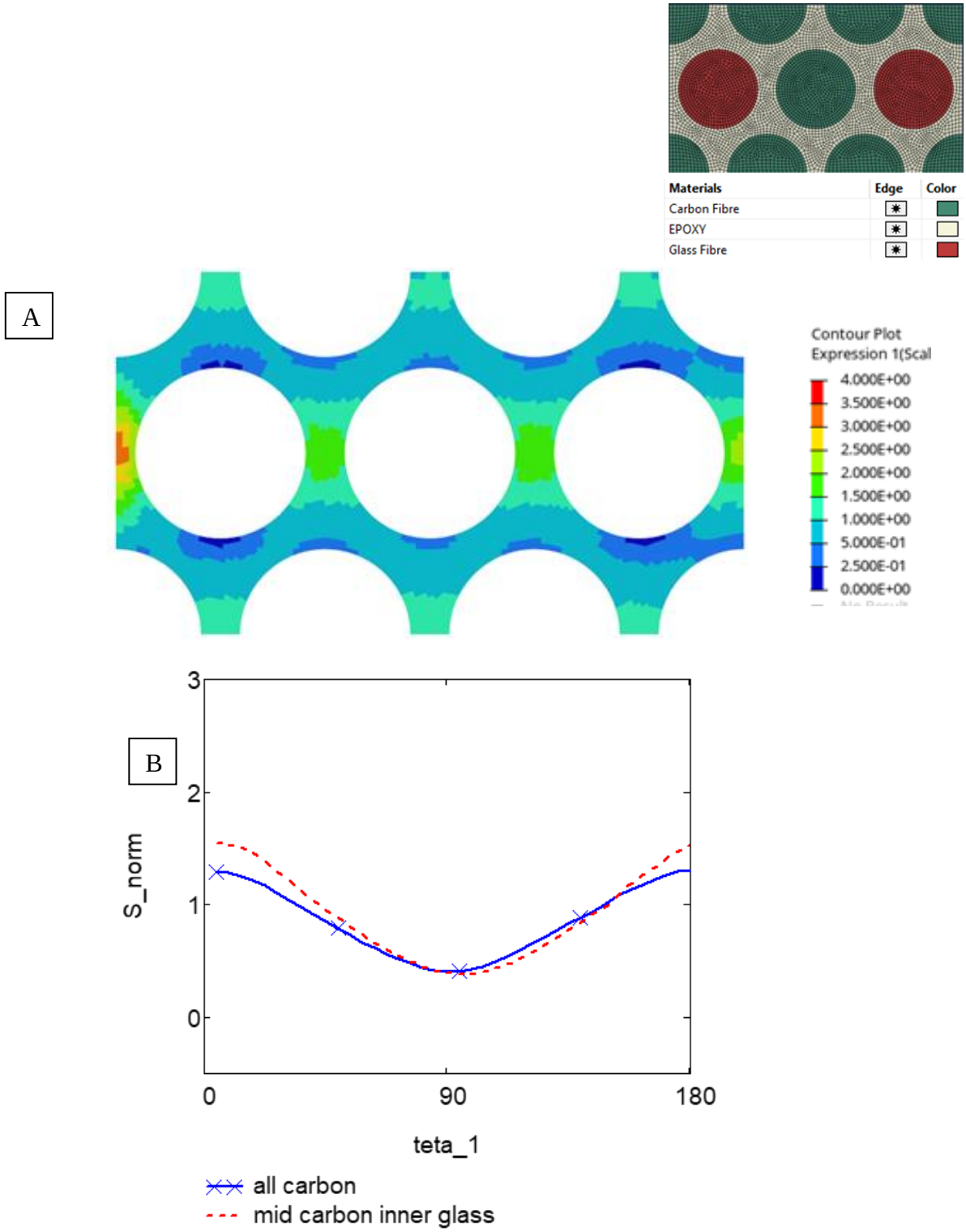

Figure 4.39 Triple hex hybrid composite results; (a)normalized contour plot for inner row glass and center fiber carbon material configuration ;(b) stress concentration distribution regarding homogenous all carbon and hybrid inner row glass and center fiber carbon material configuration cases

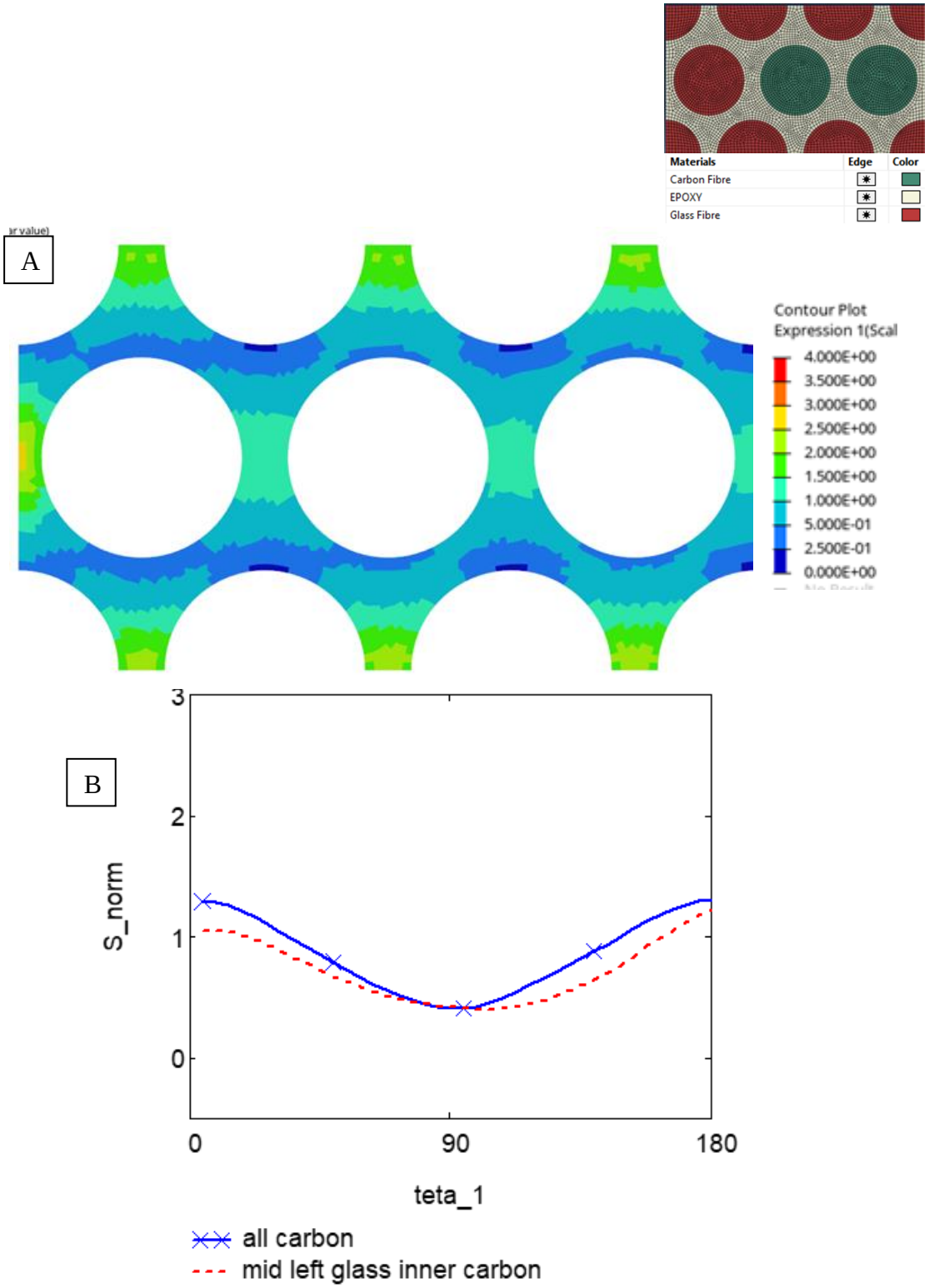

Figure 4.40 Triple hex hybrid composite results; (a)normalized contour plot for inner row 1 glass and 2 carbon fiber with carbon center fiber material configuration ;(b) stress concentration distribution regarding homogenous all carbon and hybrid inner row 1 glass and 2 carbon fiber with carbon center fiber material configuration cases

In Figure 4.38-Figure 4.40 stress concentration plots around carbon fiber with a variety of different fiber material combinations are given. Stiffer row explanation that is made before can be seen here too. This situation determines stress concentration around center fiber. When the inner row is set as carbon as in Figure 4.38, load carried by middle row decreases, and stress concentration around the center fiber decreases. On the contrary, when the upper and lower rows are set as carbon fiber and inner row set as glass fiber as in Figure 4.39, load carried by middle row increases and stress concentration around the middle fiber increases. In Figure 4.40 when two fibers in the middle row are set as carbon and load carried by that row decreases due to the different fiber material, a difference around center fiber occurs, and a decrease in stress concentration value can be observed.

Also, a summary table is given below in Table 4.8

Table 4.8 stress concentration values

Stress concentration	All glass 1	All carbon 2	Mid row glass 3	Mid row carbon 4	Mid row second fiberglass 5	Mid row first fiberglass 6	Mid row second fiber carbon 7	Mid row first fiber carbon 8
Zero degree	1.562	1.298	1.873	1.033	1.227	1.057	1.543	1.848
180 degree	1.567	1.308	1.853	1.003	1.221	1.219	1.532	1.537

Regarding results given in Table 4.8 mid, row glass&all glass comparison and mid row carbon & all carbon comparison, results strengthen the previous observations made with hexagonal RVE as changing outer fibers with stiffer fibers decreases the amount of load carried by the center fiber and decreases the stress concentration around the center fiber.

When we compare 2., 4. ve 7. Model's stiffer rows carry higher amount of loads than other rows; because of this, stress concentration in 7 is higher than 2, and it has the lowest in 4.

To summarize it is found that when stiffer fibers placed on upper and lower rows these rows carries higher load than middle row and stress concentration around center fiber decreases, effect of different fiber materials of neighboring fibers at middle row becomes minimal.

4.2. Random RVE Results

4.2.1. General Information about Random RVE Modeling & Results

In this section, results of the studies which are made with a variety of random RVE models have been revealed. In each section, normalized stress concentration plots and contour graphs are represented. In all of the studies represented here, stress concentration around selected fiber is employed, fiber configurations for each model given within the symbolic representation of each plot. Since inter-fiber distances are not exact and same in random models, all of the plots are drawn for 360 degrees. In these plots counter clockwise (CCW) path direction is employed.

4.2.2. Material Effect

Random RVE results of material effect are given under this heading. In these studies, radial stress results of a model with constant fiber radius are used. All of the results stated under this heading are the collection of stress data around the fiber, which is selected as taking the fiber with the highest stress value reached. Fiber volume ratio is set as $vf = 0.6$. In each model, material configuration is given with a colored small RVE stated in each analysis set. Figure 4.41 reveals results of homogenous RVE and used as a control group. In each of these plot, stress distribution is given for the fiber with largest stress concentration. Results for different combinations are shown in Figure 4.41- Figure 4.47.

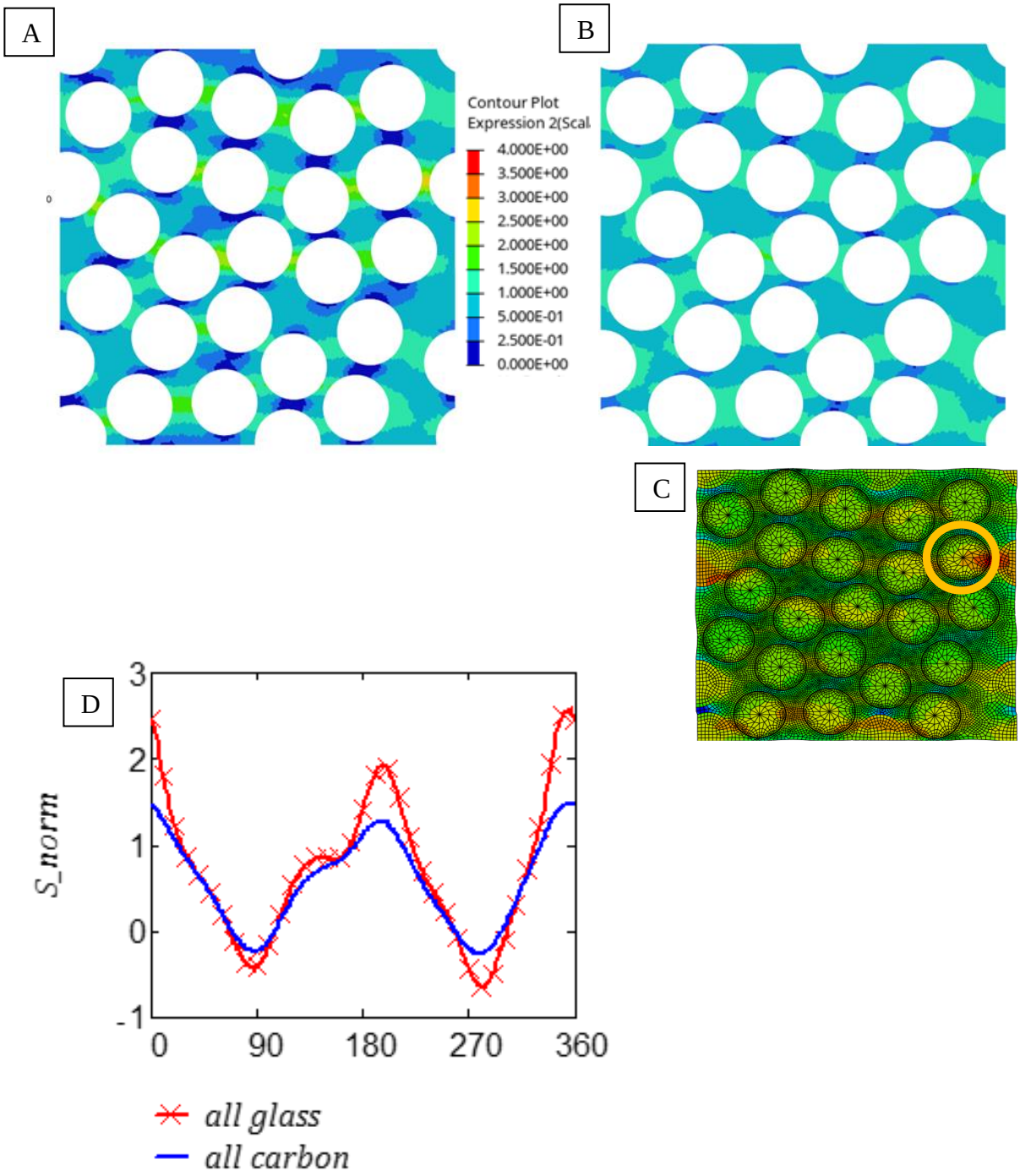

Figure 4.41 Random RVE homogenous results for the fibers with largest stress concentration: (a) all glass stress concentration contour plot; (b) all carbon stress distribution contour plot; (c) representation of selected fiber of which results in data are taken; (d) stress concentration distribution plots

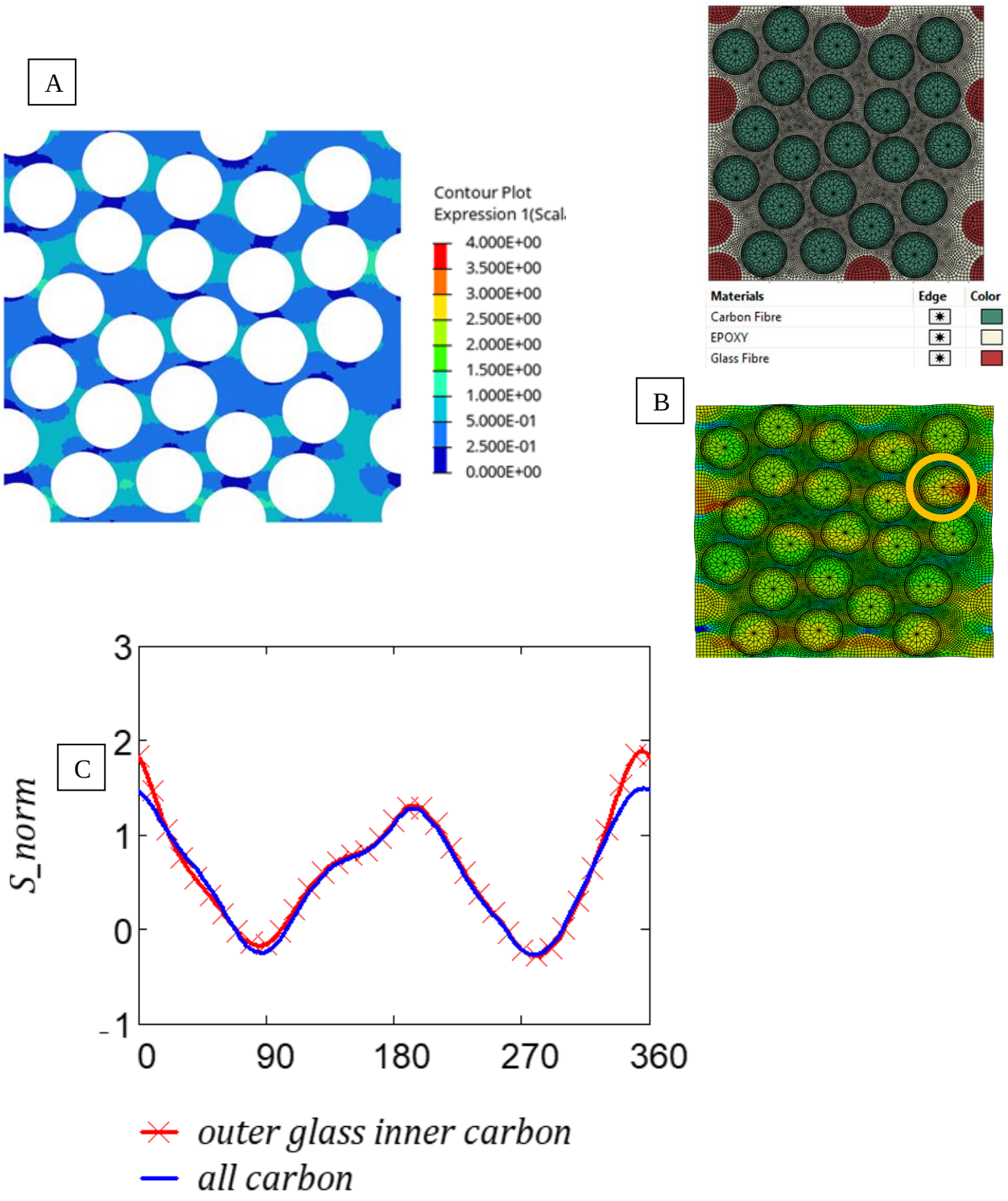

Figure 4.42 Random RVE hybrid results for the fiber with highest concentration: (a) outer glass fiber inner carbon fiber stress concentration contour plot; (b) representation of selected fiber of which results data are taken; (C) stress concentration distribution plots

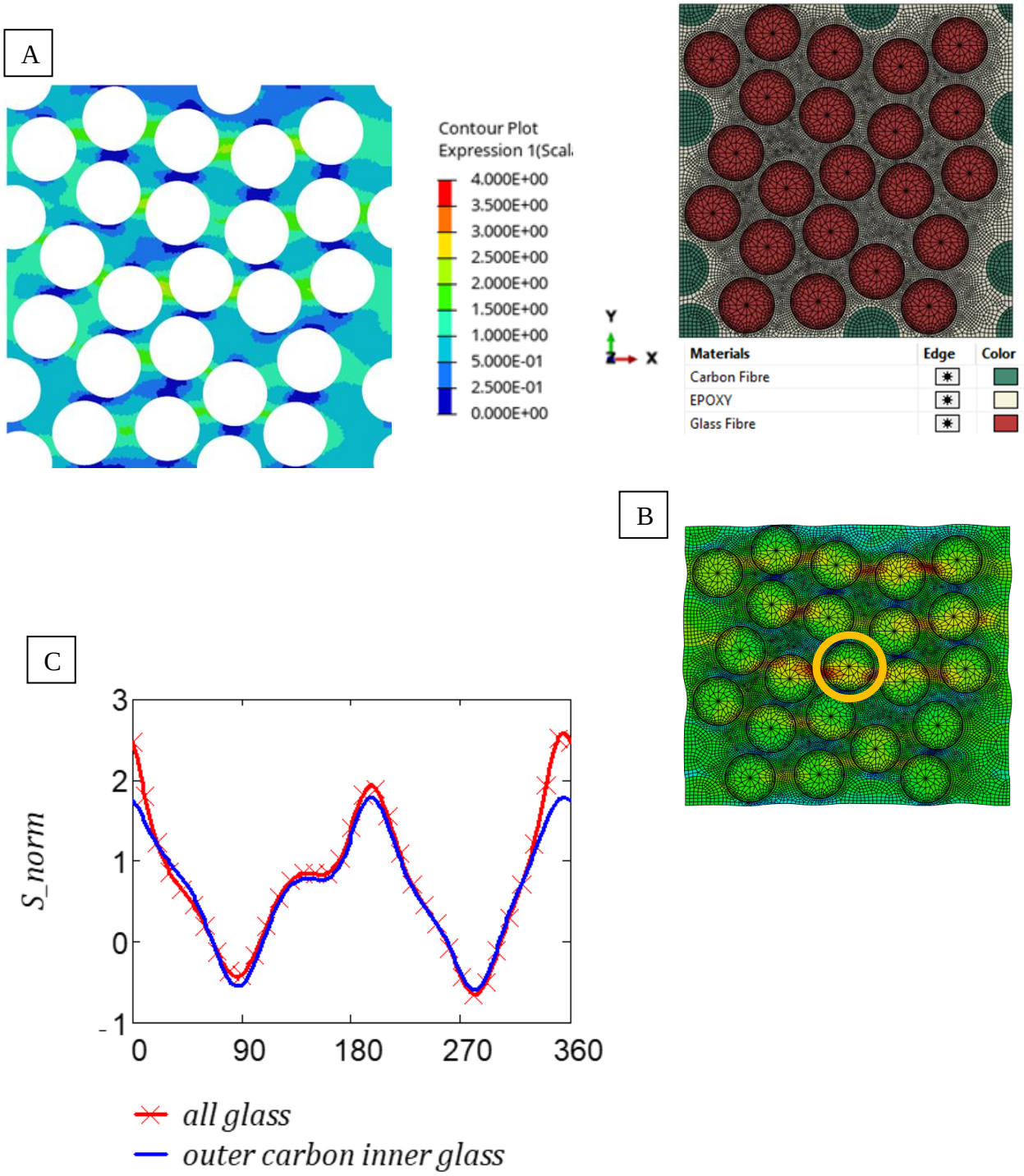

Figure 4.43 Random RVE hybrid composite studies: (a) outer carbon fiber inner glass fiber stress concentration contour plot; (b) representation of selected fiber of which results data are taken; (C) stress concentration distribution plots regarding outer carbon inner glass fiber and homogenous random all glass RVE's.

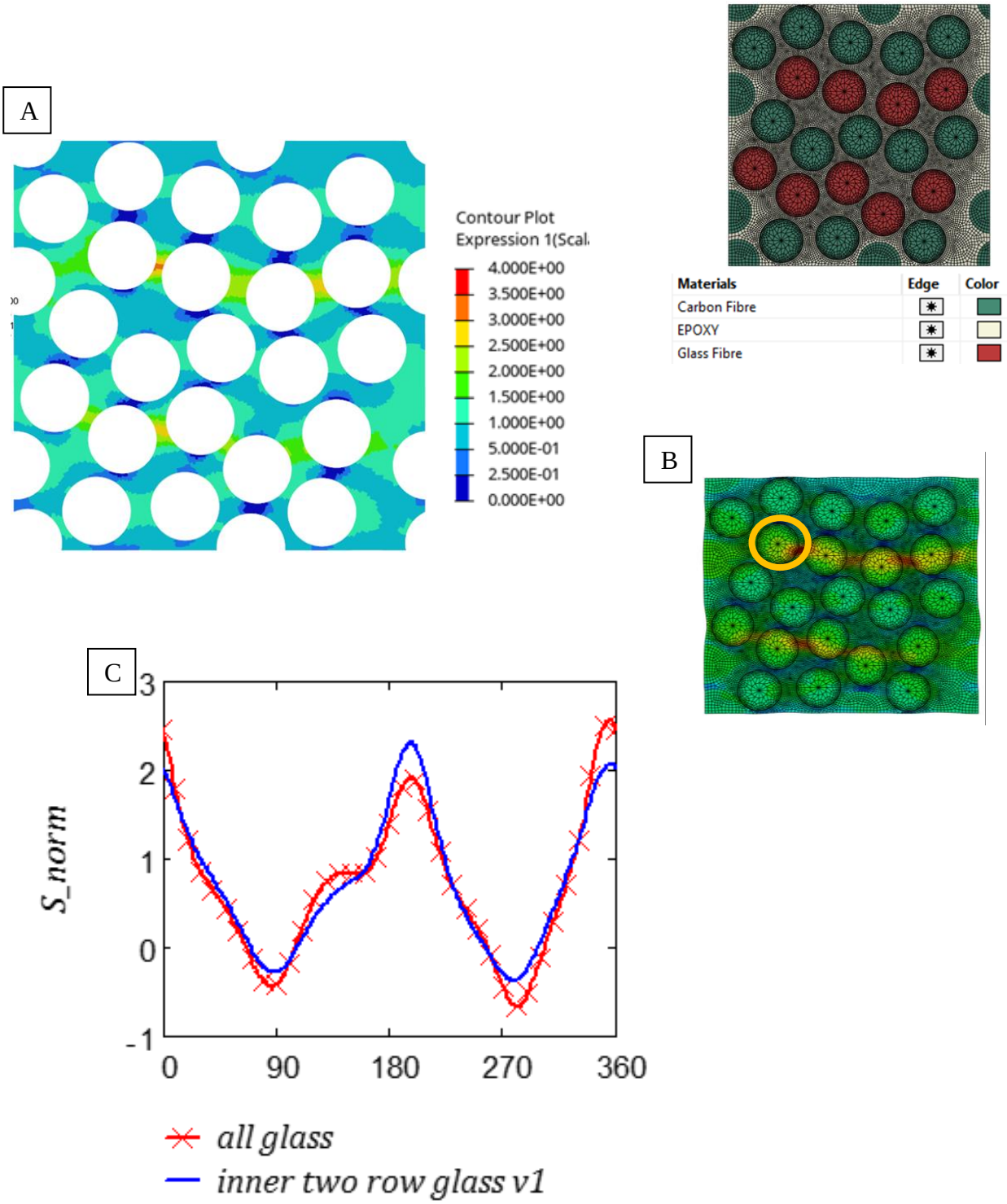

Figure 4.44 Random RVE hybrid results for the fiber with highest stress concentration: (a) inner two row glass fiber rest carbon fiber stress concentration contour plot; (b) representation of selected fiber of which results date is taken; (C) stress concentration distribution plots.

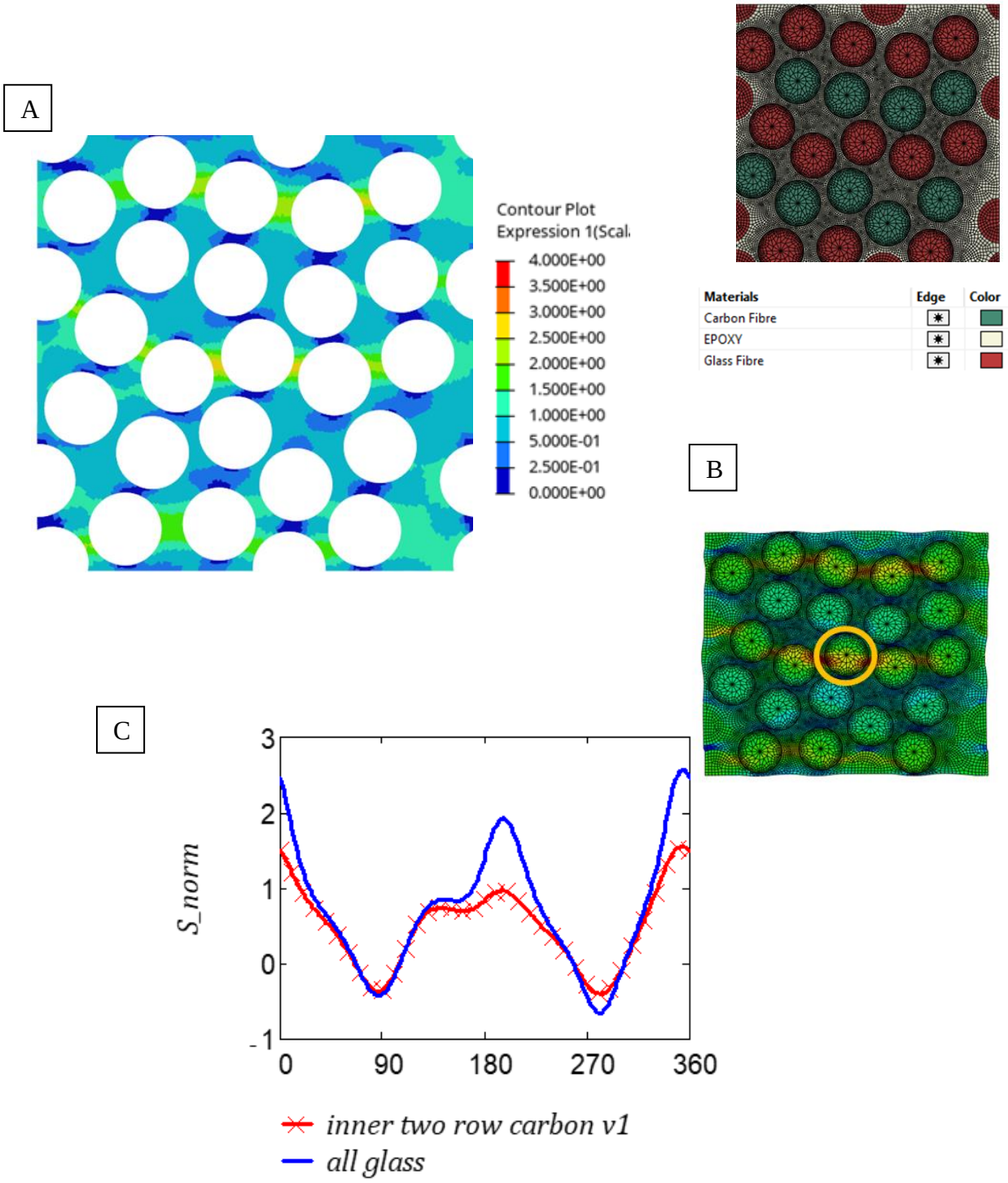

Figure 4.45 Random RVE hybrid results for the fiber with largest stress concentration: (a) inner two row carbon fiber rest glass fiber stress concentration contour plot; (b) representation of selected fiber of which results date is taken; (C) stress concentration distribution plots.

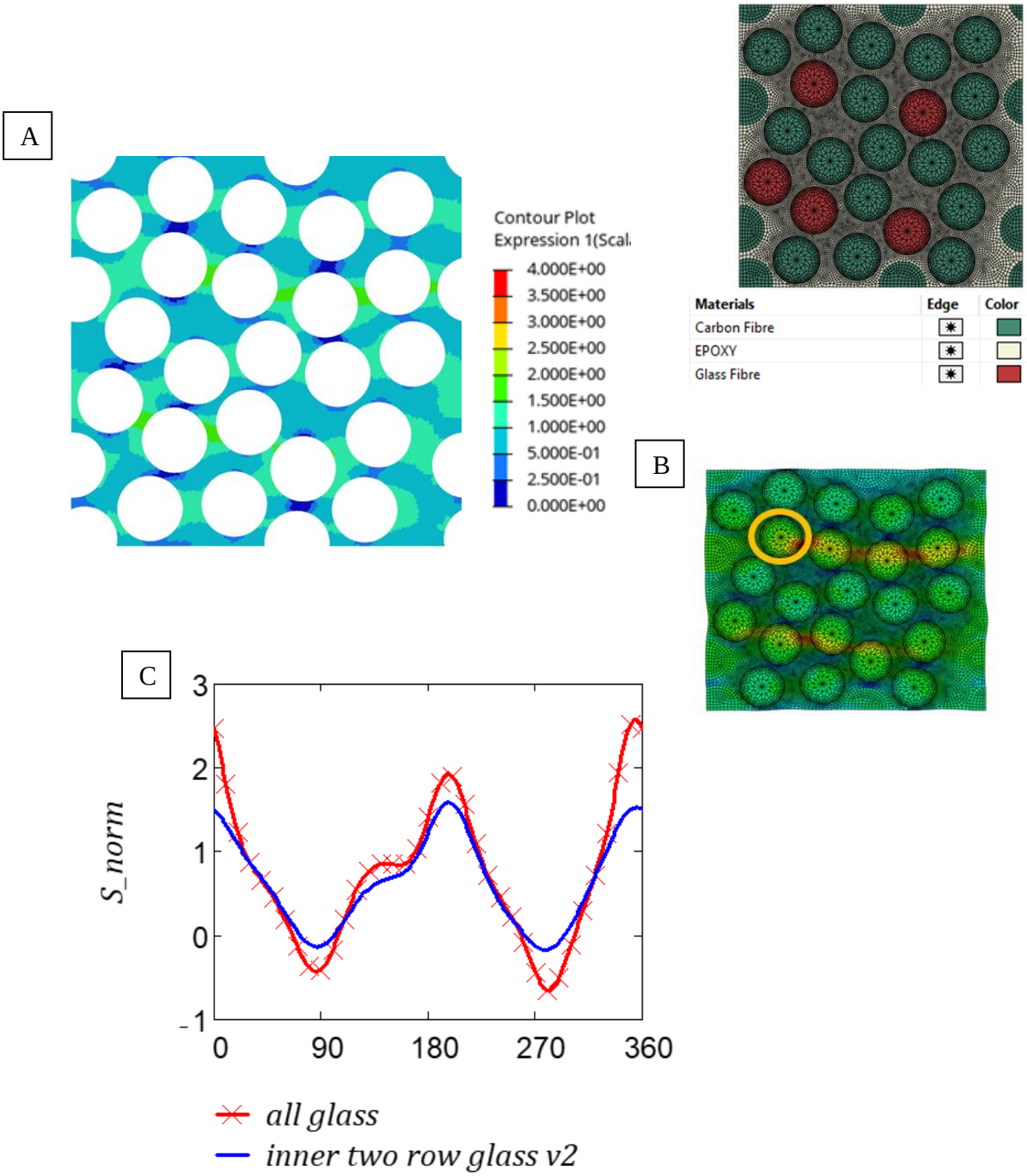

Figure 4.46 Random RVE hybrid results for the fiber with largest stress concentration: (a) inner randomly selected glass fibers rest carbon fiber stress concentration contour plot; (b) representation of selected fiber of which results date are taken; (C) stress concentration distribution plots.

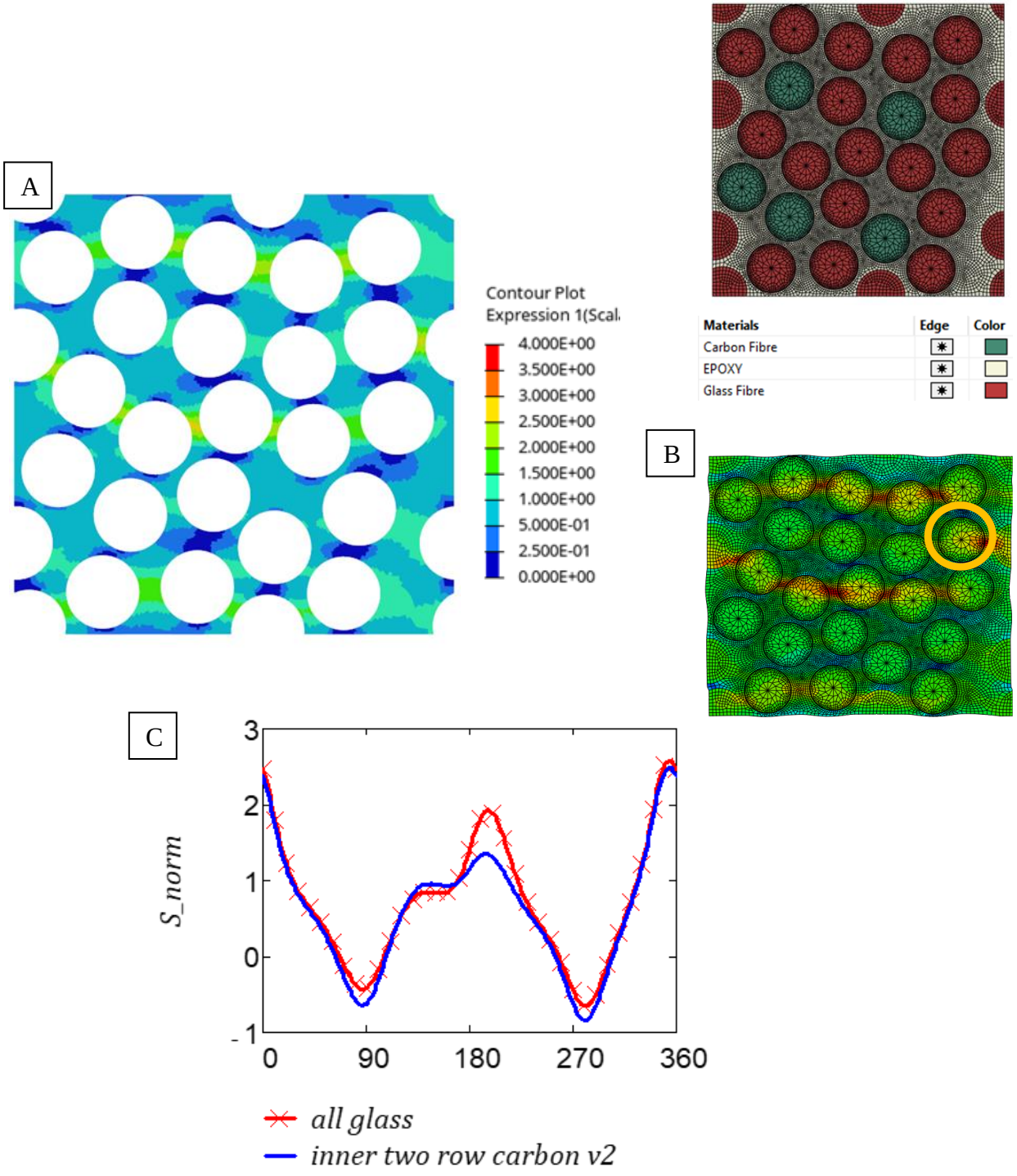

Figure 4.47 Random RVE hybrid results for the fiber with largest stress concentration:(a) inner randomly selected carbon fiber rest glass fiber stress concentration contour plot; (b) representation of

selected fiber of which results date are taken; (C) stress concentration distribution plots.

Results stated under this heading shows similar behavior with hexagonal RVE results under transverse loading, in Figure 4.42 highest concentration value is observed on a fiber that is near the stiffer outer carbon fiber, that is an expected result and stress concentration on the fiber is higher than homogenous all carbon composite. In Figure 4.43 inner fibers set stiffer as selecting glass and they carry higher amount of load, this creates a higher stress concentration than homogenous glass on the shown fiber. In Figure 4.44 inner two row set as glass this creates stiffer paths and load localizes on these rows so stress concentration distribution on one of shown the stiff fibers is higher than that of homogenous case. In Figure 4.45, stress concentration value of the selected fiber is lower than that of homogenous case due to the effect of carbon rows on amount of load carried by these fibers. In Figure 4.46, stress concentration distribution is lower than that of the homogenous case it can be assumed that lowering effect of carbon fibers are also observed here. In Figure 4.47, stress concentration distribution values are similar with that of homogenous glass case since number glass fiber to carbon fiber is high, effect of carbon fibers are minimal.

4.2.3. Fiber Volume Effect

Random RVE results of material effect with fiber volume ratio $vf = 0.4$ are given under this heading. In these studies, radial stress results of a model with constant fiber radius are used. All of the results stated under this heading are the collection of stress data around the fiber, which is selected as taking the fiber with the highest stress value reached. In each model, material configuration is given with a colored small RVE stated in each analysis set. Figure 4.48 reveals results of homogenous RVE. Homogenous RVE results and results of the models set with $vf = 0.6$ are used as control group. Similar to the previous case, since inter-fiber distances are not exact and same in random models, all of the plots are drawn for 360 degrees. Results for different combinations are shown in Figure 4.48-Figure 4.54.

A

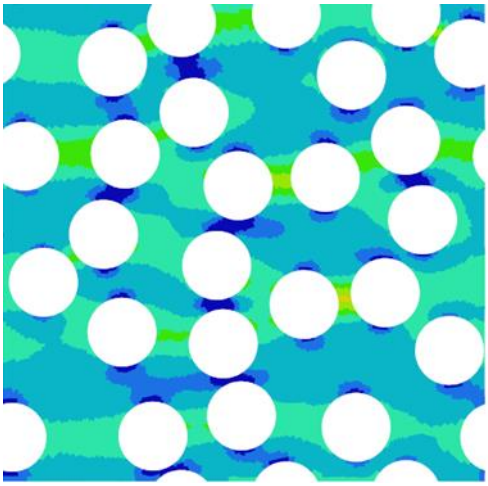

B

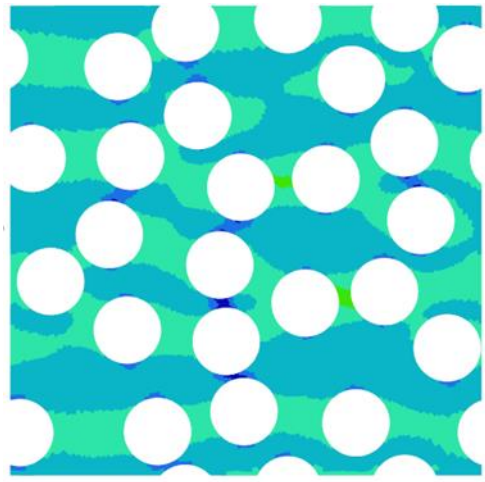

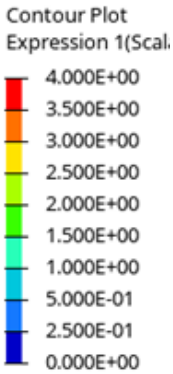
Contour Plot
Expression 1(Scal
4.000E+00
3.500E+00
3.000E+00
2.500E+00
2.000E+00
1.500E+00
1.000E+00
5.000E-01
2.500E-01
0.000E+00

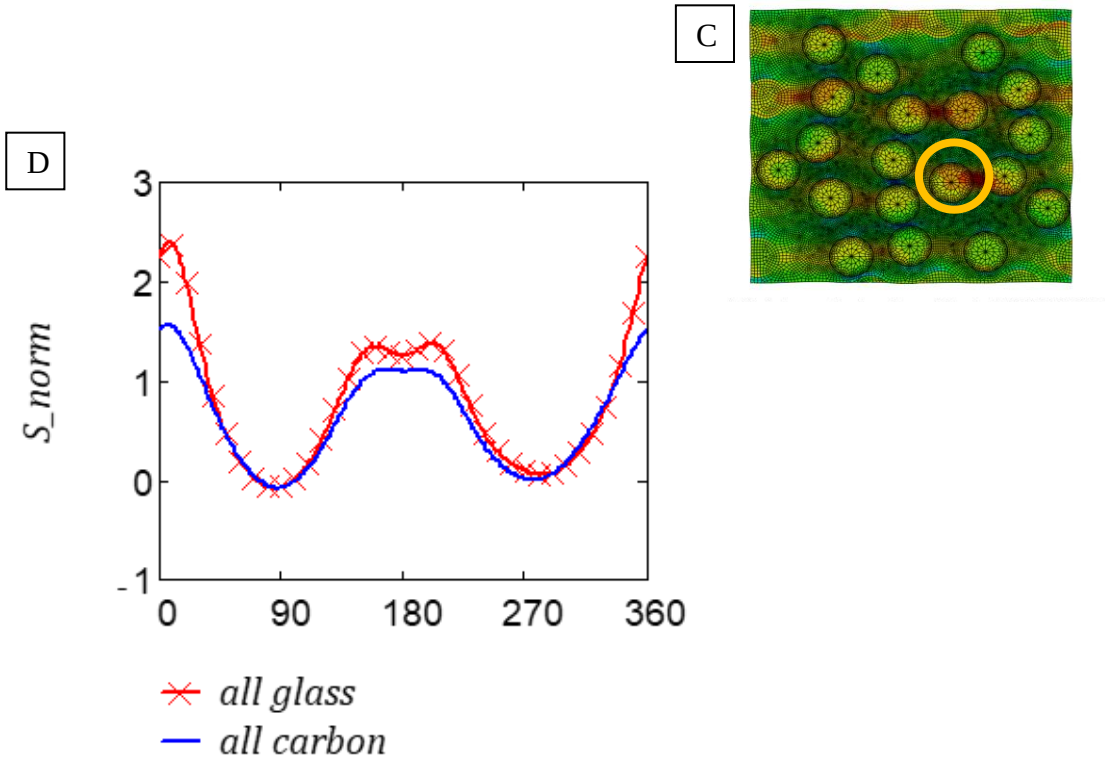

Figure 4.48 Random RVE homogenous results for the fibers with hghest stress concentration with fiber volume ratio is 0.4 : (a) all glass stress concentration contour plot; (b) all carbon stress distribution contour plot; (c) representation of selected fiber of which results date are taken; (d) stress concentration distribution plots.

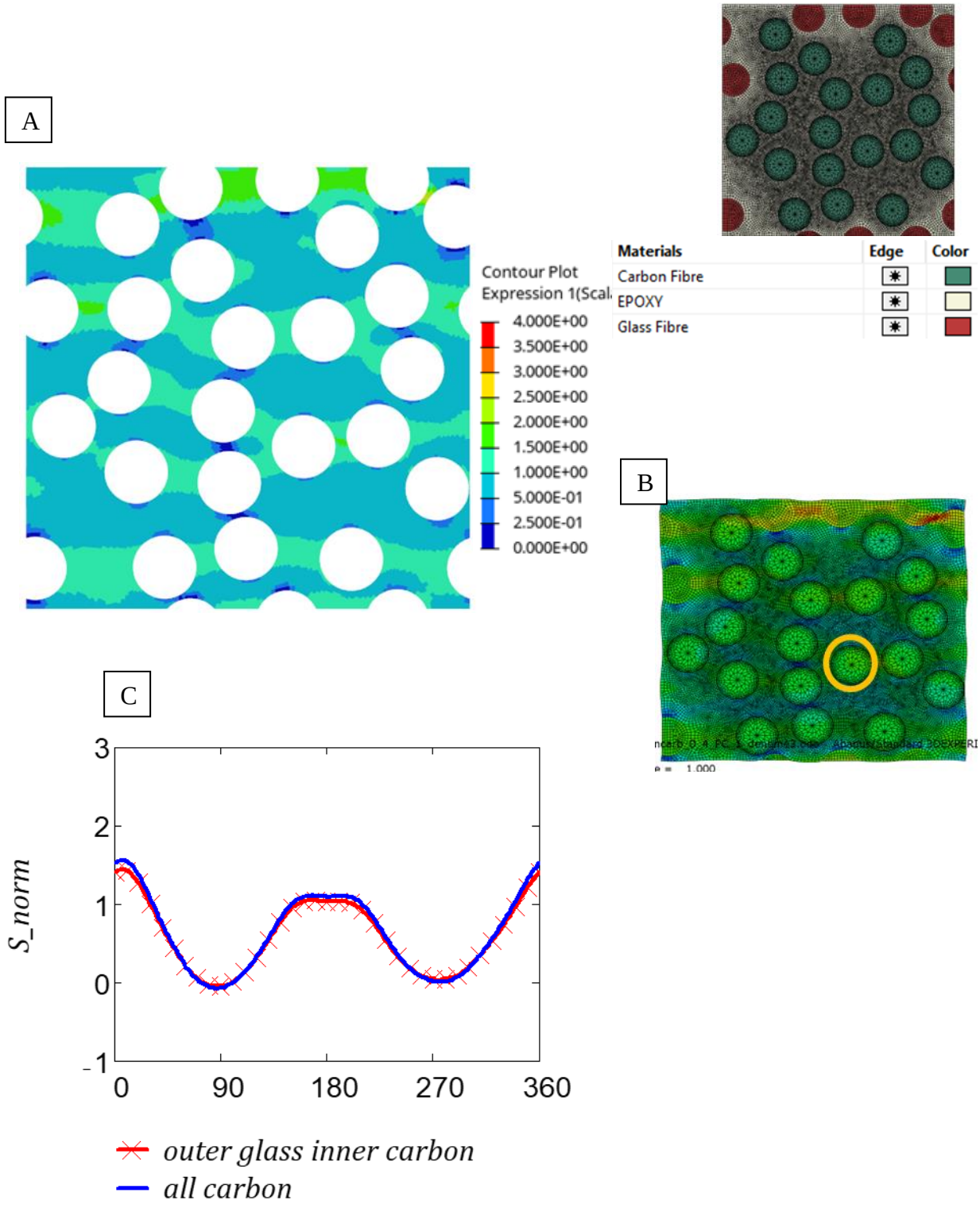

Figure 4.49 Random RVE hybrid results for the fibers with largest stress concentration with fiber volume ratio is 0.4 : (a) outer glass fiber inner carbon fiber stress concentration contour plot; (b) representation of selected fiber of which results date are taken; (C) stress concentration distribution plot.

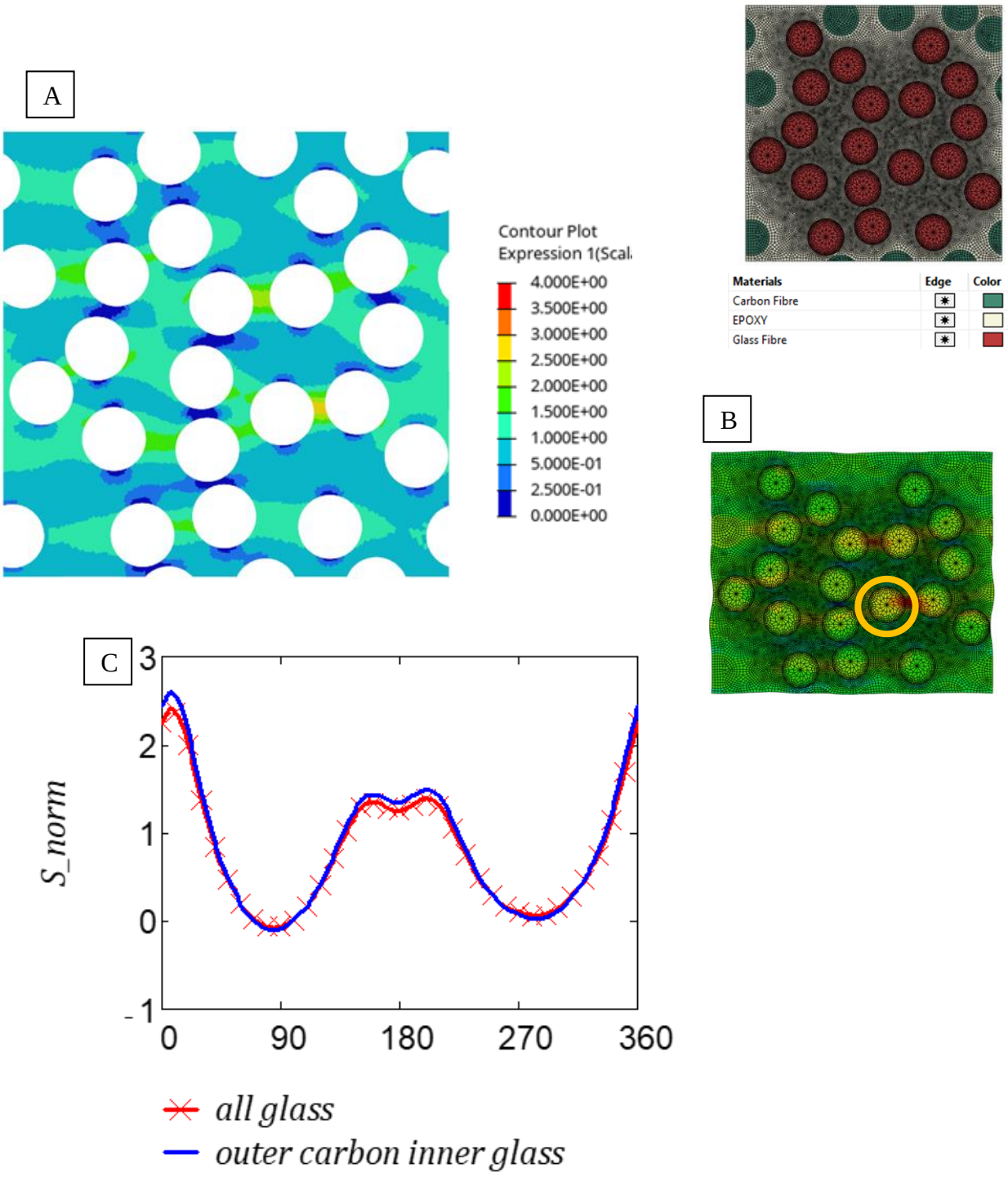

Figure 4.50 Random RVE hybrid results for the fibers with highest stress concentration with fiber volume ratio is 0.4 : (a) outer carbon fiber inner glass fiber stress concentration contour plot; (b) representation of selected fiber of which results date are taken; (C) stress concentration distribution plots.

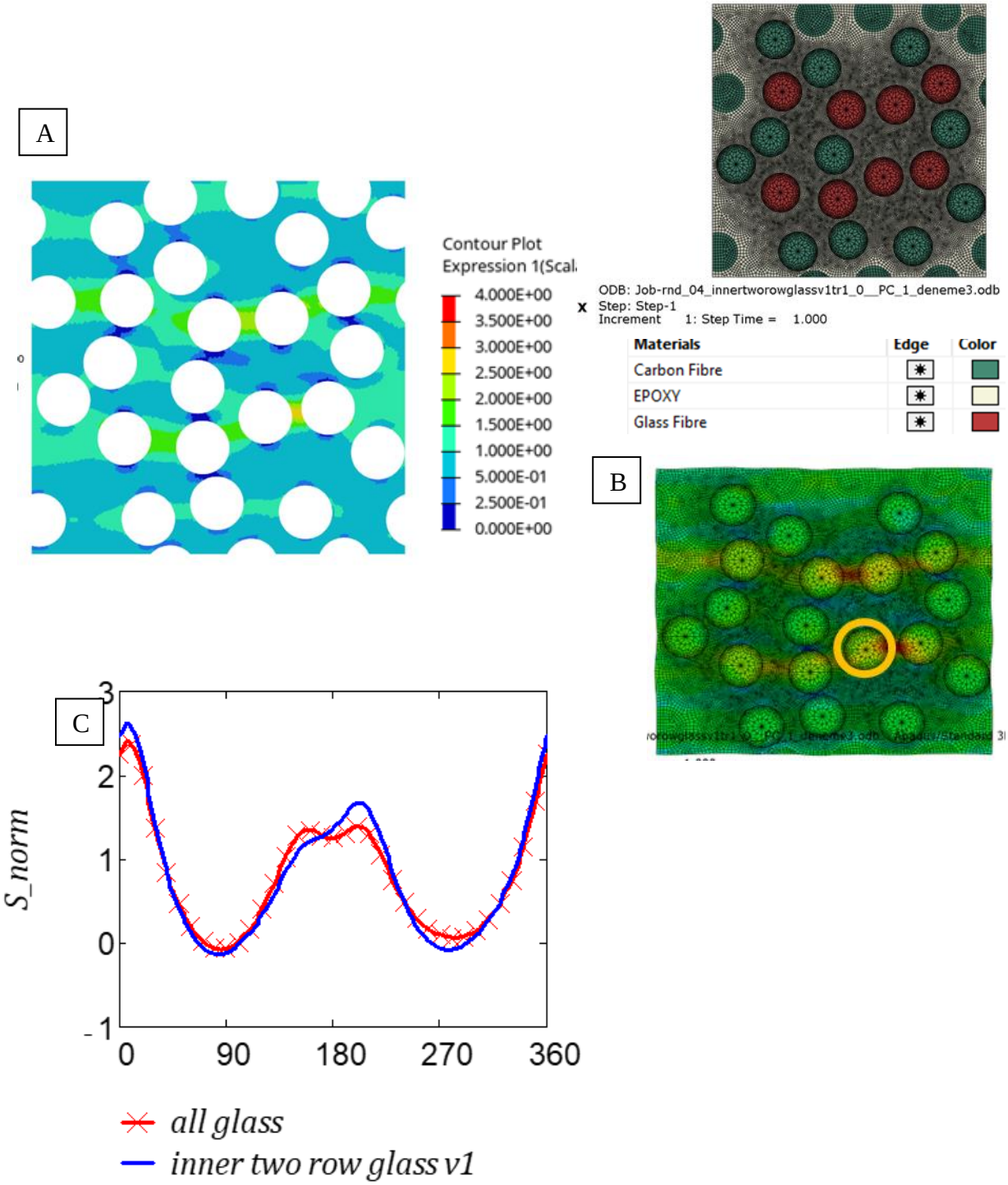

Figure 4.51 Random RVE hybrid results for the fibers with largest stress concentration with fiber volume ratio 0.4: (a) inner two row glass fiber rest carbon fiber stress concentration contour plot; (b) representation of selected fiber of which results data are taken; (C) stress concentration distribution plot.

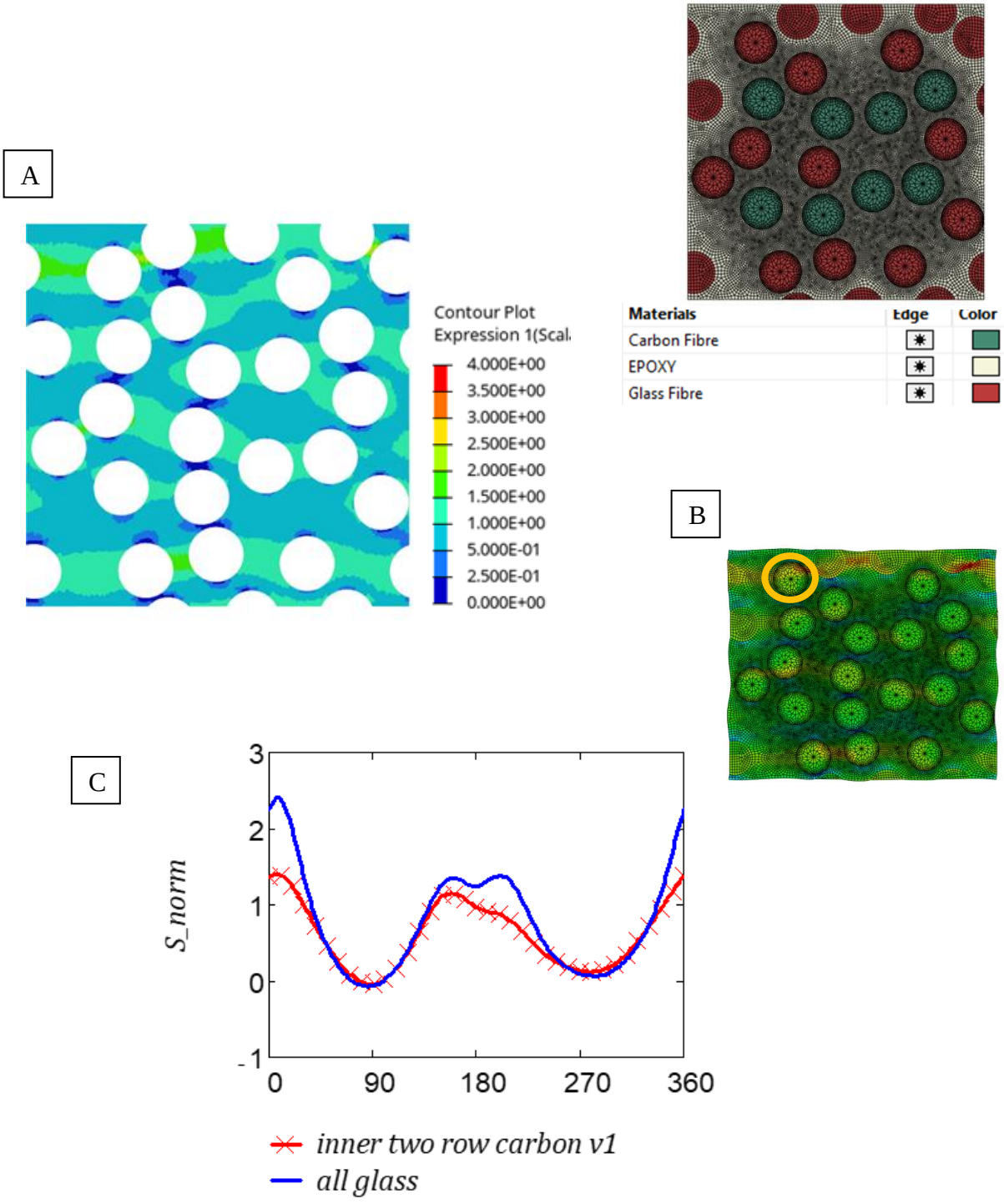

Figure 4.52 Random RVE hybrid results for the fiber with highest stress concentration with fiber volume ratio 0.4: (a) inner two row carbon fiber rest glass fiber stress concentration contour plot; (b) representation of selected fiber of which results data are taken; (C) stress concentration distribution plots.

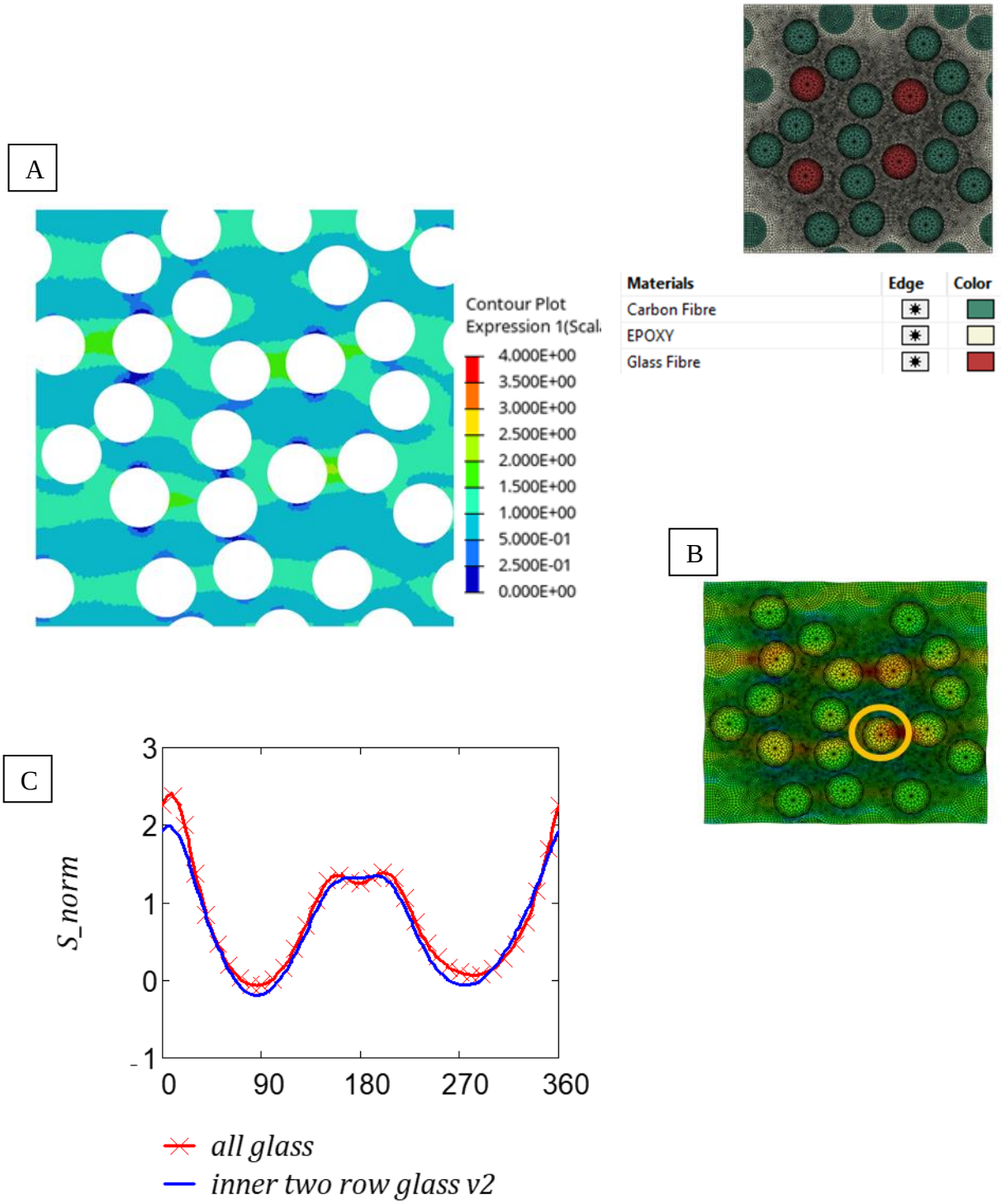

Figure 4.53 Random RVE hybrid results for the fibers with highest stress concentration with fiber volume ratio 0.4 : (a) inner randomly selected glass fibers rest carbon fiber stress concentration contour plot; (b) representation of selected fiber of which results data are taken; (C) stress concentration distribution plots.

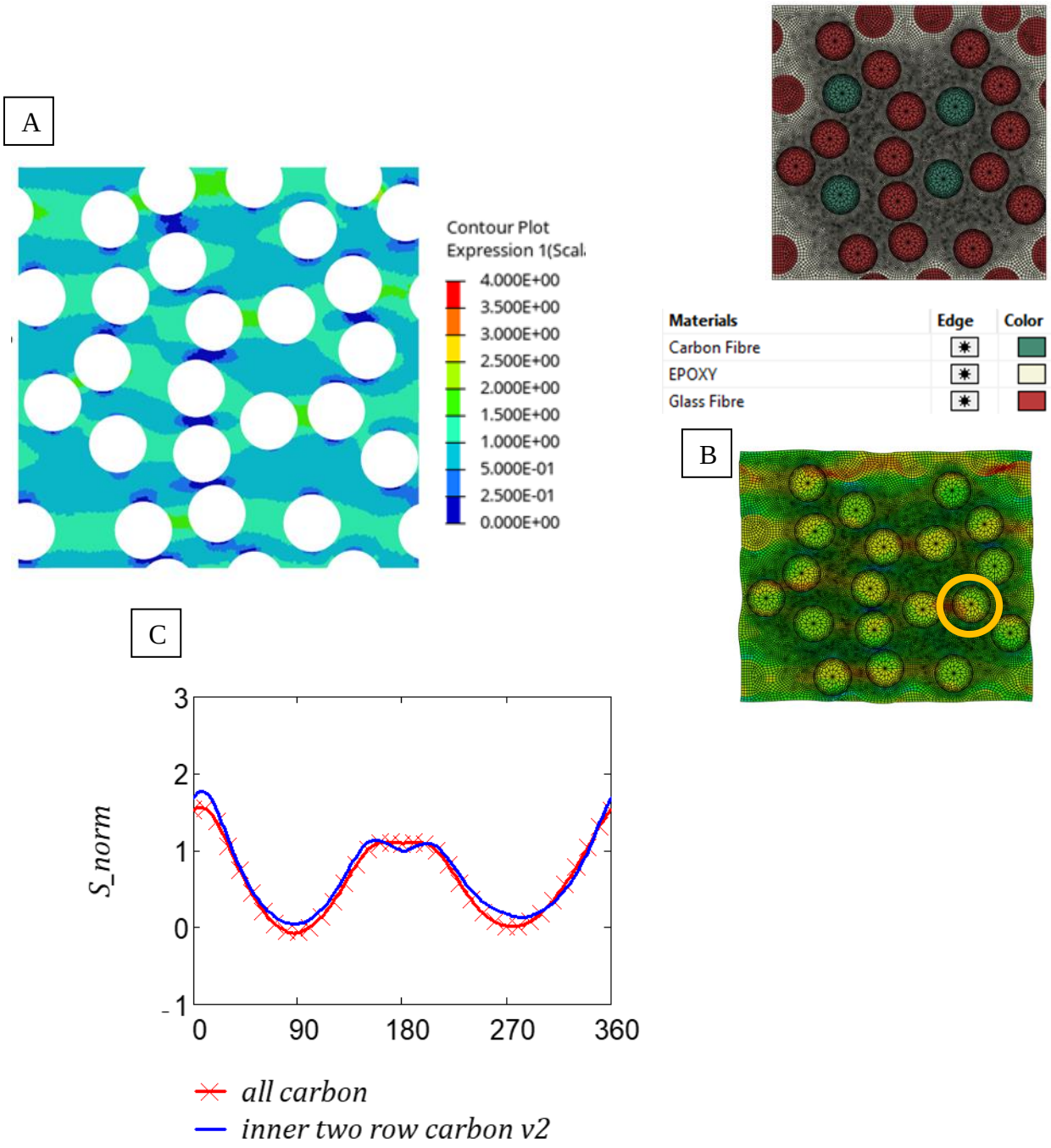

Figure 4.54 Random RVE hybrid results for the fibers with highest stress concentration with fiber volume ratio 0.4: (a) inner randomly selected carbon fibers rest glass fiber stress concentration contour plot; (b) representation of selected fiber of which results data are taken; (C) stress concentration distribution plots

Results show a decrease in hybridization effect due to the decreased fiber volume ratio. Similar observation with the ones of which fiber volume ratio set as 0.6 can be observed in all of the results. Due to the effect of low fiber volume ratio and low hybridization effect, difference in stress concentration values is lower and in most of the stress concentration distribution plots behavior of stress distribution around fiber shows a behavior that is in agreement with homogenous cases. In Figure 4.49 concentration value is almost same with homogenous case effect of the stiffer outer carbon fiber is minimal. In Figure 4.50 inner fibers set stiffer as selecting glass, but stress concentration value difference is minimal. In Figure 4.51 inner two row set as glass, stiffening effect of these rows can be observed as an increase in stress concentration distributions. In Figure 4.52, stress concentration value of the selected fiber is lower than that of homogenous case due to the effect of neighboring carbon fiber on amount of load carried by these fibers decreases. In Figure 4.53, stress concentration distribution is lower than that of the homogenous case it can be assumed that lowering effect of carbon fibers are also observed here but behavior is the same with homogenous case. In Figure 4.54, stress concentration distribution values are similar with that of homogenous glass case since number glass fiber to carbon fiber is high, effect of carbon fibers are minimal but an increase on stress concentration value of the selected fiber can be observed.

4.2.4. Fiber radius Effect

Random RVE results of fiber radius effect with varying fiber radius are given under this heading. In these studies, radial stress results of a variety of fibers are given. All of the results stated under this heading is the collection of stress data around a set of fiber that are selected as taking the fiber with the highest stress value reached. In general, 4 carbon and 4 glass fiber are selected each fiber is numbered as given in Figure 4.55. In each result case, fiber number stated in plot headings. Fiber volume ratio is set as $vf = 0.6$. In each model, material configuration is given with a colored small RVE stated in each figure. Figure 4.56 reveals results of homogenous RVE and used as a control group. Results for different combinations are shown in Figure 4.56-Figure 4.60. Identification of each investigated fiber can be seen in Figure 4.55.

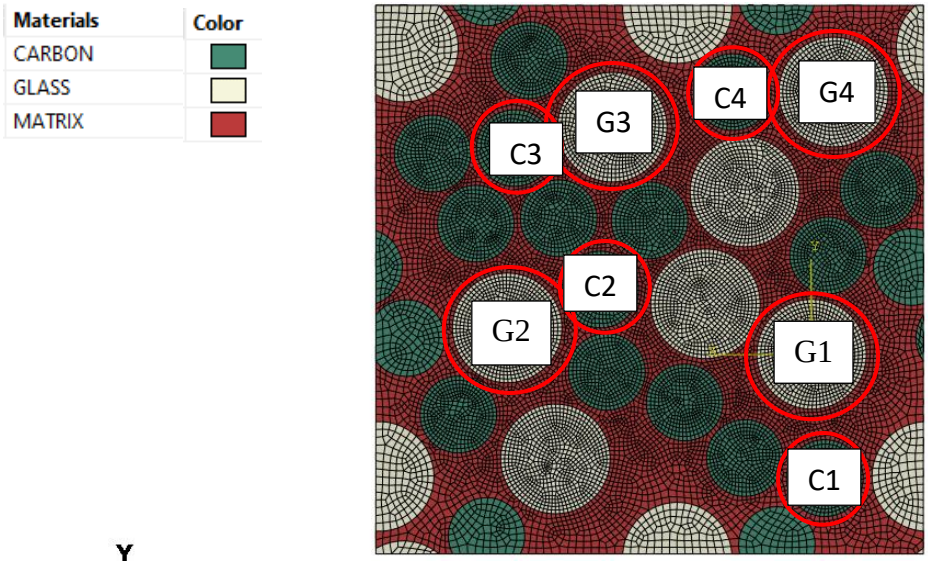

Figure 4.55 Representation of random RVE with varying fiber radius, selected fibers of which results are revealed.

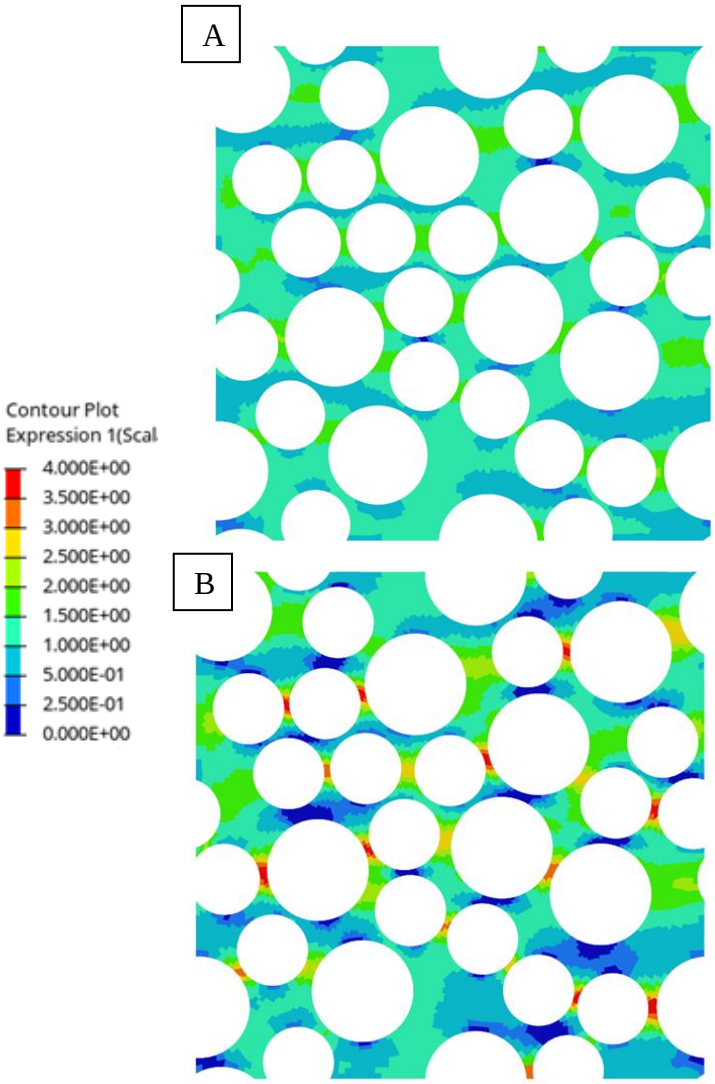

Figure 4.56 Random RVE with varying radius contour plots: (a) all carbon material; (b) all glass material.

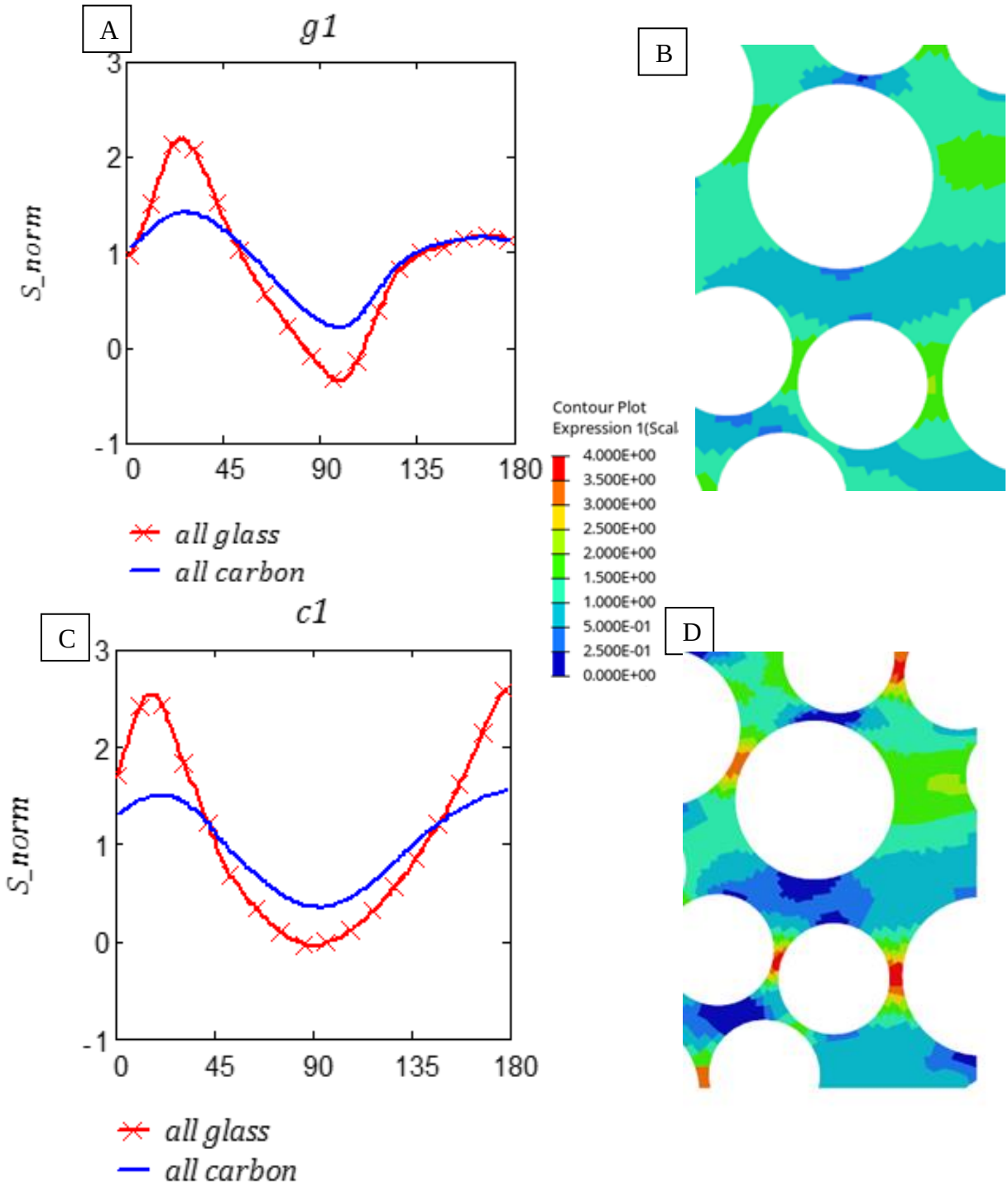

Figure 4.57 Results of Random RVE varying fiber radius g1-c1 : (a) stress concentration distribution plot for g1,comparing with all glass and all carbon ;(b)all carbon contour plot for g1-c1 region;(c) stress concentration distribution plot for c1,comparing with all glass and all carbon ;(b)all carbon contour plot for g1-c1 region ;(d)) all glass contour plot for g1-c1 region

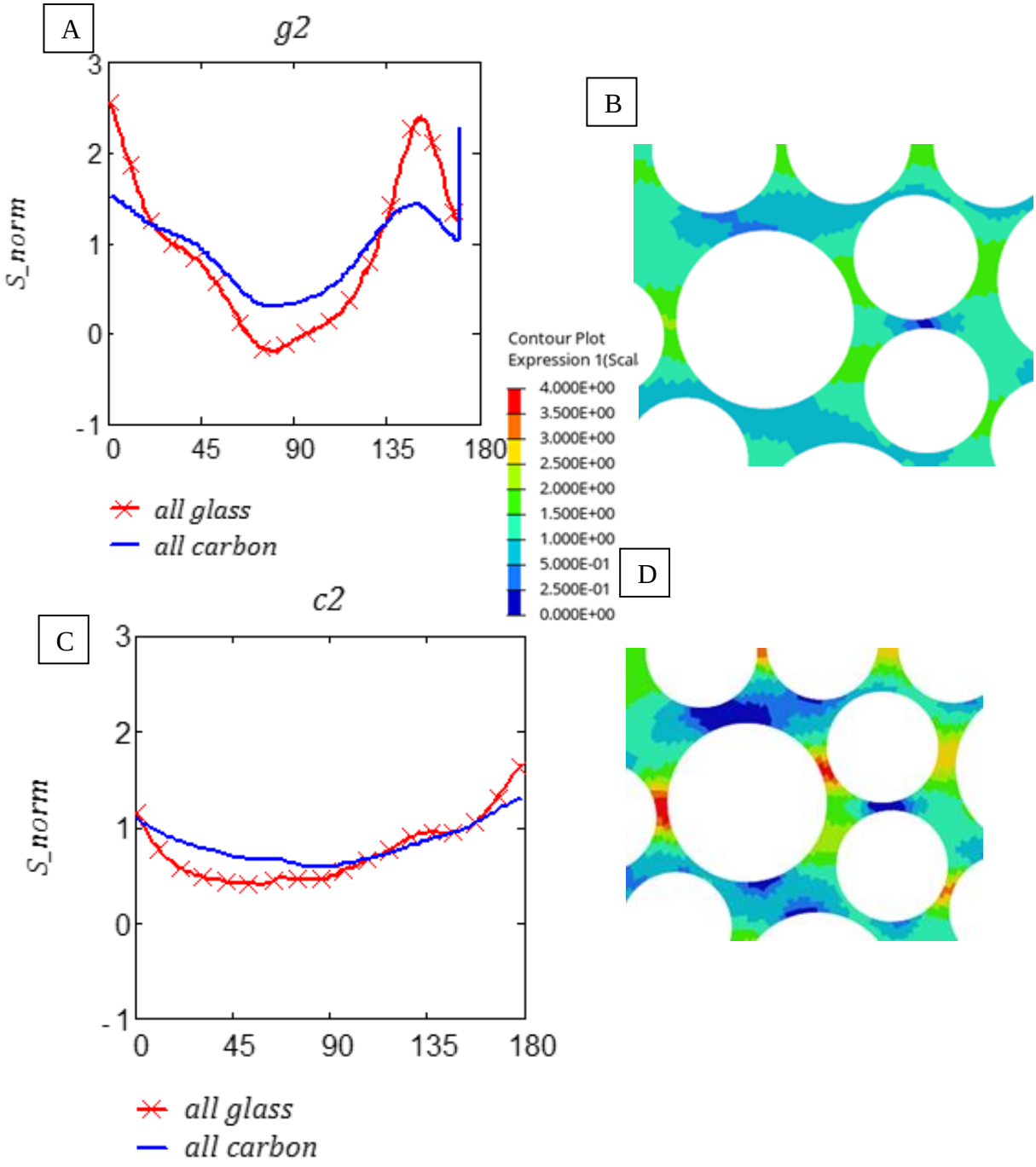

Figure 4.58 Results of Random RVE varying fiber radius g2-c2 : (a) stress concentration distribution plot for g2, comparing with all glass and all carbon ;(b)all carbon contour plot for g2-c2 region;(c) stress concentration distribution plot for 21, comparing with all glass and all carbon ;(b)all carbon contour plot for g2-c2 region ;(d)) all glass contour plot for g2-c2 region

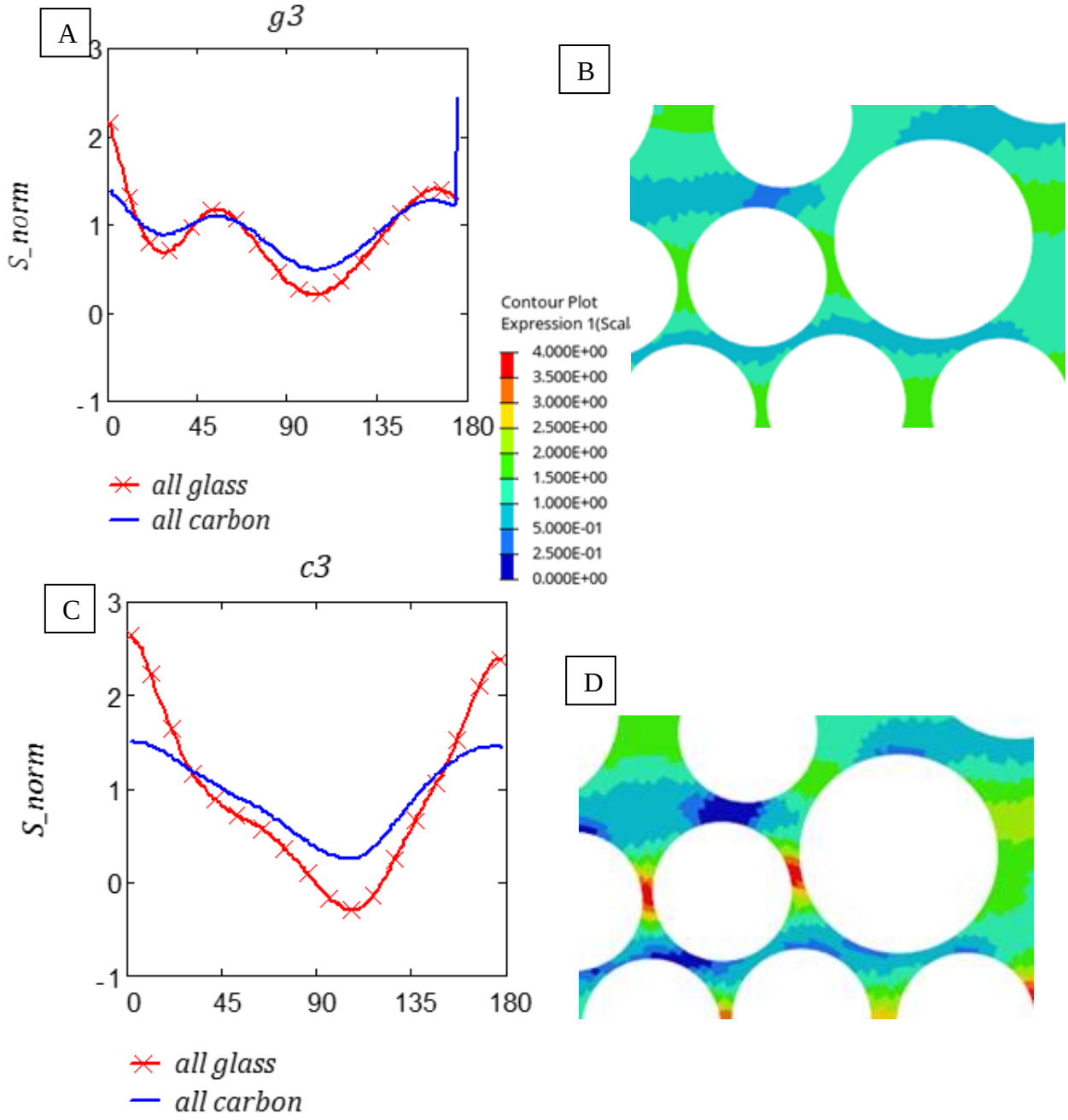

Figure 4.59 Results of Random RVE varying fiber radius g3-c3 : (a) stress concentration distribution plot for g3,comparing with all glass and all carbon ;(b)all carbon contour plot for g3-c3 region;(c) stress concentration distribution plot for c3,comparing with all glass and all carbon ;(b)all carbon contour plot for g3-c3 region ;(d)) all glass contour plot for g3-c3 region

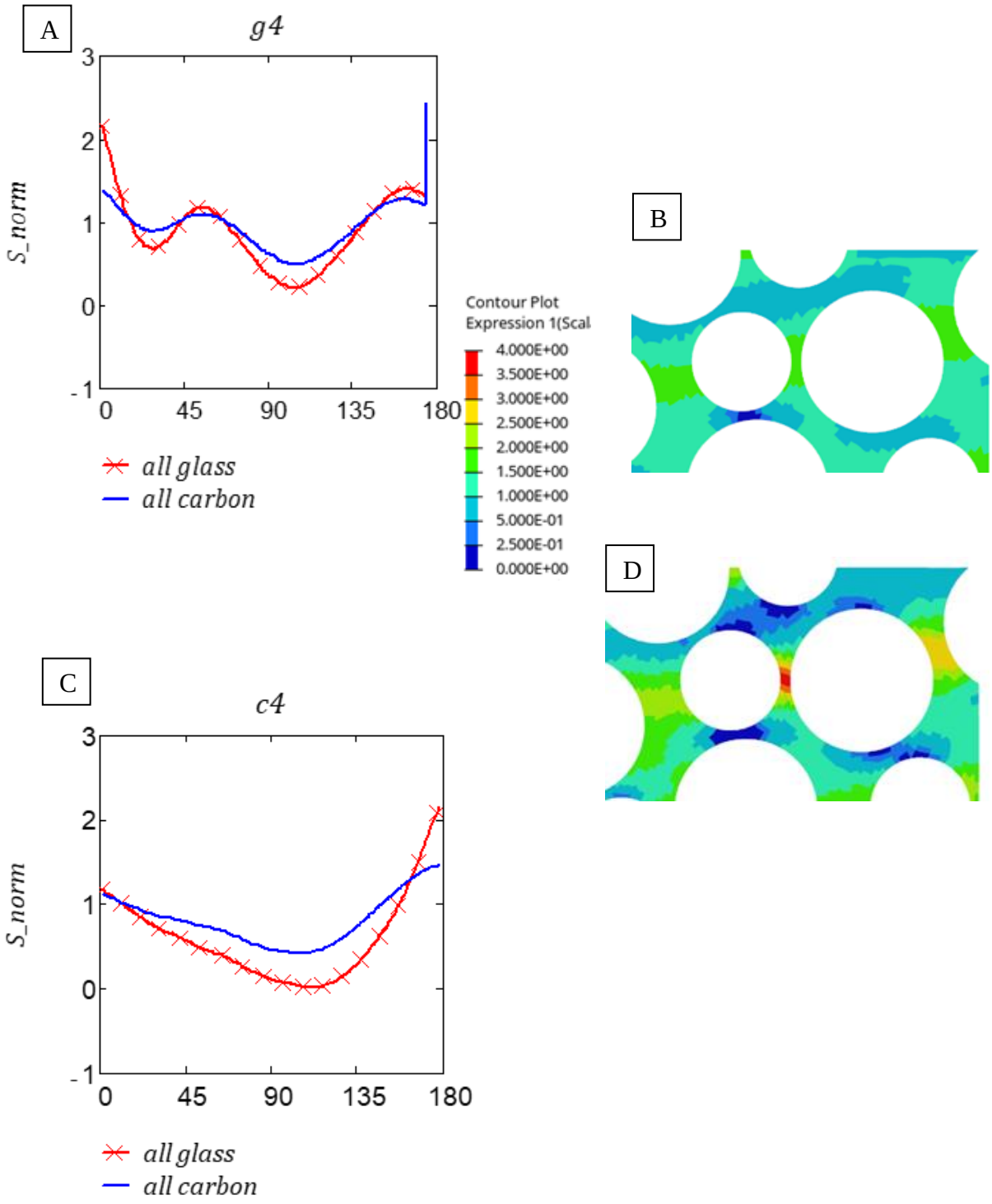

Figure 4.60 Results of Random RVE varying fiber radius g4-c4 : (a) stress concentration distribution plot for g4,comparing with all glass and all carbon; (b)all carbon contour plot for g4-c4 region;(c) stress concentration distribution plot for c4,comparing with all glass and all carbon ;(b)all carbon contour plot for g4-c4 region ;(d)) all glass contour plot for g4-c4 region

When the results of random RVE with varying radius regarded following observations can be made. In Figure 4.57, Figure 4.58, Figure 4.59 and Figure 4.60 when fiber material set as glass load carried by fibers becomes more significant than that of all fibers set as carbon in terms of material. Because of this situation in all of the data it can be seen that stress concentration distribution values becomes higher when all fiber material set as glass. In Figure 4.58, Figure 4.59 and Figure 4.60 a jump in plots (a) can be observed when all materials set as carbon, but this jump doesn't observed in stated figures plots (b) contour graphs so it can be concluded that this jump can be caused by an error at data extraction stage. Regarding results given above it can be stated that, inter fiber distance has an important role on stress concentration regarding fiber radius effect. For the g2&c2 and g4&c4, there is successive amount of distance between fibers and effect of higher load carrying capacity and high stress concentration around fiber with bigger radius can be observed. On the other hand, for the g3&c3 and g1&c1 inter fiber distances are not sufficient and fibers become to interact and stress concentration on smaller fibers becomes higher.

4.2.5. Fiber Radius and Material Combined Effect

Random RVE results of combination of fiber radius effect and combination of material effect with varying fiber radius are given under this heading. Similarly to previous case, stress results of a variety of fibers are given. All of the results stated under this heading is the collection of stress data around a set of fiber that are selected as taking the fiber with the highest stress value reached. In general, 4 carbon and 4 glass fiber are selected each fiber is numbered as given in Figure 4.55. This fiber numbering is utilized while giving results. In each result case, fiber number stated in plot headings In model fiber volume ratio is set as $vf = 0.6$. In each model, material configuration is given with a colored small RVE stated in each figure.

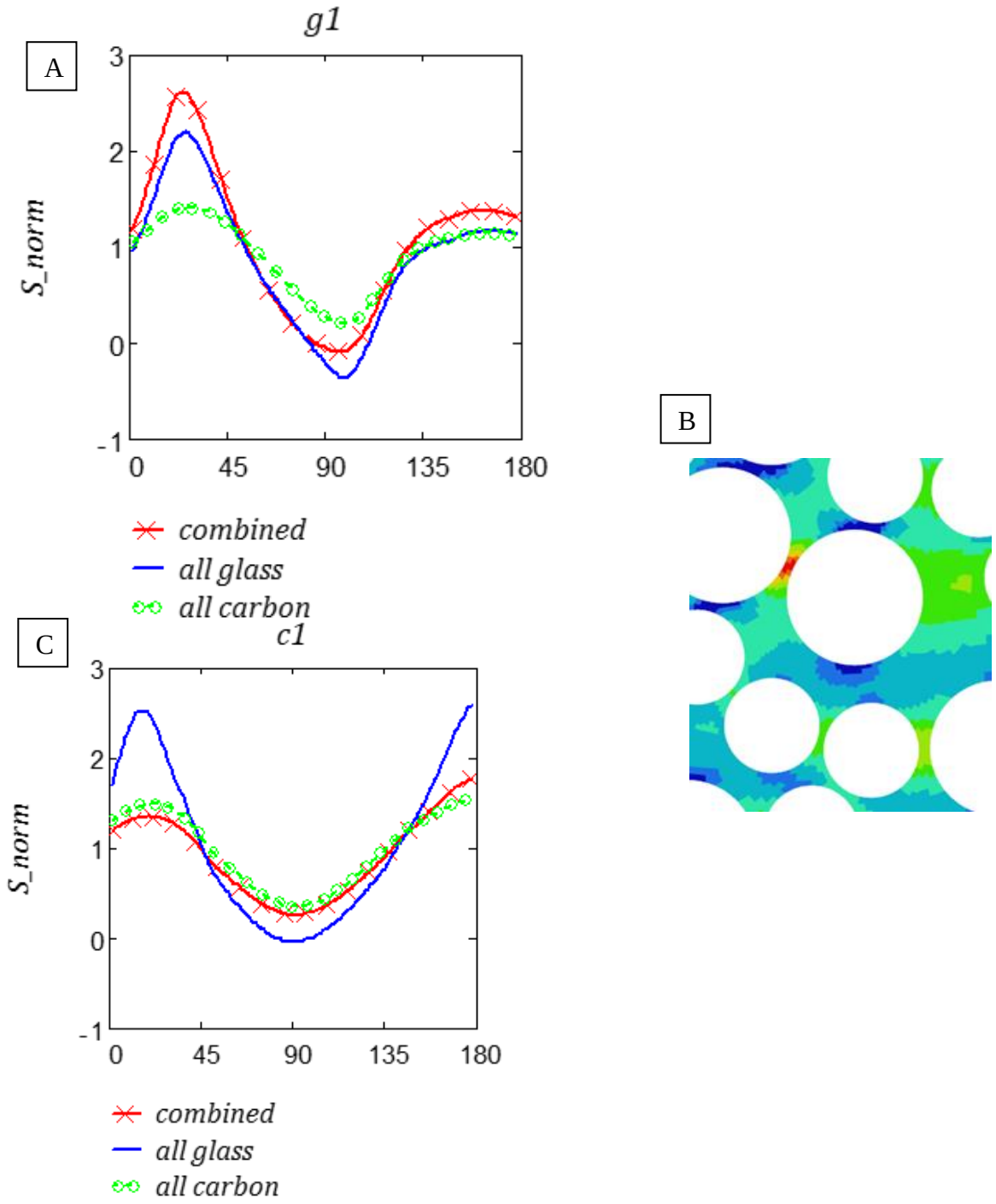

Figure 4.61 Results of Random RVE varying fiber radius and material effect combination of g1-c1region : (a) stress concentration distribution plot for g1, comparing with all glass and all carbon and combined material effect;(b)combined contour plot for the g1-c1 region;(c) stress concentration distribution plot for c1, comparing with all glass and all carbon and combined material effect.

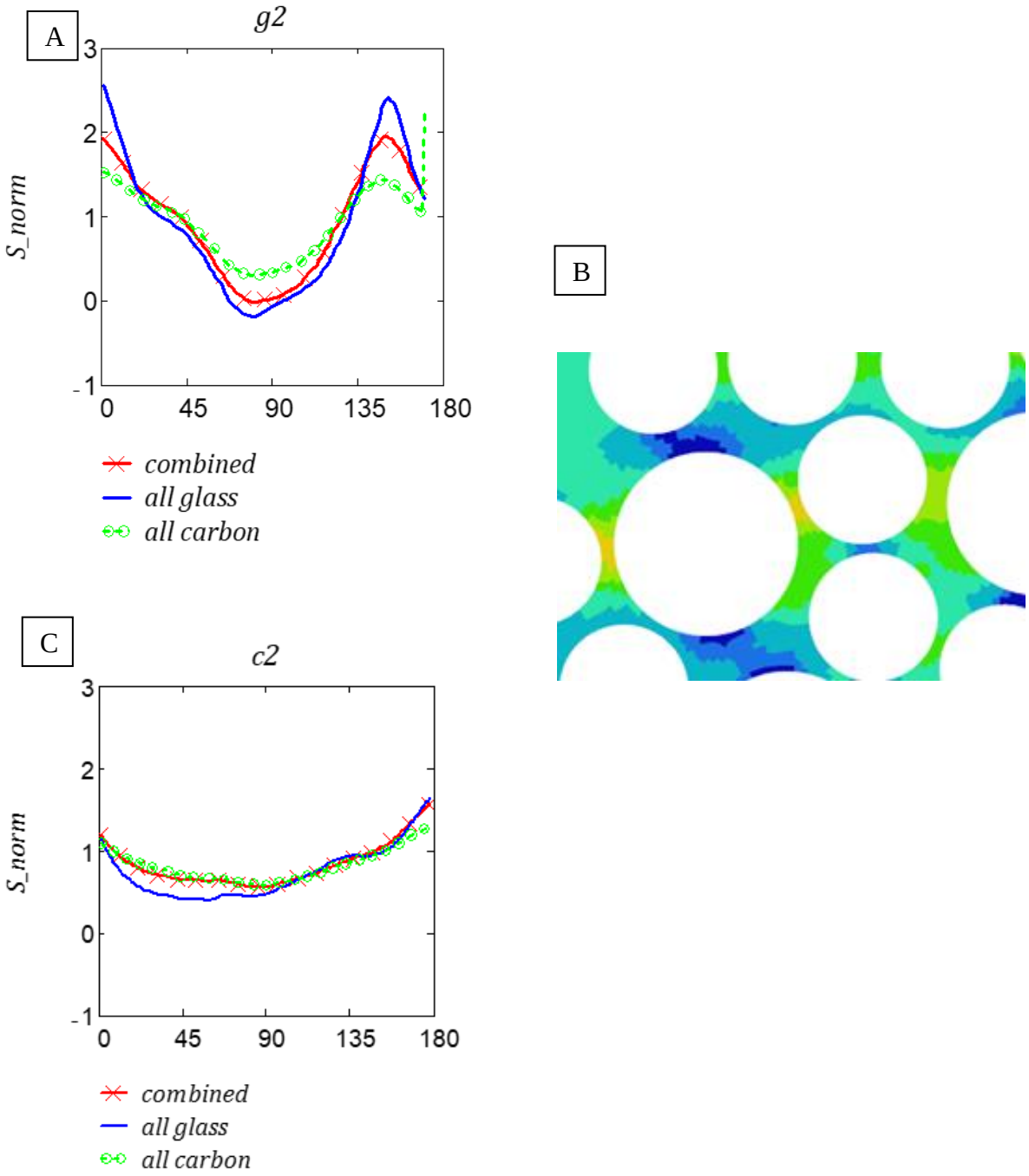

Figure 4.62 Results of Random RVE varying fiber radius and material effect combination of g2-c2region : (a) stress concentration distribution plot for g2, comparing with all glass and all carbon and combined material effect;(b)combined contour plot for g2-c2 region;(c) stress concentration distribution plot for c2, comparing with all glass and all carbon and combined material effect.

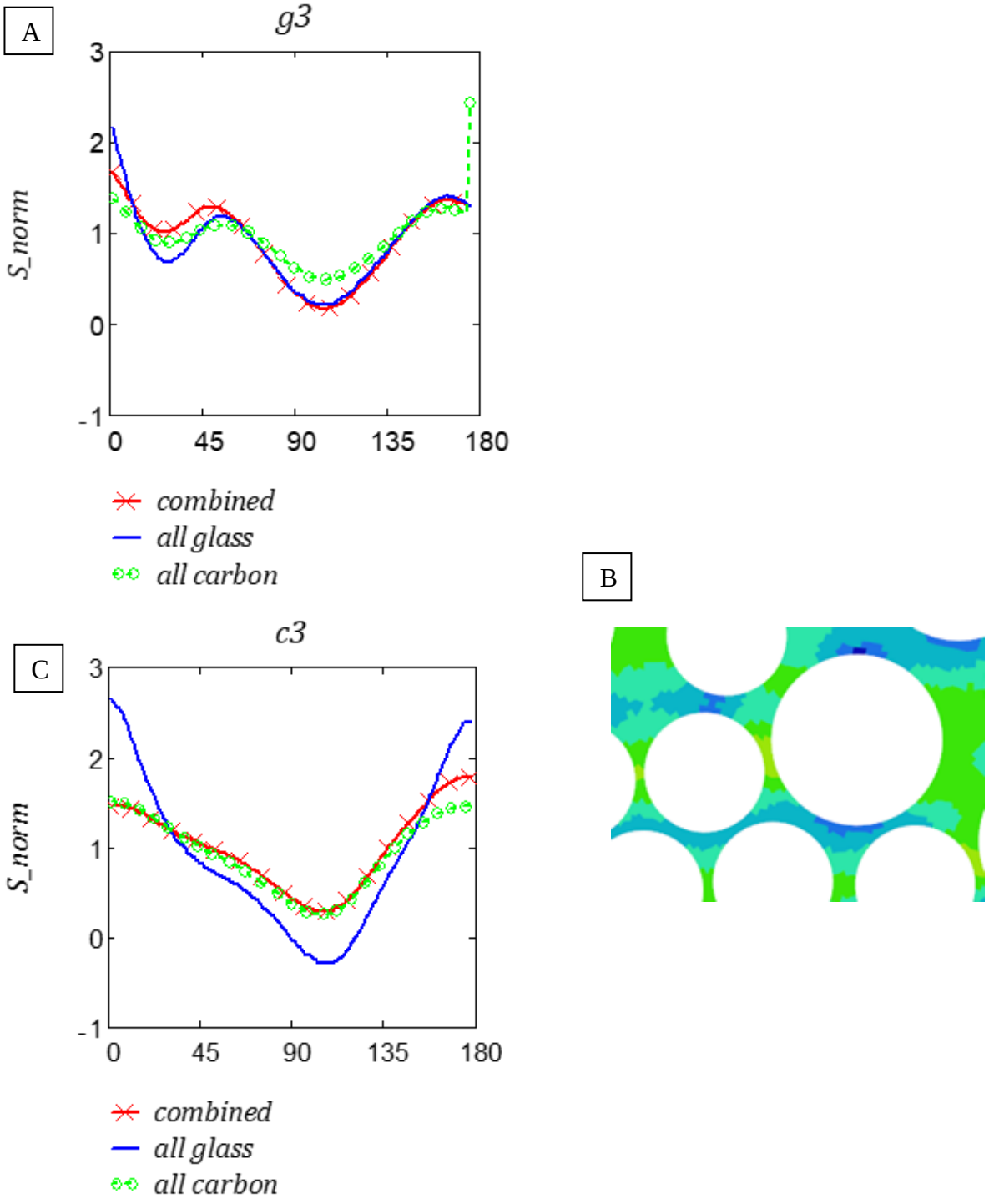

Figure 4.63 Results of Random RVE varying fiber radius and material effect combination of g3-c3 region : (a) stress concentration distribution plot for g3, comparing with all glass and all carbon and combined material effect;(b)combined contour plot for g3-c3 region;(c) stress concentration distribution plot for c3, comparing with all glass and all carbon and combined material effect.

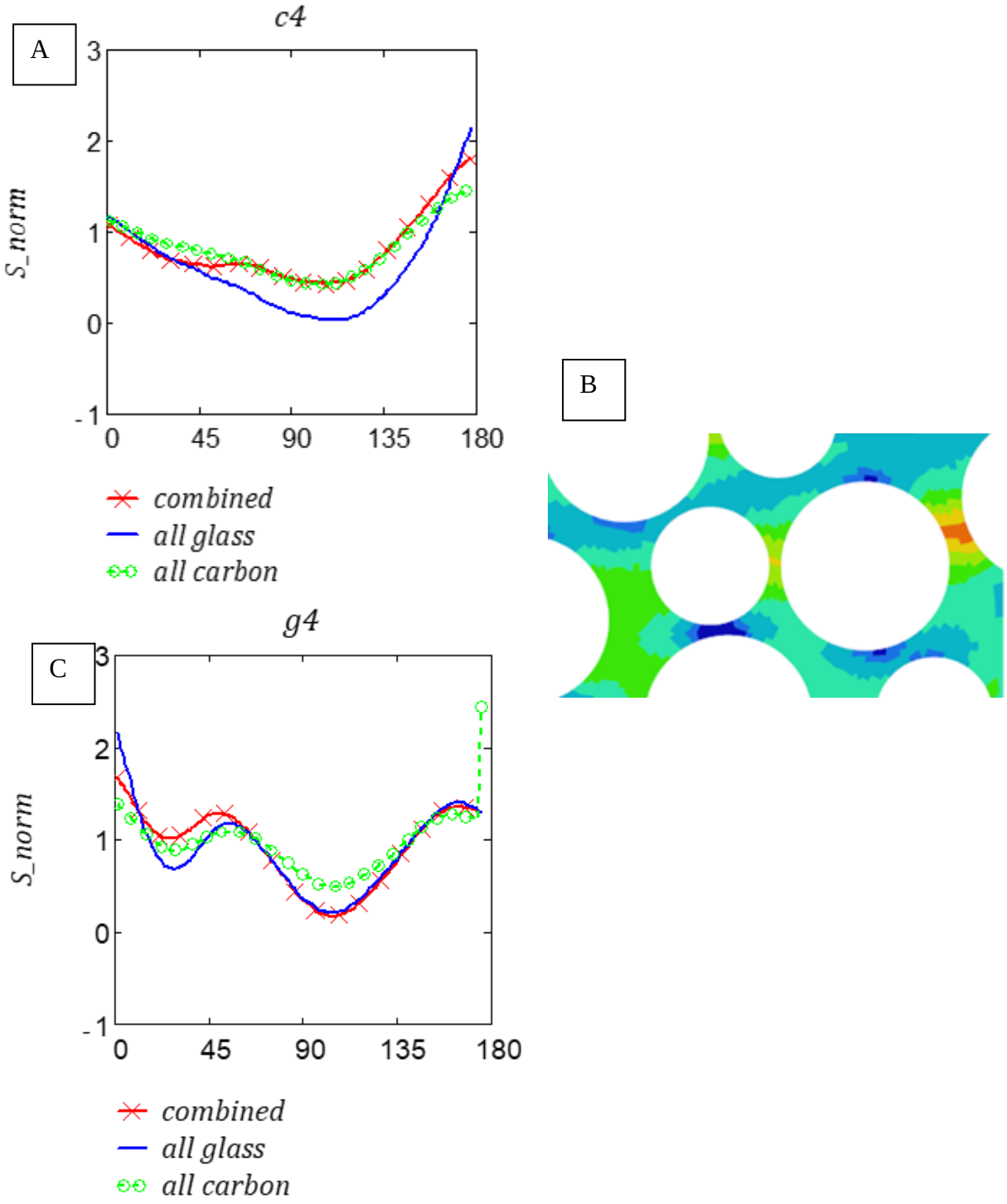

Figure 4.64 Results of Random RVE varying fiber radius and material effect combination of g4-c4region : (a) stress concentration distribution plot for g4, comparing with all glass and all carbon and combined material effect;(b)combined contour plot for g4-c4 region;(c) stress concentration distribution plot for c4, comparing with all glass and all carbon and combined material effect.

When results of the random RVE with varying radius and material effect is considered, following observations can be made. In Figure 4.61 an increase in stress concentration value for g1 can be seen because of the interaction of two stiff glass fibers, on the contrary a decrease in stress concentration value on nearby carbon fiber can be seen in c1. This observation directly strengthens results of hexagonal RVE results; as higher stress concentration around center glass fiber and lower around center carbon fiber. In Figure 4.62 interaction between g2 and c2 fibers can be seen this situation results as no change in stress concentration values since the interaction in between becomes dominant and in each case concentration value is high. In Figure 4.63 combination of these two effect creates a concentration level that is placed in between two homogenous case for g3, due to the interaction effect combined case gives an average value for the c3, too. In Figure 4.64, neighboring fiber effects becomes dominant for g4 and c4 reveals the effect of interaction with g4. To sum up, when material effect and radius effect combined, additional to explanations and resulting exceptions stated above , generally bigger fibers carry more loads and a higher stress concentration around them can be observed.

5. CONCLUSIONS

5.1. Summary and Findings

The effect of hybridization on stress concentration distribution was studied regarding different parameters. Both contour graphs and normalized stress plots on matrix are presented within each case, and each parameter was investigated in terms of the hybridization effect.

In the first case material effect was investigated. Stress concentration value, which is found in hybrid RVE constructed with inner fiber as carbon and outer fiber as glass, is decreased with a ratio of 1.41. On the other hand, the stress concentration value that is found in hybrid RVE constructed with inner fiber as glass and outer fiber as carbon is increased with a ratio of 0.774 this case, it is found that a positive hybridization effect around center fiber can be achieved by settling outer fibers with stiffer fibers.

In the second case, the fiber volume ratio effect is investigated, hybridization effect is observed similar to the first case. Ratio results calculated for $vf = 0.6$ as 1.41 and for $vf = 0.4$ as 1.2 in RVE constructed with inner carbon fiber. Ratio results calculated for $vf = 0.6$ as 0.774 and for $vf = 0.4$ as 0.856 in RVE constructed with inner glass fiber. From these, it can be stated that the amount of change in stress concentration increases with increasing fiber volume ratio, consequently, it can be said that as fiber volume ratio increases hybridization effect increases too.

In the third case, a rotated RVE was used. Same hybridization effect can be observed regarding ratio values respectively for inner carbon&outer glass fiber and vice versa as 1.3 and 0.777. When results of rotated RVE are compared with results of material effect solely, it can be said that the effect of hybridization in rotated RVE is lower than in regular RVE. This situation can be explained by the stiffness of RVE in the loading direction. Rotated RVE has higher stiffness than regular RVE under transverse loading, and consequently, stress concentration values are lower than regular RVE. Decrease in the hybridization effect in rotated RVE can be explained by the decrease in whole stress level among RVE.

Fourth and fifth cases are based on effect of fiber radii on stress concentration and the combination of fiber radii with material effect. Regarding solely radii change and material change, material change has a slightly higher effect on stress concentration than radius change. However, the highest change in stress concentration was reached with a combination of these two parameters. Since fiber with a bigger radius carries higher loads and when these fibers are located at the outer side load carried by central fiber decreases, consequently stress concentration decreases and vice versa. In addition, by placing stiffer fiber at the outer, this effect can be strengthened. Accordingly, the stress concentration value stated in the inner carbon r=3.5 case is the lowest value and stated in the inner glass r=5micrometer case is the highest value.

Sixth case set to see the behavior of the RVE under shear load and results were different than that of observed with transverse loading. When center fiber set as carbon in terms of material, stress concentration on center increases and for glass vice versa on the other hand fiber radius change results were similar with that of transverse loading. To understand the behavior better, a small angled model is set and load path observation on this model is made.

Seventh case is set as to make the load path observations and overall behavior of the model without applying a periodic BC's , instead employing neighbor RVEs in model. With the help of this model observations made with transverse loading and shear loading could be explained together as instead of single fiber effect, stiffer rows becomes dominant in terms of different loading directions. All of the stress concentrations values extracted with these models strengthened the observations made before in both shear and transverse loading.

For the last two case studies deepened by using random RVE. In these studies fiber material effect, fiber volume effect with constant fiber radius, solely fiber radius effect and combination of material effect with fiber radius effect is investigated. Different effect such as fiber interaction is taken into consideration, since inter fiber distance is set variable these effects become more significant, and general theories about stress concentration values are strengthened.

To sum up, different cases that have an effect on stress concentration value around the central fiber in hexagonal RVE and selected fibers in random RVE. Effects of the parameters stated in the study are investigated and results are examined through this thesis study. In general, it is observed that, creating stiffer regions around center fiber by employing glass fiber outer section decreases load carried by center fiber and decreases stress concentration under transverse loading, on the other hand, same configuration increases stress concentration under shear loading since this configuration causes an increase on load carried by center fiber due to creating stiffer regions in loading direction. Random RVE studies also showed an effect of inter fiber distance and fiber interaction on stress concentration. Differences related to these issues are observed as deviation from expected behavior.

5.2. Future Work

Regarding findings of this study , a further investigation about this topic can be made as extending these analysis to dynamic analysis and fatigue analysis. Also , another point of view can be strengthening the theoretical background with an experimental practical aspects could be beneficial

REFERENCES

1. Kaw, A.K., *Mechanics of composite materials*. 2005: CRC press.
2. *Abaqus Analysis User's Guide*, simulia, Editor. 2014.
3. Van Rossum, G., & Drake Jr, F. L, *ython 3 Reference Manual, Scotts Valley, CA: CreateSpace*. 2009.
4. Van Rossum, G.D.J., F.L., *python reference manual, Centrum voor Wiskunde en Informatica Amsterdam*. 1995.
5. Mathsoft, I., *Mathcad: User's Guide with Reference Manual : Mathcad 2001 Professional*. 2001: MathSoft, Incorporated.
6. Altair, *User's Guide Altair*. 2021.
7. Swolfs, Y., L. Gorbatikh, and I. Verpoest, *Stress concentrations in hybrid unidirectional fibre-reinforced composites with random fibre packings.* Composites Science and Technology, 2013. **85**: p. 10-16.
8. Singh, S.B. and H. Chawla, *Hybrid effect of functionally graded hybrid composites of glass–carbon fibers.* Mechanics of Advanced Materials and Structures, 2019. **26**(14): p. 1195-1208.
9. Swolfs, Y., L. Gorbatikh, and I. Verpoest, *Fibre hybridisation in polymer composites: A review.* Composites Part A: Applied Science and Manufacturing, 2014. **67**: p. 181-200.
10. Swolfs, Y., I. Verpoest, and L. Gorbatikh, *Recent advances in fibre-hybrid composites: materials selection, opportunities and applications.* International Materials Reviews, 2019. **64**(4): p. 181-215.
11. Crookston, J., A. Long, and I. Jones, *Modelling effects of reinforcement deformation during manufacture on elastic properties of textile composites.* Plastics, rubber and composites, 2002. **31**(2): p. 58-65.
12. Zweben, C., *Advanced composites for aerospace applications: A review of current status and future prospects.* Composites, 1981. **12**(4): p. 235-240.
13. Gururaja, M. and A.H. Rao, *A review on recent applications and future prospectus of hybrid composites.* International Journal of Soft Computing and Engineering, 2012. **1**(6): p. 352-355.

14. Zin, M., et al. *A review on the fabrication method of bio-sourced hybrid composites for aerospace and automotive applications*. in *IOP Conference Series: Materials Science and Engineering*. 2016. IOP Publishing.

15. Hayashi, T. *On the improvement of mechanical properties of composites by hybrid composition*. in *Proc. 8th Intl. Reinforced Plastics Conf.* 1972.

16. Swolfs, Y., I. Verpoest, and L. Gorbatikh, *Maximising the hybrid effect in unidirectional hybrid composites.* Materials & Design, 2016. **93**: p. 39-45.

17. Rajpurohit, A., et al., *Hybrid Effect in In-Plane Loading of Carbon/Glass Fibre Based Inter-and Intraply Hybrid Composites.* Journal of Composites Science, 2020. **4**(1): p. 6.

18. Kretsis, G., *A review of the tensile, compressive, flexural and shear properties of hybrid fibre-reinforced plastics.* Composites, 1987. **18**(1): p. 13-23.

19. Manders, P.W. and M. Bader, *The strength of hybrid glass/carbon fibre composites.* Journal of materials science, 1981. **16**(8): p. 2246-2256.

20. Sevkat, E., et al., *Effect of repeated impacts on the response of plain-woven hybrid composites.* Composites Part B: Engineering, 2010. **41**(5): p. 403-413.

21. Dickson, R., et al., *Fatigue behaviour of hybrid composites.* Journal of materials science, 1989. **24**(1): p. 227-233.

22. Fernando, G., et al., *Fatigue behaviour of hybrid composites.* Journal of materials science, 1988. **23**(10): p. 3732-3743.

23. Dong, C. and I.J. Davies, *Flexural strength of bidirectional hybrid epoxy composites reinforced by E glass and T700S carbon fibres.* Composites Part B: Engineering, 2015. **72**: p. 65-71.

24. Sabuncuoglu, B., *On the high stress concentrations in steel fiber composites under transverse loading.* Journal of Reinforced Plastics and Composites, 2014. **33**(21): p. 1941-1953.

25. Sabuncuoglu, B., et al., *Micro-scale finite element analysis of stress concentrations in steel fiber composites under transverse loading.* Journal of Composite Materials, 2015. **49**(9): p. 1057-1069.

26. Sabuncuoglu, B., O. Cakmakci, and F.S. Kadioglu, *Fiber/matrix interface stress analysis of flax-fiber composites under transverse loading considering material nonlinearity.* Journal of Reinforced Plastics and Composites, 2020. **39**(9-10): p. 345-360.

27. Sabuncuoglu, B., et al. *Micro-scale computational analysis of the effect of matrix properties on the stress distribution of steel fiber composites*. in *SICOMP Conference on the Manufacturing and Design of Composites, Date: 2013/05/30-2013/05/31, Location: Linkoping, Sweden*. 2013.

28. Sabuncuoglu, B., et al., *Stress redistribution around fiber breaks in unidirectional steel fiber composites considering the nonlinear material behavior*. Composite Structures, 2020. **239**: p. 111959.

29. Chevalier, J., et al., *Multi-scale characterization and modelling of the transverse compression response of unidirectional carbon fiber reinforced epoxy.* Composite Structures, 2019. **209**: p. 160-176.

30. Sun, Q., et al., *Failure criteria of unidirectional carbon fiber reinforced polymer composites informed by a computational micromechanics model.* Composites Science and Technology, 2019. **172**: p. 81-95.

31. Sharma, A., et al., *On the prediction of the bi-axial failure envelope of a UD CFRP composite lamina using computational micromechanics: Effect of microscale parameters on macroscale stress–strain behavior*. Composite Structures, 2020. **251**: p. 112605.

32. Sun, C.-T. and R.S. Vaidya, *Prediction of composite properties from a representative volume element.* Composites science and Technology, 1996. **56**(2): p. 171-179.

33. Maligno, A., N. Warrior, and A. Long, *Finite element investigations on the microstructure of fibre-reinforced composites.* Express Polymer Letters, 2008. **2**(9): p. 665-676.

34. Li, S., *General unit cells for micromechanical analyses of unidirectional composites.* Composites Part A: applied science and manufacturing, 2001. **32**(6): p. 815-826.

35. Li, S., *On the unit cell for micromechanical analysis of fibre-reinforced composites.* Proceedings of the Royal Society of London. Series A: Mathematical, Physical and Engineering Sciences, 1999. **455**(1983): p. 815-838.

36. Li, D.S. and M.R. Wisnom, *Finite element micromechanical modelling of unidirectional fibre-reinforced metal-matrix composites.* Composites science and technology, 1994. **51**(4): p. 545-563.

37. Bayat, M. and M. Aghdam, *A micromechanics-based analysis of effects of square and hexagonal fiber arrays in fibrous composites using DQEM.* European Journal of Mechanics-A/Solids, 2012. **32**: p. 32-40.

38. Love, A.E.H., *A treatise on the mathematical theory of elasticity*. 2013: Cambridge university press.

39. Adams, D.F. and D.A. Crane, *Finite element micromechanical analysis of a unidirectional composite including longitudinal shear loading.* Computers & structures, 1984. **18**(6): p. 1153-1165.

40. Adams, D.F. and D.R. Doner, *Longitudinal shear loading of a unidirectional composite.* Journal of Composite Materials, 1967. **1**(1): p. 4-17.

41. Adams, D.F. and D.R. Doner, *Transverse normal loading of a unidirectional composite.* Journal of composite Materials, 1967. **1**(2): p. 152-164.

42. Aghdam, M. and A. Dezhsetan, *Micromechanics based analysis of randomly distributed fiber reinforced composites using simplified unit cell model.* Composite structures, 2005. **71**(3-4): p. 327-332.

43. Romanov, V., et al., *Statistical analysis of real and simulated fibre arrangements in unidirectional composites.* Composites Science and Technology, 2013. **87**: p. 126-134.

44. Wongsto, A. and S. Li, *Micromechanical FE analysis of UD fibre-reinforced composites with fibres distributed at random over the transverse cross-section.* Composites Part A: Applied Science and Manufacturing, 2005. **36**(9): p. 1246-1266.

45. Trias, D., et al., *Random models versus periodic models for fibre reinforced composites.* Computational materials science, 2006. **38**(2): p. 316-324.

46. Chen, X. and T. Papathanasiou, *Interface stress distributions in transversely loaded continuous fiber composites: parallel computation in multi-fiber RVEs using the boundary element method.* Composites science and technology, 2004. **64**(9): p. 1101-1114.

47. Buryachenko, V., et al., *Quantitative description and numerical simulation of random microstructures of composites and their effective elastic moduli.* International journal of solids and structures, 2003. **40**(1): p. 47-72.

48. Gusev, A.A., P.J. Hine, and I.M. Ward, *Fiber packing and elastic properties of a transversely random unidirectional glass/epoxy composite.* Composites Science and Technology, 2000. **60**(4): p. 535-541.

49. Melro, A., et al., *Micromechanical analysis of polymer composites reinforced by unidirectional fibres: Part I–Constitutive modelling.* International Journal of Solids and Structures, 2013. **50**(11-12): p. 1897-1905.

50. Melro, A., et al., *Micromechanical analysis of polymer composites reinforced by unidirectional fibres: Part II–Micromechanical analyses.* International Journal of Solids and Structures, 2013. **50**(11-12): p. 1906-1915.

51. González, C. and J. LLorca, *Mechanical behavior of unidirectional fiber-reinforced polymers under transverse compression: Microscopic mechanisms and modeling.* Composites Science and Technology, 2007. **67**(13): p. 2795-2806.

52. Guerrero, J.M., et al., *Size effects in hybrid unidirectional polymer composites under longitudinal tension: A micromechanical investigation.* Composites Part A: Applied Science and Manufacturing, 2021. **140**: p. 106186.

53. Guerrero, J.M., et al., *Failure of hybrid composites under longitudinal tension: Influence of dynamic effects and thermal residual stresses.* Composite Structures, 2020. **233**: p. 111732.

54. Guerrero, J.M., et al., *An analytical model to predict stress fields around broken fibres and their effect on the longitudinal failure of hybrid composites.* Composite Structures, 2019. **211**: p. 564-576.

55. Huang, Z.-m., *Micromechanical prediction of ultimate strength of transversely isotropic fibrous composites.* International journal of solids and structures, 2001. **38**(22-23): p. 4147-4172.

56. Wilczyński, A. and J. Lewiński, *Predicting the properties of unidirectional fibrous composites with monotropic reinforcement.* Composites science and technology, 1995. **55(**2): p. 139-143.

APPENDICES

```
75
76  # Import libraries and functions
77  import numpy as num
78  from Rand_uSTRU_f_Loop import RandGen
79  import time
80  # import sys
81  import multiprocessing
82  # from functools import partial
83  from joblib import Parallel, delayed
84  from Rand_uSTRU_f_HexSqPack import GenHexSqPack
85
86  #
87  ###############################################################################
88  # Input Parameters
89  ###############################################################################
90  #
91  ###############################################################################
92  # General options
93  ###############################################################################
94  #
95  OutputCaseName = 'RVE_exp_mat1_DISTMIN5e-3_'  # This determines the name of the files generated by the code.
96  # A distribution number will be included automatically. For instance if OutputCaseName='RVE_', then the name of the
97  # file will be RVE_1, RVE_2, etc.
98  FibrePackingType = 0  # 0=Generate a random packing, 1=Generate hexagonal packing, 2=Generate square packing
99  NumTimes = 2  # Number of different fibre distributions to generate, in the case of a random packing.
100 StartingSim = 1  # Starting number for the fibre distribution
101 num_cores = 1  # Number of cpu 'threads' to be used for the parallelization.
102 # Each thread will create a different distribution, all working in parallel
103 hybrid_option = 1  # 0=Generates a non-hybrid (Fibre_type_1, see below, must be equal to 1), 1=Generates a Hybrid.
104 Hybrid_type = 0  # If hybrid_option=1, type of hybrid to make:
105 # 0=fiber-by-fiber (intrayarn), 1=layer-by-layer (interlayer), 2=Bundle-by-bundle (intralayer)
106 R = 3.5e-3 # fibre 1 average radius
107 R1 = 5e-3  # fibre 2 average radius
108 # Note: when doing non-hybrid composites, use the same radius for R and R1.
109 VariableFibreRadius = 0  # Whether to use a variable fibre radius for each fibre population, accordingly to
110 # a normal distribution, see below. 0=No, 1=Yes
111 R_STDEV = 0.000227014  # Standard deviation for fibre type 1, used if VariableFibreRadius=1.
112 # Must be in the same units of fibre radius (in mm)
113 R1_STDEV = 0.000227014  # Standard deviation for fibre type 2, used if VariableFibreRadius=1.
114 # Must be in the same units of fibre radius (in mm)
115 Vol_fibre_req = 0.6  # Overall fibre volume we wish to obtain
116 # Note: values up to 0.65 are possible. Larger values are hard to obtain.
117 Fibre_type_1 = 0.5  # Fibre volume fraction of population 1 over the total fibre volume fraction:
118 # (e.g. 0.5 would mean 50% of the overall volume fraction are type 1 fibres, the other 50% are type 2 fibres),
119 # (e.g. 0.7 would mean 70% of the volue fraction is occupied by type 1 fibres, 0.3 by type 2 fibres)
120 # If non-hybrid, set this to 1 (so that all fibres are type 1 fibres).
121 delta_width = 10  # 155.96330275229357 # Ratio (Total RVE width/Fibre radius).
122 # Note: in hexagonal and squares packings, this value is approximate.
123 delta_height = 10  # Ratio (Total RVE height/Fibre radius).
124 # Note: in hexagonal and squares packings, this value is approximate.
125 #
126 ###############################################################################
127 # Other random packing options
128 ###############################################################################
129 #
130 DIST_MIN = 2.15  # Minimum distance multiplier between two consecutive fibre centres
```

Figure 5.1 Input view of random RVE with varying radius Python code.

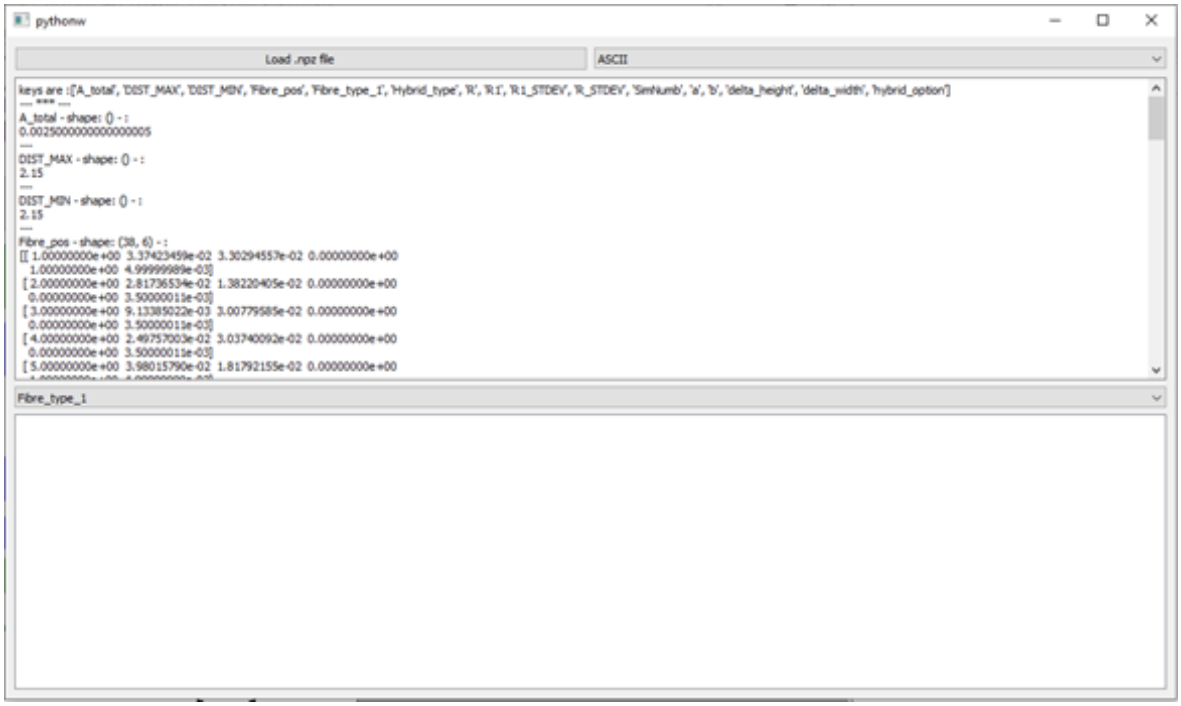

Figure 5.2 Output npz file of random RVE with varying radius Python code

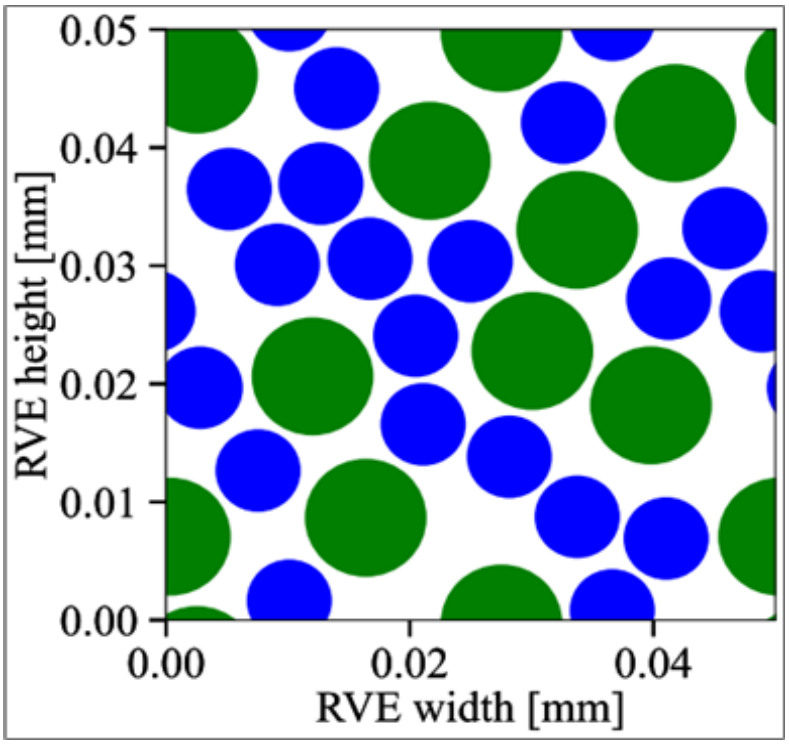

Figure 5.3 Output review picture of random RVE with varying radius Python code